

**AN INVESTIGATION ON FLOW OSCILLATIONS DUE TO SHEAR
LAYER INSTABILITY AND VORTEX DYNAMICS**

A THESIS

Submitted by

SUNIL A. S.

for the award of the degree

of

DOCTOR OF PHILOSOPHY



**MECHANICAL ENGINEERING DIVISION
SCHOOL OF ENGINEERING
COCHIN UNIVERSITY OF SCIENCE AND TECHNOLOGY, KOCHI**

NOVEMBER 2019

THESIS CERTIFICATE

This is to certify that the thesis entitled “**AN INVESTIGATION ON FLOW OSCILLATIONS DUE TO SHEAR LAYER INSTABILITY AND VORTEX DYNAMICS**” submitted by Sunil A.S. to the Cochin University of Science and Technology, Kochi for the award of the degree of Doctor of Philosophy is a bonafide record of research work carried out by him under my supervision and guidance at the Division of Mechanical Engineering, School of Engineering, Cochin University of Science and Technology. The content of this thesis, in full or in parts, have not been submitted to any other University or Institute for the award of any degree or diploma.

I further clarify that the correction and modifications suggested by the audience during the pre-synopsis seminar and recommended by the Doctoral committee have been incorporated in this thesis.

Kochi-682022

7th November 2019

Dr. TIDE P.S.

(Supervising Guide)

DECLARATION

I hereby declare that the work presented in the thesis entitled “**AN INVESTIGATION ON FLOW OSCILLATIONS DUE TO SHEAR LAYER INSTABILITY AND VORTEX DYNAMICS**” is based on the original research work carried out by me under the supervision and guidance of Dr. Tide P.S. for the award of degree of Doctor of Philosophy with Cochin University of Science and Technology. I further declare that the contents of this thesis, in full or in parts, have not been submitted to any other University or Institute for the award of any degree or diploma.

Kochi-22

7th November 2019

Sunil A .S.

Research Scholar

ACKNOWLEDGEMENTS

All praise and thanks are due to the GOD the Almighty, who always guide me to the right path, for blessing me with health, knowledge, and environment required for the completion of this work as well as getting along with life.

I want to express my sincere gratitude to my supervising guide Dr. Tide P. S., Professor in Mechanical Engineering, School of Engineering, Cochin University of Science and Technology for the constant encouragement, motivation, excellent guidance, competent instruction, keen comments, and persistent reassurance during the entire course of research work. I was able to complete the work and deliver this thesis only because of his able guidance and immense perseverance. I have been fortunate to have a supervisor, and I could not have imagined having a better advisor and mentor for my entire Ph.D work.

I extend my sincere gratitude to Dr. Sreejith P. S., Professor and former Dean, Faculty of Engineering, CUSAT for his valuable suggestions and support throughout this work. I am incredibly thankful to him as his role as Professor in Mechanical Engineering and also as member of Doctoral Committee for the valuable ideas and instruction during the period of this work. Let me express my sincere gratitude to Dr. K. S. Beena, Professor and Dean, Faculty of Engineering, CUSAT, for extending support for the smooth completion of the research work.

I am incredibly thankful to Dr. Gireeshkumaran Thampi B. S. and Dr. James Varghese, former and present Heads in the Division of Mechanical Engineering, SOE, CUSAT for providing all support including administrative for the successful completion of my thesis. I take this opportunity to thank all faculty members in the Division of Mechanical Engineering, SOE, CUSAT especially Dr. Bhasi A. B., and Dr. Biju N., for their constant backing at all stages of this research. I am obliged to our former Principal, Dr. M. R. Radhakrishna Panicker, present Principal, Dr. George Mathew and office staff

members for all other logistical support. I want to thank all non-teaching staff including library staff of CUSAT who have helped and supported me during the entire course of work.

I am incredibly thankful to Dr. V.P. Mohandas, Head, Department of Mechanical Engineering, Government Engineering College Thrissur for providing me the facilities in the Computational lab for my research work. I am very much grateful to Dr. V.S. Sheeba, Principal, GEC, Thrissur for providing all support including administrative, to facilitate my research at CUSAT. I express heartfelt appreciations to Prof. Sandhya M. and Prof. Mubarak A.K., my colleagues at GEC, Thrissur, and the constant companions throughout the research at CUSAT for being good friends. I express special thanks to Prof. Abdul Samad P. A., Prof. Jayee K. Varghese and Prof. Lalu P P., my colleagues at GEC, Thrissur, for all fruitful and encouraging discussions. I express my heartiest gratitude to all my friends and colleagues for their support throughout my work.

I record my sincere and utmost gratitude to my parents, Mr. Abdul Sathar M.H. and Mrs. Nabeesa V.C., for showering love and showing faith in me. I salute you for the selfless love, attention, and expense you did to shape my life. Also, I express my thanks to my brothers, sisters, parents-in-law without whose prayers, encouragement, and loving care for me; this work would not have become a reality.

Finally, let me mention the encouragement, love, and affection that I got from my beloved son Mohammed Saleeq S. and daughter Ibza Shalia S which had been an everlasting inspiration to complete my work at a good pace. My wife, Mrs. Shaniba N.M., has been incredibly supportive to me throughout this entire process and has made countless sacrifices to help me get to this point.

SUNIL A. S.

ABSTRACT

Tall structures and deep marine risers design pose substantial challenges to designers as their premature collapse induces tremendous economic and environmental concern to the world. Significant wind and ocean currents flowing past tall structures and risers are instrumental in producing Aeolian vibrations. At times the disturbances and instabilities could lead to the catastrophic damage of structures causing colossal loss to the industrial world and society. The alternate fluid layer separation from either side of the structures leads to the formation of vortices in the wake of the structure making it more and more unstable. The suppression of intensity of vortex induced vibrations is the only solution to this phenomenon of vortex shedding.

The investigation focuses on the numerical investigation of flow characteristics when large currents flow past bluff bodies. Detailed investigations were carried out on circular and square cylinders at Mach numbers less than 0.3. The characteristic length of circular and square structures was kept the same in all computations for the sake of comparison. The flow incident angle was kept identical, and the flow is assumed to be incompressible. The square structures tend to produce low values of vortex induced vibrations as they are capable of disturbing the fluid separation layer due to their sharp edge construction. The numerical investigation was also carried out for different Reynolds numbers to study the evolution and development of Von Karman vortex streets. At low Reynolds number up to 40, only recirculation eddies are produced. However, at Reynolds number of 150, fully developed vortex streets are visible. These vortices are found to detach alternately from either side of the bluff body, then move to the wake and finally diffuse into the atmosphere.

Numerical investigations on the suppression of vortex induced vibrations were carried out in a three -dimensional computational domain incorporating pressure based solver with *RANS* equations and *SST k- ω* turbulence model. The investigations were performed by using various suppression methods including passive, active and compound methods. The predictions were found to be in reasonable agreement with the experimental data available in the literature. It was observed that vortex induced vibration got reduced considerably by the application of these methods. However, after certain level, the excessive use of these methods hurts the suppression of Aeolian vibration. The lift forces causing alteration in Strouhal frequency was reduced principally at the expense of an increase in drag force. Hence a balance must be struck between these two forces in applying suppression methods. A reduction of 85% Aeolian vibration was achieved with the use of triple start helical strakes on a circular structure. The application of compound method was found to be more effective as it combines the excellent features of both passive and active methods. A reduction in VIV of 75% was realised with the incorporation of this method.

The effect of triple start helical strakes on a tall chimney was investigated when wind blew at a velocity of 10 m/s. The numerical simulations on the tall chimney with and without helical strakes were carried out. The drag crisis was seen to get eliminated by using hemispherical dimples along the surface of long marine cylinders. Observations reveal that the use of passive devices reduces the formation of Aeolian vibration and can also save the life of the structure as well as humans. The comparison of the predictions reveals that a reduction of 75% to 80% could be obtained with the use of these suppression methods.

TABLE OF CONTENTS

ACKNOWLEDGEMENTS	iv
ABSTRACT	vi
TABLE OF CONTENTS	viii
LIST OF TABLES	xiii
LIST OF FIGURES	xiv
LIST OF ABBREVIATIONS	xix
LIST OF NOMENCLATURE	xx
CHAPTER 1 INTRODUCTION	1-5
1.1 Vortex Induced Vibrations.	1
1.2 Thesis Outline	4
CHAPTER 2 LITERATURE SURVEY	6-27
2.1 Shear Layer Instability and Vortex Dynamics	7
2.1.1 Factors Influencing VIV	9
2.1.2 Types of Vortex Induced Vibration	9
2.1.3 Prevention of Vortex Induced Vibrations.....	9
2.2 Suppression Methods for Vortex Induced Vibration.....	10
2.2.1 Physics of Vortex Induced Vibrations	11
2.3 Fluid Flow Domain and Gridding Strategy.....	11
2.4. Vortex Suppression Methods	13
2.4.1 Passive Control Methods.....	14
2.4.1.1 Straight and Helical Fins.....	14
2.4.1.2 Splitter Plates.....	16
2.4.2 Active Methods	18
2.4.3 Compound Methods	19
2.4.4 Structural Configurations	20
2.4.5 Chimney Vibrations.....	21
2.5 Numerical Simulations	23
2.6 Motivation	24

2.6.1	Gaps in Literature -----	26
2.7	Scope of the Present Work -----	26

CHAPTER 3 NUMERICAL MODELLING ----- 28-32

3.1	Governing Equations -----	28
3.2	Turbulence Modelling-----	29
3.2.1	Closure Problem in Turbulence -----	29
3.2.2	Boussinesq's Hypothesis -----	30
3.2.3	SST $k-\omega$ Turbulence Model -----	30
3.3	Fluid Flow Parameters-----	31
3.4	Summary -----	32

**CHAPTER 4 NUMERICAL INVESTIGATIONS ON VORTEX
SHEDDING PAST BLUFF BODIES----- 33-47**

4.1	Introduction -----	33
4.2	Computational Domain-----	33
4.2.1	Computational Domain for a Square Cylinder-----	33
4.2.2	Grid Independence Study -----	35
4.2.3	Computational Domain for a Circular Cylinder -----	36
4.2.4	Solution Methodology-----	37
4.3	Results and Discussion -----	37
4.3.1	Square Cylinder -----	37
4.3.1.1	Non- Vortex Shedding Flow ($Re=40$)-----	38
4.3.1.2	Vortex Shedding Flow ($Re=150$)-----	38
4.3.1.3	Flow Characteristics at $Re=40$ and 150 for a Square Cylinder -----	40
4.3.2	Circular Cylinder-----	42
4.3.2.1	Vorticity Magnitude at $Re=5$ and 40 for a Circular Cylinder -----	43
4.3.2.2	Flow Characteristics at $Re=5$ and 40 for a Circular Cylinder-----	44
4.3.2.3	Recirculation Bubble Length-----	45
4.4	Summary-----	46

**CHAPTER 5 SUPPRESSION OF AEOLIAN VIBRATIONS BY A
SPLITTER PLATE FOR FLOW PAST A BLUFF BODY ---- 48-57**

5.1	Introduction	48
5.2	Flow Domain	49
5.2.1	Computational Domain and Mesh	50
5.2.2	Discretization Method	50
5.2.3	Boundary Conditions	50
5.3	Results and Discussion	51
5.3.1	Flow Over Square Cylinder	51
5.3.2	Flow Over Square Cylinder With and Without Detached Splitter Plate	52
5.4	Summary	56

**CHAPTER 6 SUPPRESSION OF VORTEX INSTABILITIES USING
STRAIGHT FINS----- 58-65**

6.1	Introduction	58
6.2	Computational Domain	58
6.3	Results and Discussion	59
6.3.1	Flow Over a Circular Cylinder Without Attachments	59
6.3.2	Flow Over a Circular Cylinder With Fins	61
6.3.3	Effect of Fin Count	61
6.3.4	Effect of Fin Orientation	63
6.4	Summary	65

**CHAPTER 7 FLUID FLOW OSCILLATIONS IN THE WAKE OF
A CYLINDER WITH HELICAL STRAKES----- 66-78**

7.1	Introduction	66
7.2	Computational Domain and Meshing Strategy	66
7.2.1	Boundary Conditions	68
7.3	Results and Discussion	68
7.3.1	Flow Characteristics Across a Cylinder Without Strakes at $Re=22000$	68
7.3.2	Flow Over Circular Cylinder With Triple Start Helical Strakes at $Re=22000$	71
7.4	Summary	77

**CHAPTER 8 EFFECT OF ACTIVE AND COMPOUND METHODS ON
VORTEX DYNAMIC IN THE FLOW FIELD ----- 79-96**

8.1	Introduction -----	79
8.2	Flow Domain for Active method -----	80
8.2.1	Computational Domain.-----	80
8.2.2	Boundary Conditions -----	81
8.3	Results and Discussion -----	81
8.3.1	Flow Over a Stationary Square Cylinder -----	81
8.3.2	Flow Over Oscillating Square Cylinder at Different Amplitudes-----	82
8.3.2.1	Effect of Drag -----	84
8.3.2.2	Effect of Lift -----	85
8.3.2.3	Variation of Strouhal Number With Amplitude of Oscillations-----	86
8.4	Comparison of Passive and Active Methods-----	87
8.4.1	Gridding Strategy-----	87
8.4.2	Boundary Conditions -----	88
8.5	Results and Discussion -----	88
8.5.1	Case 1: Cylinder Without Splitter Plate in the Wake – Baseline Simulation -----	89
8.5.2	Case 2: Cylinder With a Splitter Plate in the Wake – Passive Method -----	90
8.5.3	Case 3: Cylinder with an Oscillating Splitter Plate– Compound Method -----	92
8.6	Summary -----	95

**CHAPTER 9 AN INVESTIGATION ON REDUCTION OF VORTEX
INDUCED LOADS ON TALL CHIMNEYS AND MARINE
RISERS -----97-125**

9.1	Introduction-----	97
9.2	Computational Flow Domain for a Chimney-----	98
9.2.1	Chimney -----	98
9.2.2	Simulation Parameters-----	99
9.2.3	Computational Domain and Mesh. -----	99
9.2.4	Boundary Conditions -----	100
9.3	Results and Discussion -----	100
9.3.1	Flow Characteristics Across a Chimney Without Strakes -----	100
9.3.2	Flow Over the Chimney with Triple Start Helical Strakes at a velocity of 10 m/s-----	104
9.4	Computational Domain for A Marine Riser -----	110

9.4.1	Marine Riser-----	110
9.4.2	Domain and Mesh Selection-----	111
9.4.3	Boundary Conditions-----	111
9.5	Results and Discussion-----	112
9.5.1	Flow Characteristics for Fluid Flow Across a Marine Riser Without Dimples-----	112
9.5.2	Flow Over Marine Riser With Dimples on the Surface at a Velocity of 1 m/s-----	116
9.5.3	The Effect of Sizing and Sequencing of Dimples on the Riser Surface-----	121
9.6	Summary.-----	123

CHAPTER 10 CONCLUSIONS----- 126-134

10.1	Analysis of Fluid Flow Parameters on Circular and Square Structures-----	126
10.2	Effect of Splitter Plate in the Reduction of Vortex Induced Forces on a Square Cylinder-----	128
10.3	Passive Control of Vortex Induced forces on a Circular Geometry Fitted with Straight Fins-----	128
10.4	Suppression of Vortex Induced Forces on Circular Geometry Fitted with Helical Strakes-----	129
10.5	Active method of VIV Suppression on a Square Structure-----	130
10.6	Analysis of Compound Method in the Suppression of Vortex Induced Forces-----	131
10.7	Suppression of Vortex Shedding Using Helical Strakes Attached on a Tall Chimney-----	132
10.8	Novel Concept of Suppression of Vortex Shedding on a Marine Riser Engraved with Dimples on the Surface-----	133
10.9	Future Work-----	134

REFERENCES----- 135-138

LIST OF PUBLICATIONS----- 139

CURRICULUM VITAE----- 140

LIST OF TABLES

Table	Title	Page
4.1	Comparison of C_D , C_L and St obtained for square cylinders.....	42
4.2	Comparison of C_D , and St obtained for square cylinders.....	45
5.1	Flow properties.....	51
6.1	Strouhal number variation with fin count	63
7.1	Flow properties.....	68
7.2	Flow conditions for a fluid flow past a circular cylinder without strakes.....	71
7.3	(a) Flow parameters for fluid flow over a bare cylinder	76
	(b) Flow parameters for fluid flow over a cylinder with strakes	76
8.1.	Flow properties.....	81
8.2	Flow properties.....	88
8.3	Flow parameters for a stationary cylinder.....	89
8.4	Flow parameters for a stationary splitter plate	92
8.5	Flow parameters at different amplitudes of oscillations	94
9.1	Flow properties.....	100
9.2	Flow characteristics across a circular chimney without strakes.....	104
9.3	Flow characteristics across a circular chimney with strakes.....	110
9.4	Fluid flow properties	112
9.5	Flow characteristics across a bare marine riser (without dimples)	116
9.6	Flow characteristics across a cylinder with dimples on the surface	121
9.7	Flow characteristics by varying sequence of dimples on the surface	122
9.8	Flow characteristics by varying size of dimples on the surface.....	123

LIST OF FIGURES

Figure	Title	Page
2.1	Vortex shedding behind a circular cylinder	8
2.2	Formation of vortex street in the wake of a structure	8
2.3	Three dimensional flow domain and grid design	12
2.4	Flow domain for a square cylinder	12
2.5	Passive devices	14
2.6	Triple start helical strake fitted on a circular cylinder.....	16
2.7	Instantaneous flow structures from 0.15D, 0.25D, 0.5D and Velocity profile along the gap	18
2.8	Active method illustrating inline and transverse vibrations	19
2.9	Tall chimney fitted with helical strakes	21
2.10	Steel chimney depicting crosswind vibrations	22
4.1	(a) Flow domain for a square cylinder	34
	(b) 2D Computational Grid	34
4.2	Mean axial velocity distribution along centre line of the wake	35
4.3	(a) Vorticity magnitude contour at $Re=40$	38
	(b) Stream function contour at $Re=40$	38
4.4	(a) Vorticity magnitude contour at $Re=150$	39
	(b) Stream function contour at $Re=150$	39
4.5	Velocity along the wake centre line for $Re=40$ and $Re=150$	40
4.6	Wall shear stress along the surface for $Re = 40$ and $Re = 150$	40
4.7	Pressure variation along the surface for $Re=40$ and $Re=150$	41
4.8	(a) Vorticity magnitude contour at $Re=5$	43

	(b) Stream function contour at $Re=5$	43
4.9	(a) Vorticity magnitude contour at $Re=40$	44
	(b) Stream function contour at $Re=40$	44
4.10	Velocity along the wake centre line of domain.....	45
5.1	(a) Domain of fluid flow with boundary conditions	49
	(b) 3D Computational Grid	49
5.2	Variation of coefficient of pressure with domain length	52
5.3	Velocity contours at different amplitudes of oscillations	53
5.4	Variation of coefficient of drag C_D with splitter plate	55
6.1	Computational domain of fluid flow with boundary conditions.....	59
6.2	Contours of vorticity magnitude	60
6.3	(a) Pressure coefficient along cylinder surface	61
	(b) Wall shear stress along cylinder surface.....	61
6.4	Geometry of cylinders with fins.....	61
6.5	Contours of vorticity at different orientations.....	62
6.6	Percentage reduction in Strouhal number with fin count.....	63
6.7	Vorticity contours for different fin orientations.....	64
6.8	(a) Coefficient of lift at different orientations	64
	(b) Strouhal number variation with fin orientations	64
7.1	Flow domain for a circular cylinder	67
7.2	Coefficient of lift and coefficient of drag	69
7.3	Mean pressure distribution along the central plane.....	69
7.4	Contours of vorticity magnitude in the central plane.....	70
7.5	(a) Distributions of Static pressure along central plane	70

	(b) Velocity magnitude along central plane	70
7.6	(a) Strouhal frequency (b) Strouhal number	71
7.7	Circular cylinder fitted with triple start helical strakes	72
7.8	Velocity vector at different z planes.....	72
7.9	Contours of vorticity magnitude at(a) pitch = $5d$ (b) pitch = $10d$ and (c) pitch = $15d$	74
7.10	Strouhal number variation with diffrenet pitches.....	74
8.1	Domain of fluid flow with boundary conditions.....	80
8.2	(a) Domain of fluid flow with mesh (b) C_D Vs cell count.....	81
8.3	Contours of vorticity magnitude.	82
8.4	(a) C_D with flow time (b) C_L with flow time.....	82
8.5	Contours of vorticity magnitude at different amplitudes of oscillations for the cylinder	84
8.6	(a) C_D with flow time for a stationary cylinder.....	85
	(b) C_D with flow time at different amplitudes of oscillations.....	85
8.7	(a) C_L with flow time (Non- oscillating case)	86
	(b) C_L with flow time (with oscillation amplitudes)	86
8.8	(a) Strouhal number with different amplitude of oscillations	87
	(b) Strouhal frequency with amplitudes of oscillations	87
8.9	Domain of fluid flow with boundary conditions	87
8.10	(a) Coefficient of lift with flow time	89
	(b) Coefficient of drag with flow time	89
8.11	Contours of vorticity magnitude in 2D and 3D	90
8.12	(a) Coefficient of lift with time	91

	(b) Coefficient of drag with time.....	91
8.13	Contours of vorticity magnitude in 2D and 3D	91
8.14	Vorticity magnitude contours at different amplitudes of oscillation	93
8.15	Strouhal number with different amplitudes of oscillation	95
9.1	Chimney	98
9.2	Computational domain for a chimney without strakes	99
9.3	(a) Coefficient of lift with flow time	101
	(b) Coefficient of drag with flow time	101
9.4	Pressure distribution in the central plane	102
9.5	Velocity distribution in the central plane.....	102
9.6	(a) Contours of vorticity magnitude (b) 3D view.....	103
9.7	(a) Strouhal frequency (b) Strouhal number	103
9.8	Computational domain for a chimney with strakes	105
9.9	Coefficient of lift and drag with flow time	107
9.10	Pressure distribution in the central plane	107
9.11	Velocity distribution in the central plane.....	108
9.12	(a) Contours of vorticity magnitude in central plane (b) 3D view	108
9.13	(a) Strouhal number (b) Strouhal frequency	109
9.14	Marine riser.....	110
9.15	Computational domain for a bare marine riser	111
9.16	(a) Coefficient of lift with flow time	113
	(b) Coefficient of drag with flow time.....	113
9.17	Pressure distribution in the central plane.....	114
9.18	Velocity distribution in the central plane.....	114
9.19	(a) Contours of vorticity magnitude in the central plane(b)3D view.....	115

9.20	(a) Strouhal frequency (b) Strouhal number	115
9.21	Computational domain for marine riser with dimples on the surface.....	117
9.22	Pressure distribution in the central plane	118
9.23	Velocity distribution in the central plane	119
9.24	(a) Contours of vorticity magnitude in the central plane(b) 3D view	119
9.25	(a) Strouhal number (b) Strouhal frequency	120

LIST OF ABBREVIATIONS

VIV	Vortex Induced Vibration
CFD	Computational Fluid Dynamics
LES	Large Eddy Simulation
DNS	Direct Numerical Simulation
RANS	Reynolds Averaged Navier-Stokes
SST	Shear Stress Transport
St	Strouhal number
Re	Reynolds number

NOMENCLATURE

A	Area	m^2
D	Cross sectional diameter	m
M	Mach number	-
P	Pressure	N/m^2
p_a	Ambient pressure	N/m^2
a	Amplitude	m
ρ	Density	kg/m^3
μ	Dynamic viscosity	$N\ s/m^2$
ν	Kinematic viscosity	m^2/s
k	Turbulent kinetic energy	m^2/s^2
μ_t	Turbulent viscosity	m^2/s
ε	Viscous dissipation rate	m^2/s^3
ω	Specific dissipation rate	$1/s$
γ	Ratio of specific heats	-

CHAPTER - 1

INTRODUCTION

1.1 VORTEX INDUCED VIBRATIONS

Tall industrial chimneys and deep marine structures cause a severe challenge to designers as they are always subjected to Vortex Induced Vibrations (VIV) when large currents blow across them regularly. The premature collapse of these structures incurs enormous losses. The design challenges of tall structures make the suppression of vortex induced instabilities an area of intense research. The collapse of the Tahoma hanging bridge brought this complicated issue to the attention of the scientific world. The reduction of VIVs has become a topic of research and analysis in fluid dynamics owing to its vast application in industrial safety area in the last few decades.

The flow characteristics around a structure can be obtained analytically, experimentally or numerically. The solutions by analytical method are difficult where as the experimental methods is costly and time consuming. Numerical simulations of low speed flow parameters using standard turbulence models provide better insight into the flow field with limited computational resources. Numerical simulations of subsonic fluid flow using RANS equations and turbulence models such as SST $k-\omega$ and $k-\varepsilon$ models were used by researchers for the study of fluid flow oscillations in the wake of a structure. These methods are relatively inexpensive and can provide better knowledge of the flow field. It also provides accurate information on flow field characteristics based on the changes in flow parameters. The reduction of vortex induced vibrations by different methods has now become a topic of intense research in academic and practical fields. The understanding on fluid flow instabilities was

obtained from numerical predictions and experimental measurements along the flow field. The fundamental aspects of aerodynamics related to lift and drag seem to be highly relevant in the study on the suppression of flow instabilities behind structures. Several numerical studies have been carried out to study the effect of different methods to suppress VIV by modifying the structural configurations and flow conditions.

Current research on vortex instabilities highlights three major areas such as, the study of the impact of fluid currents on the flow field during flow past bluff bodies, the phenomenon of the flow instabilities and the suppression of vortex induced vibrations. Certain passive devices such as straight fins, splitter plates and helical strakes are seen to modify the flow and hence may be used with different orientations for effectively reducing VIVs. Computational fluid dynamics demand extreme numerical accuracy and high computational resources for the accurate prediction of flow characteristics in the wake of a structure. Even though LES meets the accuracy requirement for the prediction of flow instabilities, it requires higher order numerical schemes and high resolution grids which do not lend themselves well to complicated grid topologies. To evaluate the performance of new concepts a more reliable method for modelling the source mechanism is essential. The new designs incorporating passive and active methods intended to reduce the VIV in the wake can more easily be evaluated using computationally less expensive RANS simulation which can capture the trends exhibited by simulations reasonably well while altering the structural configuration, or flow velocities. Sohanker (2006) has carried out experimental measurements of the flow field behind the wake of square and circular structures for subsonic Mach numbers and reported in the literature.

Urge for reduction in Aeolian vibration in the wake of bare structures led to the idea of various passive devices that could be attached in the wake. The structure is placed against the incoming fluid flow so that the vortex instabilities can be accurately distinguished and analysed. Researchers have experimentally proved that bare structures produce more significant vortex induced instabilities around the structure. It was observed that the passive devices explicitly reduce the VIV in the wake. However, the use of helical strake as well as splitter plate has to be evaluated with different orientations for reduction in VIV for fluid flow past structures. It may be observed that passive devices offered better VIV reduction for fluid flow with different velocities. Numerical simulation of fluid instabilities in the wake of a structure using RANS calculations with a standard turbulence model can provide reasonably accurate flow field data. This fact enables the designers to easily evaluate the VIV reduction capabilities of various structural configurations and passive devices. The influence of various fluid parameters on the flow field and the corresponding VIV reduction may also be analysed with limited computational resources. Active methods provide energy to the structure or to the attachments and comparison of the turbulent characteristics of the unstable wake may be made with bare stationary structures using numerical simulations.

The complex interactions in the wake of a cylinder resulted in increased instabilities in the wake that can be compared more accurately by using compound method. An oscillating splitter plate in the wake strongly influences the flow fields behind the square structure. The major drawback of using passive devices and active methods simultaneously is that the mechanism may result in an increase of drag forces acting on the structure along with the reduction in lift forces. This aerodynamic interference was reported by Hwang (2003) in his experiments with helical grooves

on structures. The transition from a circular to a square cross-section of structures has a significant role in the character of the vortical structures generated in the wake. The present work basically focuses on aerodynamic and hydrodynamic characteristics of fluid flow past a structure such as a tall chimney or a marine riser with and without passive or active vortex suppression devices.

1.2 THESIS OUTLINE

Chapter 1 discusses the relevance of the present work in the present scenario. The current status of research happening in a flow field with the aid of computational fluid dynamics is briefly described.

A detailed review of the available literature on experimental and numerical investigations of incompressible subsonic fluid flow past bluff bodies is presented in Chapter 2. The review also focuses on the passive and active methods employed for the reduction in vortex induced vibrations due to flow separation in and around structures. The scope of the work is derived from motivation on a wider perspective.

The different parameters that characterise the flow instabilities in the wake of a cylinder, governing equations, turbulence models and solution procedures are discussed in Chapter 3.

The gridding strategy and computational scheme with solution procedure for square and circular cylinders are explained in Chapter 4.

The flow characteristics predicted from the numerical simulation of a circular structure with and without passive devices such as splitter plate, straight fins, and helical strakes are presented in Chapters 5, 6 and 7 respectively.

Numerical predictions on the effect of VIV suppression by employing active as well as compound methods on a square cylinder are reported and comparison of the flow characteristics with passive devices is deliberated in Chapter 8.

The numerical simulations of tall industrial chimneys with helical strakes are described in Chapter 9. The study is also extended to deep marine risers with and without dimples enabled on surfaces. The effectiveness of these passive devices in the suppression of Aeolian vibrations is discussed in detail.

Chapter 10 presents the overall conclusion and the scope for future work.

CHAPTER - 2

LITERATURE SURVEY

Aeolian vibrations occur in tall industrial structures and marine risers in offshore ventures when large currents blow across them. Low pressure zone created in the rear of the structure is mainly instrumental in the detachment of fluid layers from the surface of the structure in the form of vortices. These structures are subjected to both drag and lift forces due to vortex shedding phenomenon. The structure experiences vibration in a crosswise direction and these vibrations are termed as vortex induced vibrations (VIV). When the frequency of VIV comes in resonance with the natural frequency of the structure, it vibrates violently leading to catastrophic failure. These undesirable vibrations are usually annihilated by making different modifications to the structure. The use of active methods as applied to the structure or passive devices placed in the wake is effective in diminishing vortex instabilities to a significant extent. A review of the available literature on the experimental and numerical investigations of vortex and shear instabilities is presented in this chapter. The discussions on numerical studies are based on different parameters such as inflow, outflow, boundary conditions and the interpretation of flow parameters predicted from the simulation.

Shear layer instability due to flow separation was studied comprehensively by Roshko (1954). Measurements of flow characteristics obtained from experiments on fluid flow oscillations for Reynolds number less than 40 were analyzed. It was observed that the flow remains laminar, two-dimensional and steady, but can become unstable under the influence of external excitation. Behr *et al.* (1996) studied the influence of the location of the lateral boundaries on the unsteady flow past a circular

cylinder at $Re = 100$ and suggested that the lateral boundaries should be away from the cylinder by a distance of at least eight cylinder diameters. Faruquee *et al.* (2007) conducted domain independent study for flow past a circular cylinder using a circular domain. The influence of the far-field boundary on the drag coefficient was investigated. Sumner *et al.* (2004) reported that the flow field over the circular cylinder is symmetric at low values of Reynolds number. As the Reynolds number increases, flow begins to separate behind the cylinder, causing vortex shedding which is an unsteady phenomenon.

2.1 SHEAR LAYER INSTABILITY AND VORTEX DYNAMICS

Structures in contact with fluid flow, whether natural or human-made, are inevitably subject to flow-induced forces and flow-induced vibration. It applies from plant leaves to traffic signs and more substantial structures, such as bridge decks and heat exchanger tubes. Under certain conditions, the vibration may be self-excited, usually referred to as instability. These instabilities and, more specifically, the conditions under which they arise are of great importance to designers and operators of the systems concerned because of the significant potential to cause damage in the short term. Shear layer instability causes a vortex roll-up. Flow speed outside wake is much higher than inside and hence vorticity gathers at down crossing points in the upper layer and vice versa in the lower layer. Induced velocities due to these vortices amplify this perturbation.

When a fluid flows past a bluff body (such as a circular cylinder) in a direction that is perpendicular to the axis of the body, boundary layers develop around the body. At a low Reynolds number, the fluid flows past the body sustaining an attached flow. However, as the Reynolds number increases, the vortices tend to separate

(Figure 2.1) from the body surface and roll up at the downstream side of the fluid flow. Further increase in Reynolds number leads to alternate shedding of vortices due to the adverse pressure gradient which leads to a phenomenon known as vortex shedding.



Fig. 2.1 Vortex shedding behind a circular cylinder

Consequently, as vortices are shed (Figure 2.2) on the surface of the cylinder, the cylinder experiences forces which are periodic. These forces cause the cylinder to vibrate as long as vortices are shed continuously. Vortex induced vibration occurs anytime when a sufficiently bluff body is exposed to a fluid flow that produces vortex shedding near the natural frequency of the body. This information implies that vortex induced vibration occurs when vortex shedding frequency is close to the natural frequency of the body. Continuous periodic vibration of the structure could make it susceptible to fatigue failure and hence offshore structural members must be designed to prevent VIV.



Fig. 2.2 Formation of Vortex Street in the wake of a structure

2.1.1 Factors influencing VIV

The primary factors that influence vortex induced vibrations are (i) Reynolds number, (ii) Lift and drag coefficients, (iii) Correlation of force components (iv) Shedding frequencies and their interactions and (v) Added mass (or mass ratio) and damping.

2.1.2 Types of Vortex Induced Vibration

The following are the three types of vortex induced vibrations observed, based on the actuating forces:

1. In-line Vortex Induced Vibrations
2. Cross-flow Vortex Induced Vibrations
3. Hybrid Vortex Induced Vibrations

In-line vortex induced vibrations is caused by symmetric shedding of vortices on the surfaces of a bluff body. Cross-flow vortex induced vibrations occur when vortex shedding is asymmetric. As the name suggests, hybrid vortex induced vibrations are somewhat in between in-line and cross-flow vortex induced vibrations and usually a combination of both oscillations.

2.1.3 Prevention of Vortex Induced Vibrations

Different approaches that can be taken to prevent vortex induced vibrations include:

1. Design: This involves designing structural members with a natural frequency that is far away from the vortex shedding frequency.

2. Active methods: In active method of VIV suppression, energy is applied to impart an oscillation on either the bluff body or a passive device placed in the wake.
3. Vortex suppression devices: VIV can be prevented in structures by the use of vortex suppression devices such as strakes, shroud, axial slats, fairings, splitter, and ribboned cables. These devices operate by disrupting the near wake region and disturbing the correlation between the vortex shedding and vibration, thereby preventing vortex street formation. However, an increase in steady drag is observed on the stationary structure.

2.2 SUPPRESSION METHODS FOR VORTEX INDUCED VIBRATION

Fairings are designed to rotate, to align with the current effectively, minimising vortex shedding and drag loading. They operate most efficiently in structural members which are in a near vertical configuration. Even though fairings are expensive, they can reduce drag force to as low as one-third of its original value and suppress VIV almost entirely. The less expensive alternatives include strakes which are not as effective as fairings, but are adequate in many instances.

Strakes are external ribs placed on the cylindrical structure, most commonly in a helical shape. Helical strakes disrupt the flow pattern by creating shorter and weaker vortices. Even though the amplitude of vibration is reduced, the strakes augment 30-50% additional drag force, which can increase the potential for interference. Although strakes increase drag, they can reduce wave induced fatigue by damping the dynamic response caused by vessel motions. Strakes destroy the correlation of vortex shedding along a structural member by creating a large number of small vortices. Therefore,

regular vortex shedding pattern is disturbed and a street of smaller and weaker vortices begins to appear several diameters downstream of the body.

2.2.1 Physics of vortex induced vibrations

Vortex induced vibrations may occur when vortices are shed alternately from opposite sides of a structure in a range of wind velocity. This influence gives rise to a fluctuating load perpendicular to the wind direction. As the vortices are shed alternately first from one side, then the other, a harmonically varying lateral load with the same frequency as the frequency of the vortex shedding is formed. The expression

gives the frequency $St = \frac{fD}{U_\alpha}$

where, St is the Strouhal number, U_α is the mean velocity of the approaching wind, and D is the cross-wind dimension of the structure considered. Significant vibrations may occur if the dominating frequency of vortex shedding f is the same as the natural frequency f_n of the structure vibrating in the cross-wind direction with a particular mode shape.

2.3 FLUID FLOW DOMAIN AND GRIDDING STRATEGY

Sohanker *et al.* (2006) constructed a non-uniform mesh (Figure 2.3) near the wall of a square cylinder and a uniform mesh at five diameters away from the cylinder surface. The size of the smallest cell was located at the leading edge of the cylinder with a cell size of $h/d = 0.004$, where h/d is the size of cell non-dimensionalised by the diameter of the square cylinder.

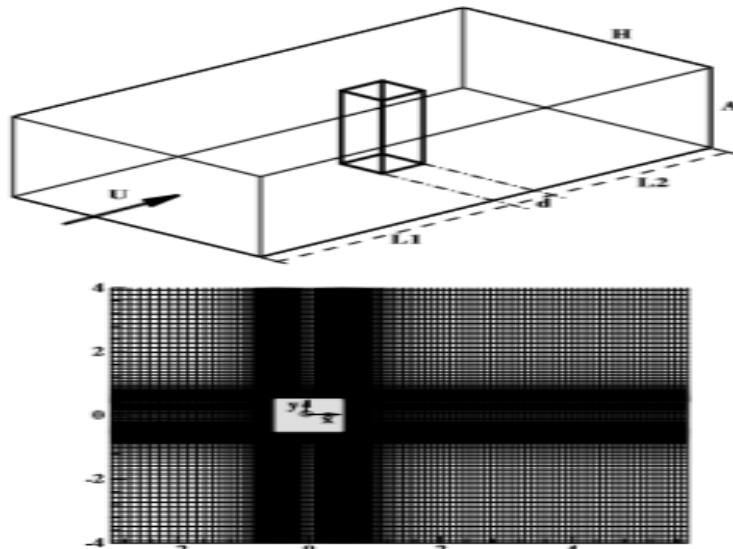


Fig. 2.3 Three dimensional flow domain and grid design (Sohanker, 2006)

Ali *et al.* (2009) investigated the grid convergence for three different grid resolutions (Figure 2.4) by conducting Direct Numerical Simulation (DNS) of fluid flow around a square cylinder and found that the solution converged when the smallest cell size along the square cylinder edge was $h/d = 0.0167$.

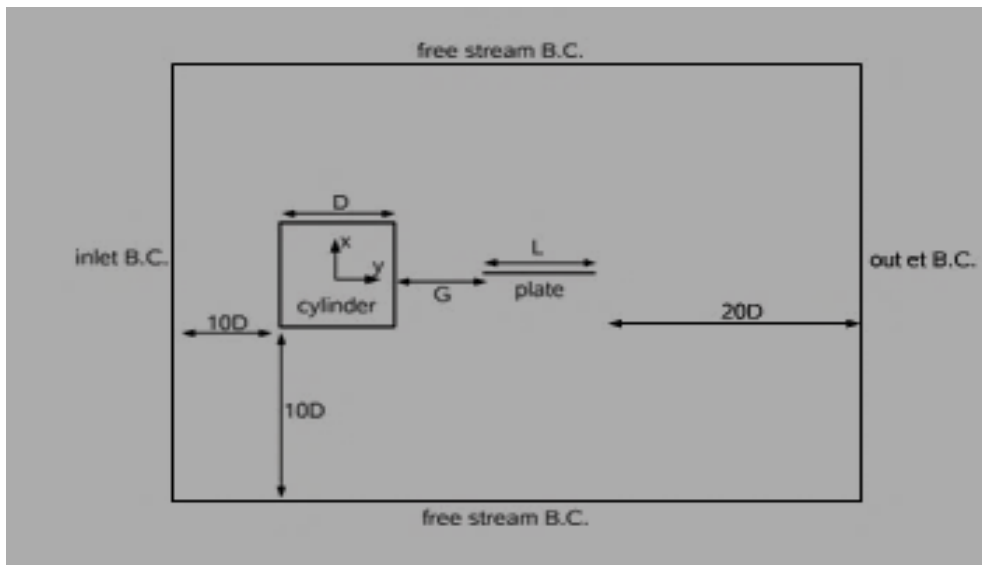


Fig. 2.4 Flow domain for a square cylinder (Ali *et al.*, 2012)

Inoue *et al.* (2006) built a non-uniform mesh with in computational domain and divided into three regions, each with a different grid ratio. The smallest cell was located along the edges of the square cylinder with a value of $h/d = 0.01$.

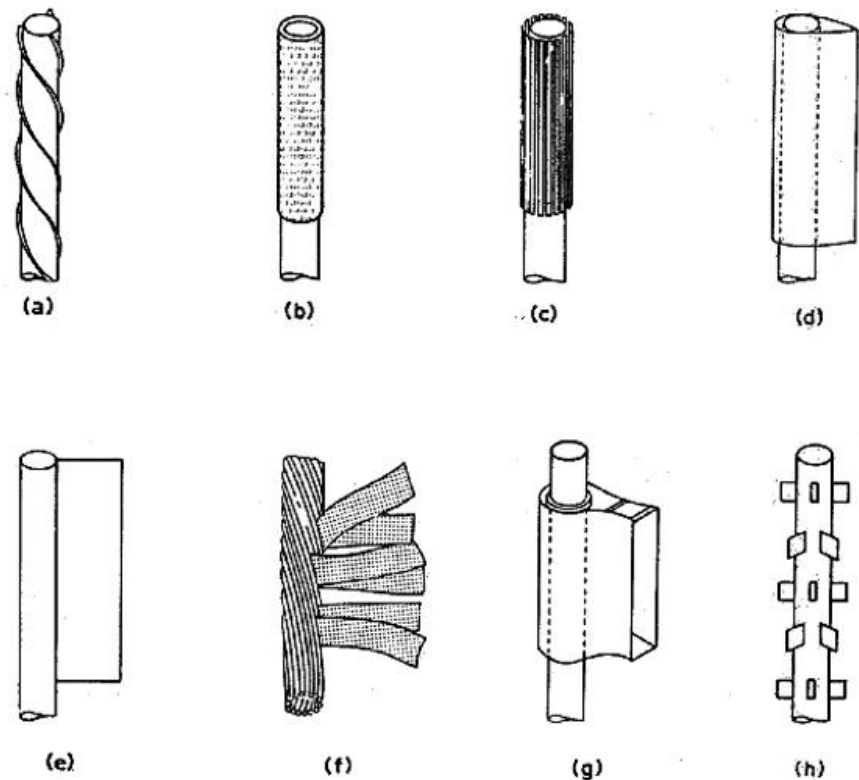
2.4 VORTEX SUPPRESSION METHODS

Many researchers have used different passive devices and active methods to control vortex shedding and vortex instabilities and found out that these methods are highly effective in decreasing vortex induced vibrations. Zdrakovich (1981) had categorised passive vortex shedding suppression methods as surface protrusions, shrouds and near wake stabilisers after evaluating their performance in identical fluid flow conditions. The passive devices used are straight fins, helical fins, splitter plates, helical grooves, and shrouds. Passive control does not need external energy during application. In active methods, energy is supplied to the structure to reduce the vortex shedding. Active control techniques such as EHD actuators and vibrators require external energy to affect the fluid flow. The EHD method is classified as a boundary layer control method, where an electric discharge creates electric force acting on fluid particles, resulting in a change in the fluid velocity field. This force leads to a delay in the separation of the flow in the trailing side of the obstacle. The effective combination of both passive and active methods is known as the compound method and its effect on flow field has to be evaluated. However, studies on the reduction of VIV using a combination of these two methods are scarce.

2.4.1 Passive control methods

One of the structural modifications that can reduce the formation of vortices and vortex induced vibrations is surface protrusions. A surface protrusion is any device that modifies the form of the cylinder's surface without being situated predominantly in the wake of the cylinder. Some of these devices are considered as omni-directional as their effect is all around the structure. The different types of surface protrusions that can effectively counter the vortex induced vibrations are

straight fins, helical strakes, splitter plates, ribbons, shrouds, spoiler plates, pivoted guiding vanes, ropes and bumps. Some of these passive devices with extended surfaces are shown in Figure 2.5.



(a) helical strake; (b) shroud; (c) axial slats; (d) streamlined fairing; (e) splitter; (f) ribbed cable; (g) pivoted guiding vane; (h) spoiler plates.

Fig. 2.5 Passive devices (Dalton, 2000)

2.4.1.1 Straight and helical fins

Zhou *et al.* (2011) experimentally investigated the decline of vortex induced vibration of a cylinder with the application of passive devices like helical strakes. A rigid circular cylinder of diameter $d = 80$ mm attached with three-strand helical strakes of dimensions of $10d$ in pitch and $0.12d$ in height was tested in a wind tunnel. This experiment found that the helical strakes can decrease VIV by about 98%. No lock-in region was observed for the cylinder with helical strakes. On the other hand,

the bare cylinder experienced a lock-in over the velocity range of 5–8.5 m/s. Doolan *et al.* (2012) in their experimental work investigated the interaction of turbulent wake with a cylinder. Huang and Sworn (2013) carried out experiments on two fixed circular cylinders fitted with helical strakes at various staggered and tandem arrangements. It was observed that the cylinder with strakes had a higher drag coefficient in comparison with a bare cylinder. Quen (2014) had used flexible risers to find effectiveness in reducing the VIV. The study revealed that the most effective configuration of strakes in terms of the dynamic responses was observed in the model with pitch $p = 10d$ and $h = 0.15d$. However, the model having pitch $p = 10d$ and height $h = 0.10d$ was seen to perform better in reducing the hydrodynamic forces. Even though many studies were conducted in the aerodynamic flow field with cylindrical cross sections, very few similar studies were observed on flow past circular cylindrical structures provided with helically projected fins (helical strakes) at moderate Reynolds numbers. Among the different passive vortex suppression methods, the use of helical strakes on the structure is found to be more effective in suppressing VIV. Korkischko and Meneghini (2010) had investigated with triple start helical strakes in a circulating water channel. The strakes were made of rigid rubber and set at three pitches $p = 5d, 10d$ and $15d$ and three heights $h = 0.1d, 0.2d$ and $0.25d$. The straked cylinder was made of three-start helical pattern having thin plate geometry as depicted in Figure 2.6.

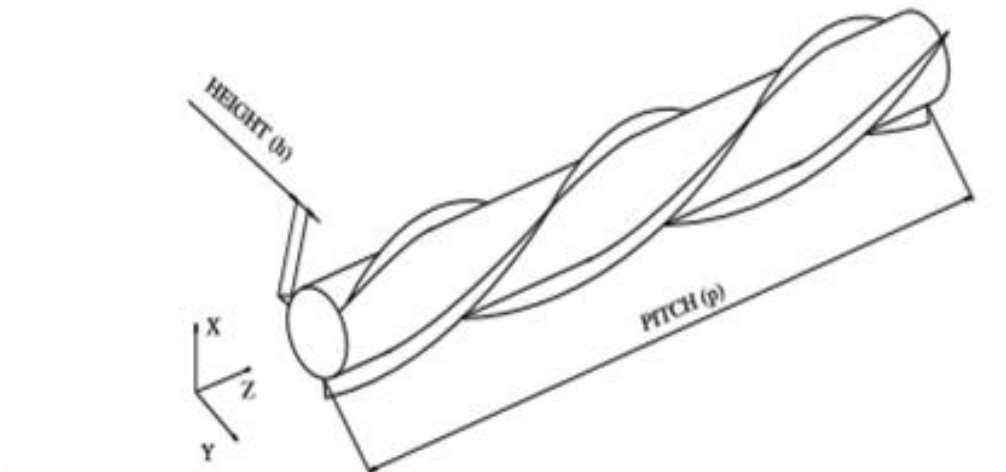


Fig. 2.6 Triple start helical strake fitted on a circular cylinder

Huang (2011) reported that the helical grooves were also instrumental in suppressing the vortex-induced cross-flow vibration amplitudes with a peak amplitude reduction of 64%. Drag reductions up to 25% was also achieved in the sub-critical range of Reynolds number tested for fixed cylinders.

2.4.1.2 Splitter plates

Numerical simulation of Kwon and Choi (1996) analysed the effect of a splitter plate behind a circular cylinder in the diminution of VIV and highlighted that the critical length of the splitter plate is proportional to the Reynolds number of fluid flow. Mittal (2003) numerically assessed the effect of plate length and its downstream location on the near wake of a circular cylinder at a Reynolds number of 100. Hwang *et al.* (2003) used a no-slip boundary condition and found that there were minimum plate length values and plate trailing edge positions for suppressing vortex shedding in the wake of structures. This work suggested that not only the spacing distance affects the near wake structure, but the length of the plate was also an essential factor. Assi *et al.* (2009) pointed out that control plates

which are free to rotate in the wake of the structure can be used to prevent the interaction of fluid masses and associated vortex and shear instabilities and asserted the reduction in VIV in line with drag reduction. Baek and Karniadakis (2009) established that a slit made on the structure parallel to the incoming flow was very constructive in suppressing vortex shedding and estimated the optimal size of the slit for different Reynolds numbers. Owen *et al.* (2001) had conducted an experimental investigation on the changes in the wake of a cylinder by the use of hemispherical bumps on the structure to study the magnitude of VIV diminution. The effectiveness of a tandem cylinder in the suppression of vortex induced instabilities reported by Strykowski and Sreenivasan (1990) pointed out that the presence of a small cylinder in the wake reduces the growth rate of instabilities in the wake significantly. The effect of thin wires attached to the surface of a cylinder in reducing the vortex shedding at various Reynolds numbers was investigated by Hover *et al.* (2001) and reported an earlier onset of frequency lock-in. The optimum position of the splitter plate placed in the rear of the cylinder in controlling vortex and shear instabilities (Figure 2.7) was estimated by Ali *et al.* (2012) while suppressing VIV.

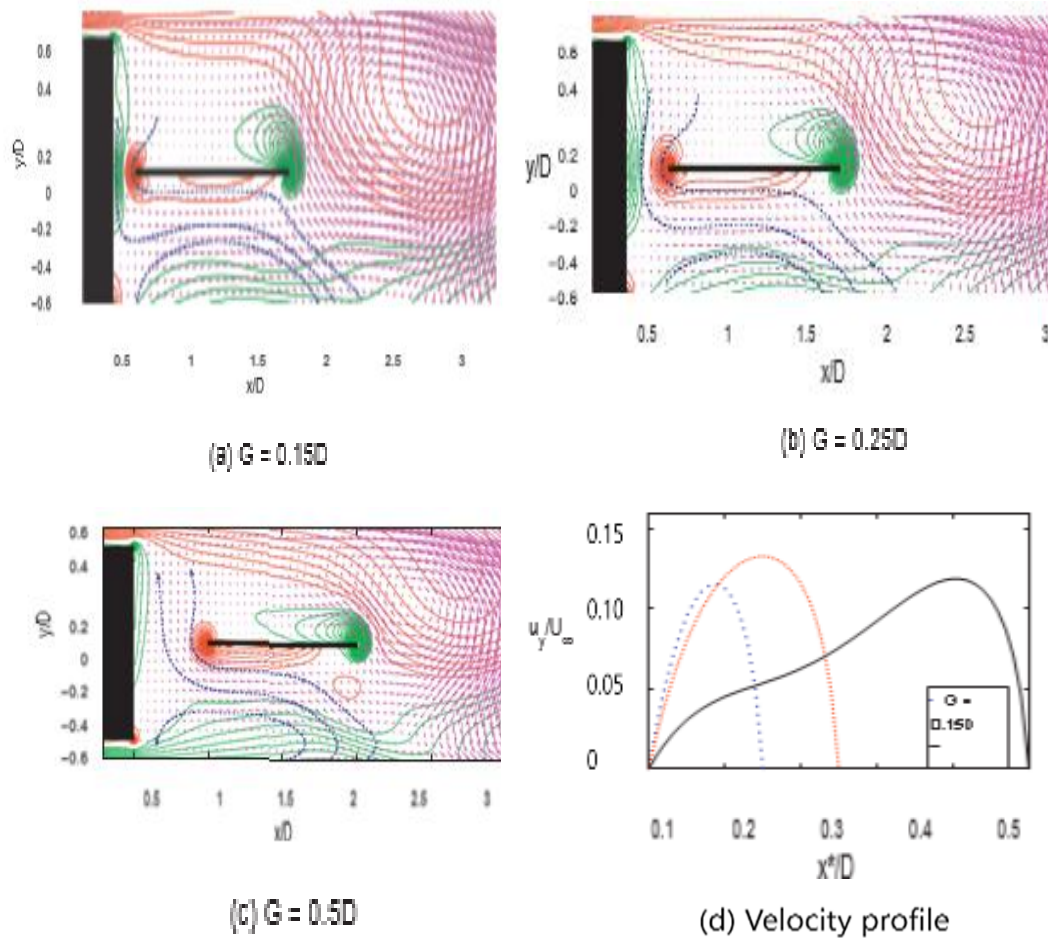


Fig. 2.7 Instantaneous flow structures from $0.15D$, $0.25D$, $0.5D$ and velocity profile along the gap (Ali *et al.*, 2012)

2.4.2 Active methods

Cheng *et al.* (2001) conducted the study of flow characteristics in the rear of an oscillating circular cylinder, using a hybrid vortex method at various velocities for a broad range of oscillations. Dong and Karniadakis (2005) made numerical investigations on fluid flows past circular cylinder which is undergoing forced harmonic oscillations at large flow velocities. Zheng and Zhang (2008) investigated an oscillating cylinder to investigate changes in the frequency of flow instabilities and studied the effect of various flow phenomena on lift and drag forces on the cylinder. Chern *et al.* (2010) numerically investigated the behaviour of vortex shedding

initiated by flow over side-by-side arranged square cylinders in a flow of oscillating nature.

Sen and Mittal (2011) have conducted experimental investigations to study the free vibration of a square cylinder at zero incidences. A stabilised space-time finite element method has been used to discretise the equations of fluid flow in two dimensions. The cylinder was mounted on elastic support and is allowed to undergo inline as well as transverse vibrations as shown in Figure 2.8.

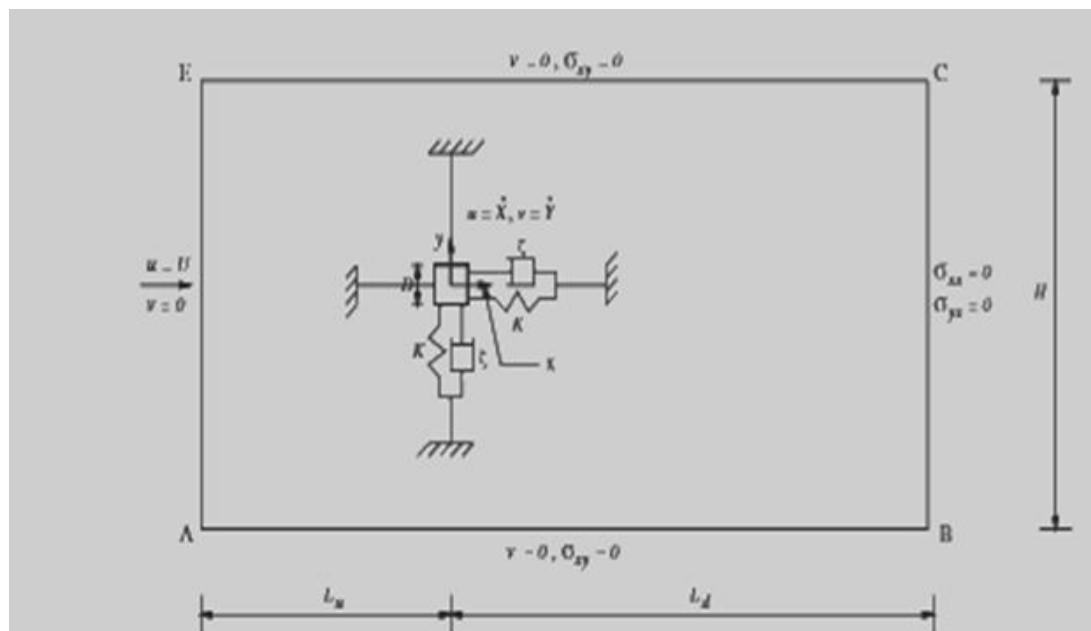


Fig. 2.8 Active method illustrating inline and transverse vibrations (Sen and Mittal, 2011)

2.4.3 Compound methods

In the previous section, a few investigations were conducted by using active methods for the suppression of vortex shedding. The compound method of providing oscillations to a passive device behind the main structure may significantly reduce vortex induced structural vibrations. Hence numerical works involving compound

methods by providing oscillating passive devices behind a structure have been carried out to investigate the effect of flow instabilities formed in the rear of a cylinder.

2.4.4 Structural configurations

Birka and Laneville (1997) conducted detailed experimental studies leading to the information on the formation of Aeolian vibration of cylindrical structures. Guilmineau and Queutey (2002) carried out a numerical investigation of VIV of oscillating circular cylinders, where cylinders were allowed to undergo oscillations, and variations in drag coefficients observed. Krishnamurthy *et al.* (2001) conducted experimental investigations to study the flow oscillations of a flow across a cylinder in a water channel at low velocities with the help of dye test and analysis of wake spectra. The experimental works conducted by Khalak and Williamson (1999) and Singh and Mittal (2005) demonstrated that a circular cylinder executing two degrees of freedom exhibits two modes of vibration at a low Reynolds number. Nakamura and Mizota (1975) and Bearman and Obasaju (1982) reported that the measurements of the fluctuating forces on a square cylinder at zero incidences constrained only to have transverse motion. Ozono (1999) conducted experiments over circular and rectangular cylinders with a horizontal short, thin splitter plate below the wake centreline and showed that vortex could get suppressed even when the splitter plate is asymmetrically behind the cylinder. Rathakrishnan (1999) comprehensively studied the vortex shedding suppression using the splitter plates attached to the end of the cylinder. In the recent past, a large number of studies had been conducted to enhance the understanding of different transition processes of flow past circular structures, but there are very few studies related to flow past square cylinders.

2.4.5 Chimney vibrations

The spirals are used to prevent the formation of Von Karman vortex streets downwind of the chimney by diverting the wind upwards on one side of the chimney and downwards on the other, creating a three-dimensional airflow pattern that disrupts the vortex sheet. The vortex shedding causes vortex-induced vibration in the chimney during strong winds and can damage the relatively thin walled and flexible structure of the chimney in the long run. As the vortices get shed on alternate sides of the chimney, each one imparts a counter-force on the surface of the chimney. Under suitable conditions, these oscillating forces could drive the chimney itself to vibrate from side to side. The helical projections on the chimney (Figure 2.9) prevent this by disrupting the vortices as they form, or at least causing them to form out of phase vortices at different altitudes.



Fig. 2.9 Tall chimney fitted with helical strakes (Blevins, 1990)

Huang and Sworn (2013) performed experimental investigations on two fixed circular cylinders fitted with helical strakes and asserted that the cylinder with strakes

had a higher drag coefficient in comparison with a bare cylinder. The studies on flow past circular cylindrical structures provided with helically projected fins known as helical strakes at moderate Reynolds numbers are scarce. Kawecki and Zuranski (2007) observed crosswind vibrations of steel chimneys at different wind velocities and assessed the relative amplitude of vibration at the top of the chimney (Figure 2.10). Cross wind vibrations of a new steel chimney 100 m high caused significant damage to the bolts. The measured damping properties of the chimney gave comparison of different approaches for the calculation of relative amplitude of vibration at a small Scruton number (Sc) as climatic conditions play a significant role. John *et al.* (2011) carried out an experimental study on Fibre Reinforced Plastic (FRP) chimney in a wind tunnel to study along-wind and the across-wind response of a chimney in terms of bending moment. The work claimed that there is a significant decrease in the magnitude of cross-wind vibrations in the presence of strakes.

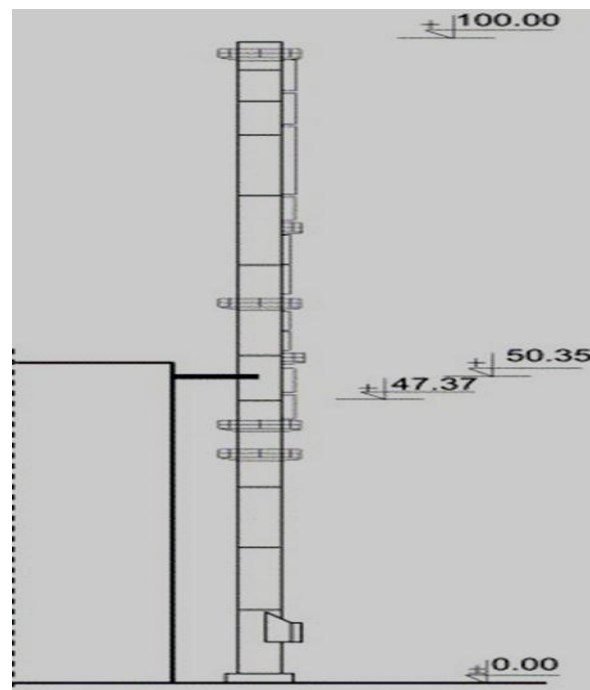


Fig. 2.10 Steel chimney depicting cross-wind vibrations (Kawecki and Zuranski, 2007)

2.5 NUMERICAL SIMULATIONS

The application of Direct Numerical Simulation (DNS) and Large Eddy Simulation (LES) provides the most accurate results in the numerical analysis of fluid flow characteristics. The DNS method is computationally expensive since it involves the simultaneous solution of a large number of equations. DNS method is rarely used by the researchers in the analysis of vortex and shear instabilities owing to its large grid size. Since most of the problems with practical interest have a high Reynolds number, an alternative method known as Large Eddy Simulation (LES) has been developed.

Large Eddy Simulation had been used extensively to compute the flow field behind a structure when large currents flow across them. LES has less computational cost compared to DNS and suitable for conducting simulations for problems of practical interest. In LES, the large scales are directly resolved, and the effect of the small scales or the subgrid scales on the large scales are modelled. As LES requires high order numerical schemes which do not lend themselves well to complicated grid topologies, LES is less preferred for the analysis of vortex induced instabilities.

RANS models have been developed based on the concept that a velocity scale and a length scale are sufficient to describe the effect of turbulence in a flow. Wilcox (1993) developed the $k-\omega$ two equations model as an alternative to cope with the deficiencies of the $k-\varepsilon$ model at the walls. The $k-\varepsilon$ model avoids using fine mesh near the wall by employing an empirical formula to predict the flow near the wall to save computational power. Although near wall treatment of $k-\varepsilon$ model saves vast amount of computational power, it is not sufficient to represent complex flow accurately. The $k-\varepsilon$ model performed well in the shear layer flow, while the $k-\omega$ model is excellent near

the wall. This information led to the development of the Shear Stress Transport (SST) model which aims to combine the advantages of these two methods. Menter (1994) introduced the SST model which combines the positive features of both models.

2.6 MOTIVATION

It is observed from the above literature review that the phenomenon of vortex shedding occurs naturally, and a vortex-street is generated when a stream flows across a bluff body. This phenomenon induces vortex induced vibrations and often encountered in tall chimneys, towers, buildings, oil rigs, offshore structures, bridges, pipelines etc. It may be noted that the pressure drag is dominant over viscous drag when flow passes over any non-streamlined body or a bluff body. Representative examples including cylinders with circular, square and rectangular cross sections are discussed briefly in the literature.

Control methods such as active and passive are seen to reduce vortex shedding behind bluff bodies successfully. Numerous investigations have so far been conducted for drag reduction and suppression of vortex shedding behind circular and square cylinders using either active (requiring external energy as input) or passive (without the aid of external energy) control methods. The passive methods primarily focus on varying the surface shapes by attaching devices such as shrouds, slits, strakes, splitter plates, bumps, small control cylinders etc. in the structure or along the flow field. The active control method of reducing VIV includes acoustic feedback system blowing/suction based flow control and EHD methods. Analytical, experimental and numerical techniques have been utilised to assess the instabilities from vortex dynamics in the flow field. Since the instabilities are to be captured precisely, the vortex shedding phenomenon must be visualized and the flow parameters predicted

accurately so that the whole information can throw light on vortex dynamics and shear layer instabilities formed in the wake of bluff bodies or structures. The estimation of suppression due to Aeolian vibration by the installation of passive and active methods on and off the structures is to be carried out meticulously. Moreover, the evaluation of the benefits attained by combining both passive and active methods into a compound method on VIV suppression has to be performed and evaluated.

Among the different numerical models employed by researchers to calculate the flow characteristics in the wake of a structure, LES appears to be the most accurate one. The small scales of turbulence can be accurately captured using LES, only if proper grid resolution is employed which makes it computationally very expensive. However, the different passive and active methods employed for reducing VIV cannot be quickly evaluated by LES. The above limitation has led to think about a quick evaluation technique employing limited computational resources, similar to RANS calculations. RANS based methods are found to be ideal in analysing the flow instabilities in the turbulent wake region as the trends exhibited by the experiments were captured reasonably well for incompressible flows. Also, focus must be given for developing optimum sized domains and grids for analysing cross flow past bluff bodies and to assess the concept of compound method employing active and passive devices. Moreover, the literature survey has given a motivation for quick assessment of vortex induced oscillations on tall industrial chimneys and deep marine risers so that its life as well as safety requirements can be evaluated easily with existing numerical models.

2.6.1 Gaps in literature

From the literature survey, it was observed that works related to the causes of generation of vortex induced vibrations and its reduction strategies adopted are scarce and further exploration is essential for getting better insight into the phenomenon.

(i) The combination of active and passive methods to suppress Aeolian vibrations must be explored.

(ii) The application of these control strategies in industrial structures such as tall chimneys and marine risers has tremendous technological and economic importance.

(iii) The drag crisis induced along with the suppression of vortex shedding and implementation of appropriate design modifications for its elimination on industrial structures subjected to flow induced aerodynamic or hydraulic loads must be evaluated.

2.7 SCOPE OF THE PRESENT WORK

The scope of the research work in a wider perspective is abridged as follows:

1. To perform computational studies of the fluid flow past bluff bodies and compare the predictions with the experimental measurements reported in the literature.
2. To conduct numerical simulations for circular and square structures fitted with passive devices and compare the turbulent characteristics of the flow with that of a bare structure.
3. To perform numerical simulations of helical strakes on the structure by varying structural dimensions such as pitch, height and diameter and to determine the optimum dimensions of strakes that can provide maximum reduction in VIV.

4. To carry out numerical simulations by employing active method on a square structure by providing different amplitudes of oscillations to the structure and analyse the turbulent fluctuating quantities such as Strouhal number, drag and lift forces.
5. To perform numerical simulations by combining passive and active methods into a novel concept of 'compound method' by means of an oscillating splitter plate along with a stationary bare cylinder and compare the flow characteristics and vortex suppression benefits obtained with that of a stationary splitter plate along with a stationary bare cylinder.
6. To extend the computational simulation on a tall industrial chimney with and without helical strakes fitted on to its surface for ensuring large extent of reduction in VIV for additional life and safety.
7. To assess a novel concept of dimples (depressions) on the structure for the suppression of Aeolian vibrations by analyzing the flow parameters for flow past a circular marine riser modified with and without dimples on the outer surface.

CHAPTER - 3

NUMERICAL MODELLING

Fluid flow analysis in the wake of a structure is governed by well-known equations that predict the changes of characteristics of the flow in time, from an initially known state. The flow of fluid is assumed to be incompressible as the Mach number is subsonic and less than 0.3.

3.1 GOVERNING EQUATIONS

The Navier-Stokes equations are derived by applying the Newton's law of conservation of momentum and forces to a fluid element in each of the spatial dimensions. In incompressible fluid flow analysis, the governing equations solved are continuity equation and momentum equations in the three directions. These four equations can ultimately determine the evolution of the four state variables.

The equation for conservation of mass is

Continuity Equation

$$\frac{\partial u}{\partial x} + \frac{\partial v}{\partial y} + \frac{\partial w}{\partial z} = 0 \quad (3.1)$$

The equation for conservation of momentum

X- Momentum Equation

$$\frac{\partial u}{\partial t} + u \frac{\partial u}{\partial x} + v \frac{\partial u}{\partial y} + w \frac{\partial u}{\partial z} = -\frac{1}{\rho} \frac{\partial p}{\partial x} + \nu \left(\frac{\partial^2 u}{\partial x^2} + \frac{\partial^2 u}{\partial y^2} + \frac{\partial^2 u}{\partial z^2} \right); \quad (3.2)$$

Y- Momentum Equation

$$\frac{\partial v}{\partial t} + u \frac{\partial v}{\partial x} + v \frac{\partial v}{\partial y} + w \frac{\partial v}{\partial z} = -\frac{1}{\rho} \frac{\partial p}{\partial y} + \nu \left(\frac{\partial^2 v}{\partial x^2} + \frac{\partial^2 v}{\partial y^2} + \frac{\partial^2 v}{\partial z^2} \right) \quad (3.3)$$

Z- Momentum Equation

$$\frac{\partial w}{\partial t} + u \frac{\partial w}{\partial x} + v \frac{\partial w}{\partial y} + w \frac{\partial w}{\partial z} = -\frac{1}{\rho} \frac{\partial p}{\partial z} + \nu \left(\left(\frac{\partial^2 w}{\partial x^2} \right) + \left(\frac{\partial^2 w}{\partial y^2} \right) + \left(\frac{\partial^2 w}{\partial z^2} \right) \right) \quad (3.4)$$

3.2 TURBULENCE MODELLING

Turbulence modelling is the construction and use of a numerical model to predict the features of turbulence. Turbulent fluid flow has features on many different length scales, which all interact with each other. A common approach is to average the governing equations of the flow to focus on large-scale and non-fluctuating features of the flow.

3.2.1 Closure Problem in Turbulence

The Navier–Stokes equations govern the velocity and pressure of the fluid flow. In a turbulent flow, each of these quantities may decompose into an average part and a fluctuating part. Averaging the equations gives the Reynolds Averaged Navier–Stokes (RANS) equations, which govern the mean flow. However, the nonlinearity of the Navier–Stokes equations causes the velocity fluctuations to appear in the RANS equations with the nonlinear term $-\overline{\rho u'_i u'_j}$ from the convective acceleration known as the Reynolds stress. The outcome on the mean flow is like that of a stress term, such as from pressure or viscosity. To obtain equations containing only the mean velocity and pressure, we need to close the RANS equations by modelling the Reynolds stress term as a function of the mean flow, removing any reference to the fluctuating part of the velocity. Suitable turbulence model are selected to overcome this closure problem in turbulence.

3.2.2 Boussinesq's Hypothesis

Boussinesq was the first researcher to attack the closure problem by introducing the concept of eddy viscosity. In 1877, Boussinesq proposed a relation (Equation 4.5) to connect the turbulence stresses to the mean flow for closing the system of equations. In the present work, the Boussinesq hypothesis is applied to model the Reynolds stress terms with a new proportionality constant μ_t , the turbulence eddy viscosity.

$$-\overline{\rho u'_i u'_j} = \mu_t \left(\frac{\partial U_i}{\partial x_j} + \frac{\partial U_j}{\partial x_i} \right) - \frac{2}{3} \rho k \delta_{ij} \quad (3.5)$$

where k is the turbulent kinetic energy, $k = \frac{1}{2} \overline{u'_i u'_i}$

$$\text{and } \delta_{ij} \text{ is Kronecker delta} = \begin{cases} 0, & \text{for } i \neq j \\ 1 & \text{for } i = j \end{cases}$$

3.2.3 SST k - ω turbulence Model

In computational fluid dynamics, the k - ω model is a standard two-equation turbulence model that used as a closure procedure for the Reynolds Averaged Navier–Stokes (RANS) equations. The model attempts to predict turbulence by two partial differential equations for two variables, k and ω , with the first variable being the turbulence kinetic energy (k) while the second (ω) is the specific rate of dissipation (conversion of the turbulence kinetic energy k into internal thermal energy). The SST k - ω turbulence model (Menter, 1993) is a two-equation eddy-viscosity model which has become very popular. The use of a k - ω formulation in the inner parts of the boundary layer makes the model directly usable down to the wall through the viscous sub-layer. Hence SST k - ω model can be used as a Reynolds number turbulence model without any extra damping functions. The SST formulation also switches to k - ε behaviour in the free-stream and thereby avoids the common k - ω concern of

sensitiveness to the inlet free-stream turbulence properties. The researchers who use the SST $k-\omega$ model merit it on its excellent behaviour in adverse pressure gradients and separating flows. The SST $k-\omega$ model does produce a bit too high turbulence levels in regions with sizeable normal strain, like stagnation regions and regions with strong acceleration. This tendency is much less pronounced than with a standard $k-\varepsilon$ model. The two variables interpreted as ‘ k ’ the turbulence kinetic energy and ‘ ω ’ the rate of dissipation of eddies.

Transport equation for k

$$\frac{\partial(\rho k)}{\partial t} + \text{div}(\rho k U) = \text{div} \left[\left(\mu + \frac{\mu_t}{\sigma_k} \right) \text{grad}(k) \right] + p_k - \beta^* \rho k \omega \quad (3.6)$$

Transport equation for ω

$$\frac{\partial(\rho \omega)}{\partial t} + \text{div}(\rho \omega U) = \text{div} \left[\left(\mu + \frac{\mu_t}{\sigma_{\omega,1}} \right) \text{grad}(\omega) \right] + \gamma \left(2\rho S_{ij} S_{ij} - \frac{2}{3} \rho \omega \frac{\partial u_i}{\partial x_j} S_{ij} \right) - \beta_2 \rho \omega^2 + 2 \frac{\rho}{\sigma_{\omega,2} \omega} \frac{\partial k}{\partial x_k} \frac{\partial \omega}{\partial x_k} \quad (3.7)$$

3.3 Fluid Flow Parameters

The flow simulations are carried out with the following assumptions in the fluid domain:

- (i) The flow of fluid across industrial structures is predominantly transient.
- (ii) The flow is assumed to be incompressible as the Mach number is less than 0.3.
- (iii) The variations in velocity along y and z directions are assumed to be negligible in all simulations.
- (iv) The conservation of mass, momentum and energy are valid in the flow domain.

Strouhal Number (St):

$$St = fD / U_{\infty} \quad (3.8)$$

where f is Strouhal frequency, D is characteristic length, and U_{∞} is velocity.

Coefficient of Drag (C_D) and Coefficient of Lift (C_L)

$$C_D = F_D / 0.5\rho U_{\infty}^2 D, \quad (3.9)$$

$$C_L = F_L / 0.5\rho U_{\infty}^2 D, \quad (3.10)$$

where F_D and F_L are drag and lift forces, D is characteristic length, U_{∞} is velocity and ρ is density.

Pressure Coefficient

$$C_p = (P - P_{atm}) / 0.5\rho U_{\infty}^2 \quad (3.11)$$

where P and P_{atm} are the pressures at the point where pressure coefficient is evaluated and free stream pressure measured respectively, D is characteristic length, U_{∞} is velocity and ρ is density.

3.4 SUMMARY

The governing equations and the approximations adopted for overcoming the closure problem in turbulence by enabling turbulence models are discussed in detail.

CHAPTER - 4

NUMERICAL INVESTIGATIONS ON VORTEX SHEDDING PAST BLUFF BODIES

4.1 INTRODUCTION

Vortices are created in the rear of a bluff body whenever a fluid flows past it. In this chapter, numerical investigations of a fluid flow past cylinders of different structural configurations (square and circular) at low Reynolds numbers were carried out and the effect of parameters such as Strouhal number, drag and lift forces investigated. Finite Volume Method was used for the discretisation of the computational domain and unsteady Reynolds Averaged Navier Stokes (*RANS*) equations with SST *k- ω* turbulence model for calculations. The numerical simulation was carried out using ANSYS CFD code which is basically a finite volume solver.

4.2 COMPUTATIONAL DOMAIN

4.2.1 Computational domain for a square cylinder

A rectangular domain having a length of $40d$ and width of $20d$, (where $d = 0.04$ m is the length of the side of the square cylinder) was used for the simulations. The cylinder centre is at a distance of $10d$ from the domain inlet and also $10d$ from the top and bottom edges of the domain. The fluid flows uniformly (with velocity U_∞) from left to right in the downstream direction of the domain. Boundary conditions are enforced at the outlet and also at the lateral boundaries of the computational domain. At domain inlet and outlet, velocity inlet and pressure outlet conditions respectively

have been employed. The symmetry boundary condition at the lateral boundaries of the domain and wall with no-slip condition has been used at the cylinder wall.

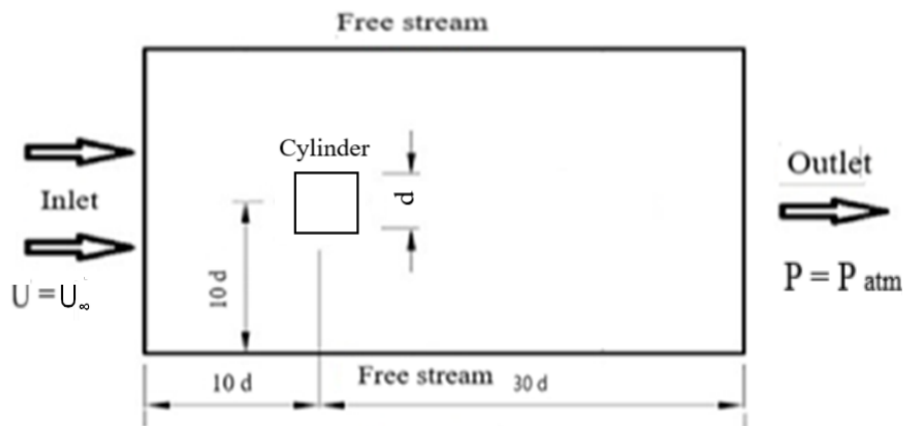


Fig. 4.1 (a) Flow domain for a square cylinder

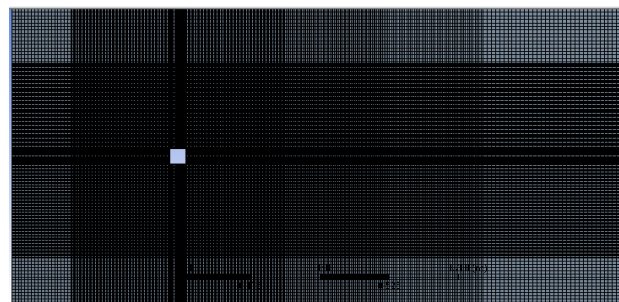


Fig. 4.1 (b) 2D computational Grid

The entire domain (Figure 4.1) has been discretised using the finite volume approach on a fixed Cartesian-staggered grid with non-uniform grid spacing. The grids in the region of the embedded boundaries were made sufficiently fine to capture the vortex shedding phenomenon with reasonable accuracy. The grid sizes used for 2D and 3D numerical simulations were 0.1 million and 1.0 million cells respectively. Mesh refinement near the no-slip surfaces is such that the area weighted wall y^+ is less

than 10. The volume weighted average of cell equi-angle skew is 0.3 and maximum value is 0.5. Furthermore, second order accurate discretization has been used for all the variables. Calculations were carried out till the residuals for all the equations were less than 10^{-6} . The temporal discretisation was made in conformity with the second-order implicit scheme and unsteady calculations were carried out. The pressure-velocity coupling was adopted in the calculation of the flow field.

4.2.2 Grid independence study

One of the reasons for variation in numerical predictions is the difference in the mesh or grid used for simulation. Six different 2D grids (Figure 4.2) were used ranging from very coarse to very fine. The dependency on the grid resolution on calculations was observed. It was observed that all the runs predict identical results in the upstream, whereas a faster recovery of mean axial velocity predicted with increase in grid resolution. The grid size with approximately 0.1 million cells captured the vortex shedding zone reasonably well with limited computational resources.

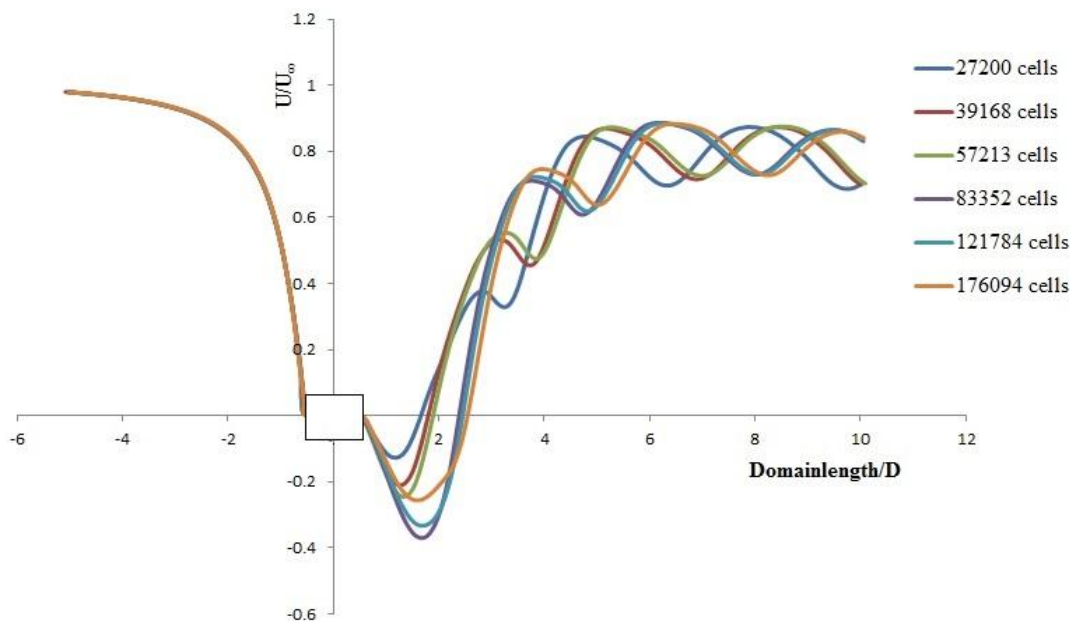


Fig. 4.2 Mean axial velocity distribution along centre line of the wake

Various parameters such as drag coefficient; $C_D = F_d / 0.5\rho U_\infty^2 d$, pressure coefficient; $C_p = (P - P_{atm}) / 0.5\rho U_\infty^2$ and Strouhal number; $St = f d / U_\infty$ have been computed to study the influence of grid on predictions. Since the predictions are not highly sensitive to the grid size, sufficient grid independency for the Reynolds number considered is observed.

The value of St predicted at $Re = 150$ was in good agreement with experimental studies of Okajima (1982) and Ozona (1999). The experimental values of St obtained by these authors were in the range of 0.148 to 0.155, and the present numerical study predicted a value of 0.15. Similarly, the value of C_D obtained experimentally was 1.40 and the present simulation predicted a value of 1.58.

4.2.3 Computational domain for a circular cylinder

The governing equations are applied in a rectangular domain for both square and circular cylinders. To minimize the effect of the far-field boundary conditions, the outer boundary of the computational domain was placed sufficiently far away from the cylinder.

A computational domain extending up to a length of $40d$ (d denotes cylinder diameter) in the downstream directions and $10d$ in the transverse direction from the centre of the cylinder was employed. The coefficient of drag (C_D) was one of the flow parameter predicted in all the simulations. Grid independence was achieved according to the procedure outlined by Cengel and Cimbala (2005). Several meshes with increasing refinement were tested to ensure that the solution was independent of the mesh. Significant variations in values of the drag coefficient (C_D) were not observed

for flow past a circular cylinder at $Re = 40$ for mesh refinement beyond 0.1 million cells.

4.2.4 Solution methodology

The application of appropriate boundary conditions at the cylinder surface and the outer boundary is crucial for accurate simulation. A uniform approach velocity was imposed at the domain inlet, while symmetry condition imposed on the axis and pressure outlet condition imposed on the domain outlet of the computational domain. The no-slip condition was appropriate along the cylinder wall and QUICK scheme of interpolation used for solving velocity and momentum. The SIMPLEC method was used for the pressure–velocity coupling with second-order interpolation scheme for pressure. Convergence criterion employed was 10^{-6} for all the conservation equations.

4.3 RESULTS AND DISCUSSION

In this section, flow characteristics at different Reynolds numbers are discussed for both square and circular cylinders.

4.3.1 Square cylinder.

The flow characteristics obtained for a Reynolds numbers of 40 (non-vortex shedding flow) and 150 (vortex shedding flow) are analysed for the flow past a square cylinder.

4.3.1.1 Non-vortex shedding flow ($Re = 40$)

The simulation was performed for the square cylinder with a Reynolds number of 40. The primary aim of this study is to analyse the flow structure around the cylinder and to obtain the flow variables, pressure variation along the surface of the cylinder and the drag coefficient. A contour plot can quickly reveal regions of high (or low) values of the property studied. Figure 4.3(a) shows the vorticity magnitude contours for Reynolds number 40 which indicate that the formation of vortex street is absent in the wake region. At Reynolds number 40, recirculation eddies alone are formed immediately downstream of the cylinder as indicated by streamlines shown in Figure 4.3(b).



Fig. 4.3(a) Vorticity magnitude contour at $Re=40$

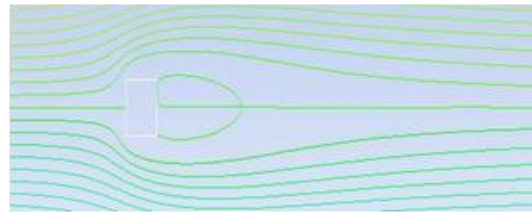


Fig. 4.3(b) Stream function contour at $Re=40$

4.3.1.2 Vortex shedding flow ($Re = 150$)

When Reynolds number is increased beyond 40, the wake behind the cylinder becomes unstable. Wake develops a slow oscillation in which the velocity is periodic in time and distance, with amplitude of oscillations increasing downstream. Periodic wake rolls up into two staggered rows of vortices with opposite sense of rotation. This staggered row of vortices behind the square cylinder was termed as Von-Karman vortex street. The vorticity magnitude and stream function contours for $Re = 150$ are shown in Figures 4.4(a) and (b).

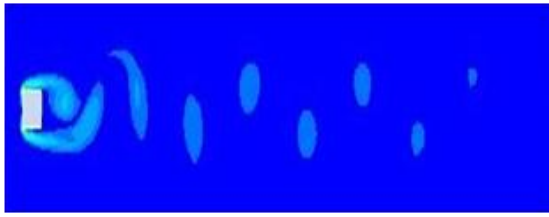


Fig. 4.4(a) Vorticity magnitude contour at $Re=150$

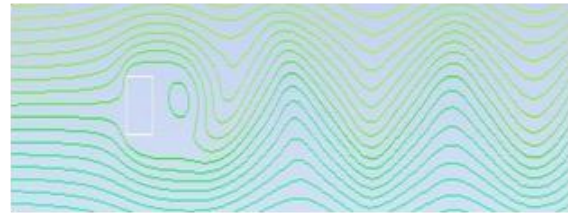


Fig. 4.4(b) Stream function contour at $Re=150$

Eddies formed in the wake periodically break off alternately from the two sides of the cylinder, as shown in Figure 4.4(a). While an eddy on one side shed, that on the other side is formed, resulting in an unsteady flow near the cylinder. The vortices of opposite circulations are shed off alternately from either side of the cylinder, resulting in an oscillating lift. This effect is obtained by plotting the variation of coefficient of lift with flow simulation time. Figure 4.4(b) shows the streamline pattern for $Re=150$, which indicates a rotating lump of fluid shed from the top portion of the cylinder. It is evident from Figure 4.4(b) that the velocity in the wake region of the cylinder at Reynolds number, $Re = 150$ is lower than that for $Re = 40$. It also observed that vortices are shed over a much larger length of the wake.

The U/U_∞ plotted in Figure 4.5 shows that the fluid comes to a complete rest at the mid-point of the incident face of the square cylinder; known as the stagnation point. The flow accelerates around the upstream corner, so that boundary layer cannot negotiate the sharp corner causing separation and reverse flow occurs in the immediate downstream of the cylinder. While moving further downstream of the wake region, flow slowly regains its velocity.

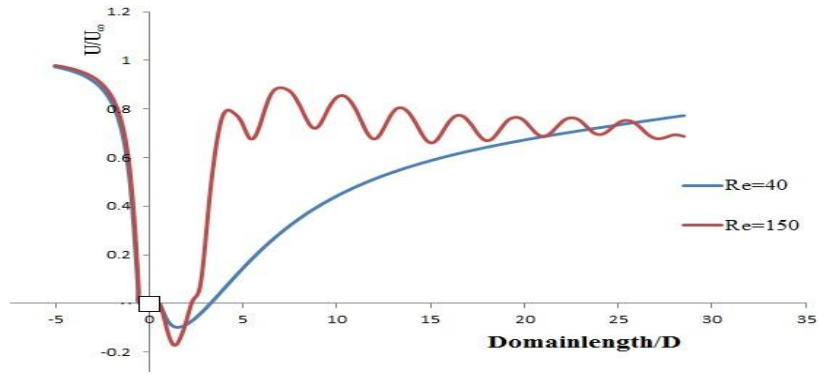


Fig. 4.5 Velocity along the wake centre line for $Re = 40$ and $Re = 150$

4.3.1.3 Flow characteristics at $Re = 40$ and 150 for a square cylinder

Apart from the velocity profile, the pressure distribution is an important parameter in the study of flow around a cylinder. The motion of vortices, in the vicinity of the body, causes changes in pressure.

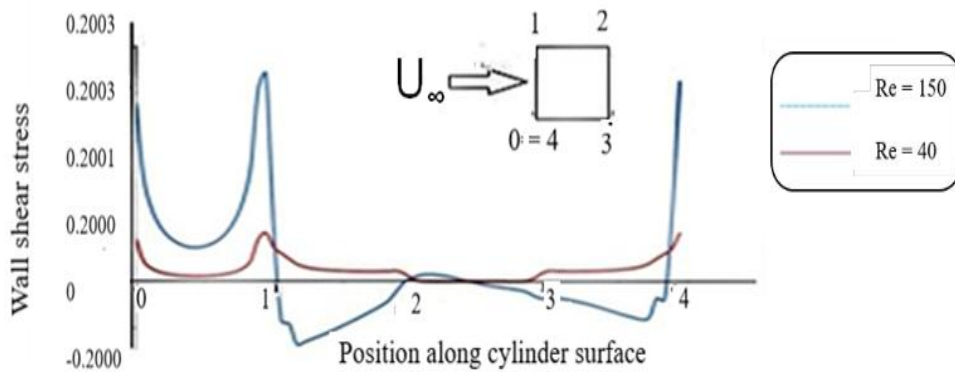


Fig. 4.6 Wall shear stress along the surface for $Re=40$ and $Re=150$

At stagnation point, located at the midpoint of face 0-1, as shown in Figure 4.6, the flow comes to rest and pressure reaches maximum value. Near the top surface of the cylinder, flow momentum is quite low due to viscous effects and is thus sensitive to changes in pressure gradient. The flow has to move against pressure force

in addition to the viscous force. This phenomenon leads to reduced velocity and wall shear stress. Flow separation occurs when shear stress cannot overcome adverse pressure gradient, and hence separation occurs just after top right corner of the square cylinder, where wall shear stress is zero as indicated in Figure 4.6.

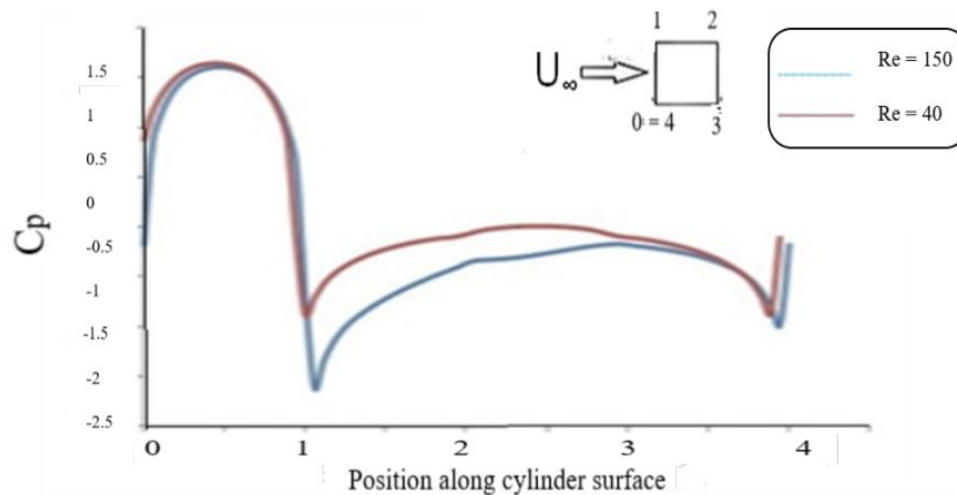


Fig. 4.7 Pressure variation along the surface for $Re=40$ and $Re=150$

The pressure variation near the top left corner and the top surface of the cylinder for $Re=150$ are much larger creating a larger adverse pressure gradient (than that of $Re=40$) opposing the flow as shown in Figure 4.7. Hence the flow around the square cylinder at $Re=150$ separates off much earlier (from the top left corner of the cylinder) as the wall shear stress approaches zero along cylinder surface (after point 1). The values of C_D , C_L , and St obtained from simulation are compared with experimental works of other researchers as shown in Table 4.1. The flow separates in a square cylindrical geometry much earlier when compared to similar circular cylindrical geometry.

Table 4.1: Comparison of C_D , C_L and St obtained for square cylinders

Experimental study	St	C_D	C_L
Okajima (1982)	0.148-0.155	1.40	0.24
Sohanker <i>et al.</i> (1998)	0.165	1.44	0.250
Doolan (2009)	0.156	1.44	0.296
Inoue <i>et al.</i> (2006)	0.151	1.40	0.40
Ali <i>et al.</i> (2009)	0.160	1.47	0.285
Present numerical study	0.150	1.58	0.196

A low value of C_L predicted in the present simulation is primarily due to slight variation in certain parameters such as size, shape and Reynolds number, when compared with other researchers. The size expressed as diameter and shape as cross sectional area of the structure considered in their works are slightly different from the present investigations. Moreover, the velocity at flow inlet is also different as the studies are based on different values of Re . It may be noted that the predicted value of C_L in the present study is 0.196, while the experimental measurements reported by other researchers are ranging from 0.24 to 0.4.

4.3.2 Circular cylinder

The flow characteristics obtained from simulations at Reynolds numbers of 5 and 40 for a circular cylinder is discussed in this section.

4.3.2.1 Vorticity magnitude at $Re = 5$ and 40 for a circular cylinder

Two dimensional steady and incompressible flow over a circular cylinder simulated at Reynolds number, $Re = 40$ has a laminar and steady flow field behaviour. As flow approaches the leading point of a circular cylinder, the fluid is brought to rest, causing a pressure rise and a boundary layer develops along the surface. The leading point is called the forward stagnation point. For very low Reynolds number ($Re = 5$), the flow splits into two symmetrically equal parts and passes around the cylinder to the rear stagnation point.

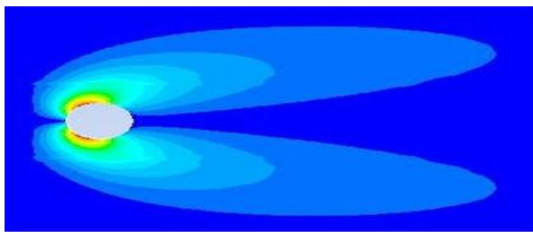


Fig. 4.8(a) Vorticity magnitude contour at $Re = 5$

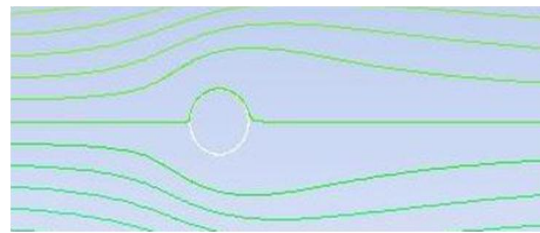


Fig. 4.8(b) Stream function contour at $Re = 5$

As Reynolds number increases, small sized eddies develop near the rear stagnation point of the cylinder, where the velocity is extremely small with an unfavourable pressure gradient. The recirculation zone remains steady and symmetrical about the stream wise centerline of the flow. The contours of vorticity magnitude and stream function at $Re = 5$ and $Re = 40$ respectively are shown in Figures 4.8 and 4.9.

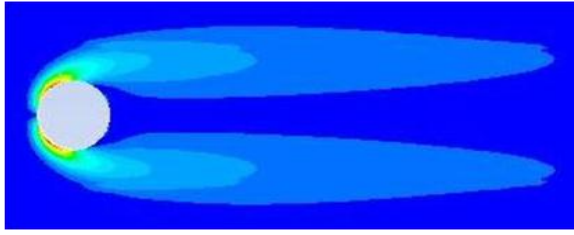


Fig. 4.9(a) Vorticity magnitude contour
at $Re = 40$

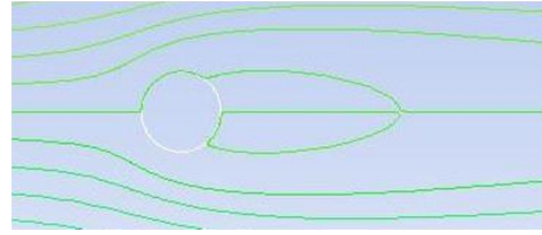


Fig. 4.9(b) Stream function
contour at $Re = 40$

4.3.2.2 Flow characteristics at $Re = 5$ and 40 for a circular cylinder

The flow separation point and nature of eddies formed are entirely different when the flow streamlines and vorticity contours for flow past a circular cylinder at $Re = 5$ and $Re = 40$ were analysed. At $Re = 40$, only recirculation eddies are formed immediately downstream of the cylinder, near the rear stagnation point as indicated by streamlines. Here, the flow separation gets originated from the middle of the lateral side, whereas, for $Re = 5$, the flow separation gets delayed and occurs at the rear side of the circular cylinder.

Lengthwise variation along the wake centerline (Figure 4.10) showed the corresponding variation of x -component of velocity along wake centerline at $Re=5$ and 40 . The coefficient of drag from the above simulation at $Re= 40$ is computed as 1.564.

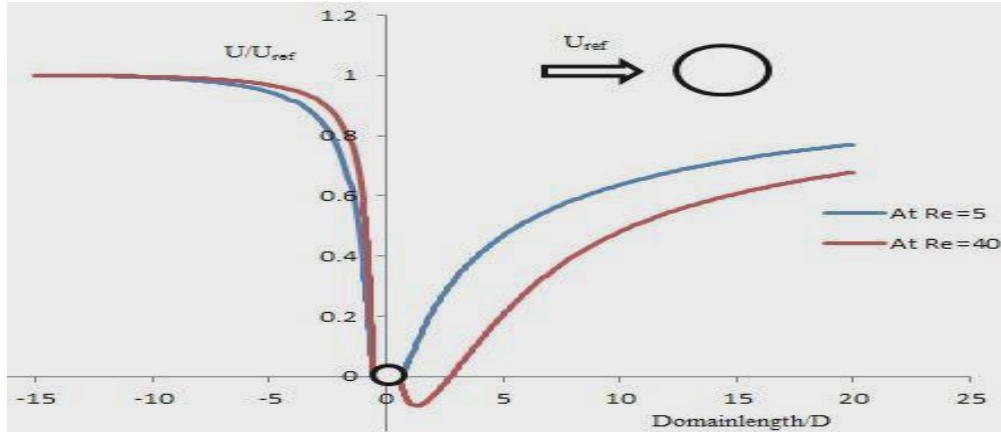


Fig. 4.10 Velocity along the wake centre line of domain

The values of C_D and St obtained for circular cylinders from the present simulations are compared with experimental data reported in literature as shown in Table 4.2.

Table 4.2: Comparison of C_D and St obtained for circular cylinders

Experimental study	St	C_D
Krishnamoorthy <i>et al.</i> (2001)	0.22	--
Mittal (2003)	0.17	--
Ozgoren <i>et al.</i> (2011)	0.21	--
Assi <i>et al.</i> (2009)	--	1.03
Present numerical study	0.2	0.9

4.3.2.3 Recirculation bubble length

At this juncture, a discussion on recirculation bubble length of laminar flow without vortex shedding seems to provide some better insight into the flow

characteristics. De and Dalal (2006) have carried out numerical simulations of flow past bluff bodies at low Reynolds numbers of 20, 30 and 35. It was reported that at subcritical range, two steady symmetrical vortices form behind the cylinder whose size increases with increase in Re was observed. Recirculation length (Lr), defined by the reattachment of the fluid layer separated from the two rear-end vertices of the cylinder, has been obtained by monitoring the stream wise velocity along the line of symmetry. The extent of recirculation region spreads with increase in Reynolds number Re . A linear $Lr-Re$ relationship has been obtained by least square fit, as shown below with other bluff configurations

$$Lr/h = 0.05 \times Re \text{ for } 4.4 \leq Re \leq 40; \text{ circular cylinder}$$

$$Lr/h = 0.0672 \times Re \text{ for } 5 \leq Re \leq 40; \text{ square cylinder}$$

By using the above relation, we get $Lr/h = 2.688$ for $Re = 40$. It may be noted that the present study predicts a value of $Lr/h = 2.60$ which is in good agreement with the published result.

4.4. SUMMARY

The flow characteristics at various Reynolds numbers around square and circular cylinders showed remarkable variation in properties. For square cylinder at $Re = 40$, only recirculation eddies are formed immediately downstream of the square cylinder, and no periodic vortex shedding noticed. The flow separates at the top right corner of the square cylinder, *i.e.* flow wraps the cylinder at the top and bottom face at $Re = 40$. For $Re > 40$, flow around square cylinder becomes unstable and results in an oscillating flow with the amplitude of oscillation increasing in the downstream direction. However, at $Re = 150$, due to its turbulent nature, the flow separates much

earlier, *i.e.* at top left corner forming a vortex street. Flow characteristics in the field such as Strouhal number (St), C_L and C_D were computed and the predictions were in reasonable agreement with the available experimental data in the literature.

Flow characteristics for flow past a circular cylinder studied at low Reynolds number. The flow separation gets much delayed for $Re = 5$ and the stagnation point is at the rear of the circular cylinder. However, the flow separation occurs at the forwarding stagnation point, and only recirculation eddies formed at $Re = 40$. When comparing the flow characteristics of the square and circular cylinders at $Re = 40$, similar recirculation eddies are formed. Nevertheless, the flow separation occurs much delayed in circular cylinders when compared to a square cylinder which is primarily due to the sharp corners of the square cylinder. The value of non-dimensional recirculation bubble length Lr/h predicted by the simulation was found to be within 3% variation with experimental data reported in the literature. The coefficient of drag computed for circular and square cylinders remains roughly the same under similar conditions.

CHAPTER - 5

SUPPRESSION OF AEOLIAN VIBRATIONS BY A SPLITTER PLATE FOR FLOW PAST A BLUFF BODY

5.1 INTRODUCTION

When wind flows past a cylindrical structure at a specific velocity, low-pressure zones are formed in the wake of the cylinder leading to the vortex shedding phenomenon. The cylinder is subjected to oscillations perpendicular to its axis resulting in transverse vibrations known as the Aeolian vibrations. The structures, when exposed to constant wind currents were prevented from catastrophic failure by employing suitable passive devices by the design engineers. The passive devices are found to be very effective in reducing Aeolian vibrations. A splitter plate placed in the downstream of the cylinder can control the flow variation in the wake effectively. The flow instabilities were analysed accurately by measuring the flow parameters such as Strouhal frequency, drag and lift forces. The flow was considered to be unsteady and turbulent in the flow field. As the Mach number is less than 0.3, the flow is subsonic and incompressible. A three-dimensional computational domain was modelled for numerical simulation and unsteady Reynolds Averaged Navier Stokes equations with SST $k-\omega$ turbulence model used for simulation. The numerical simulation was carried out using ANSYS CFD code.

5.2 FLOW DOMAIN

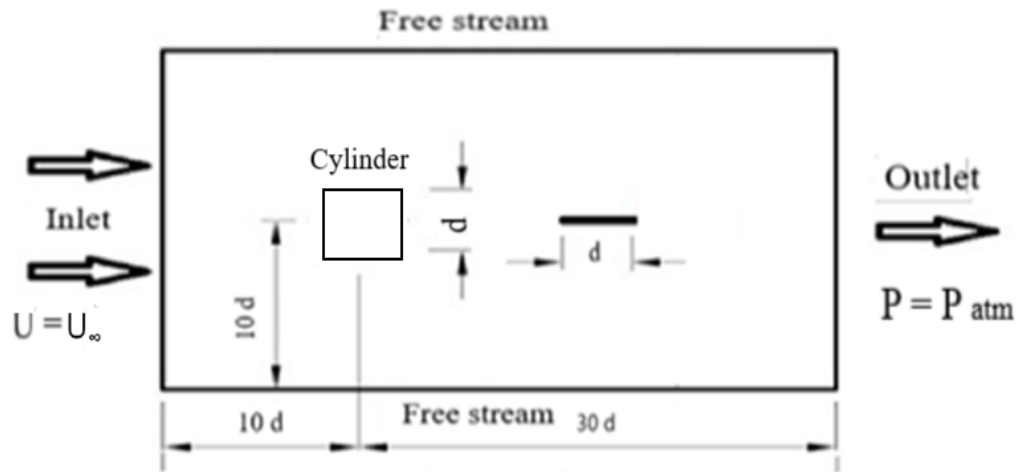


Fig. 5.1(a) Domain of fluid flow with boundary conditions

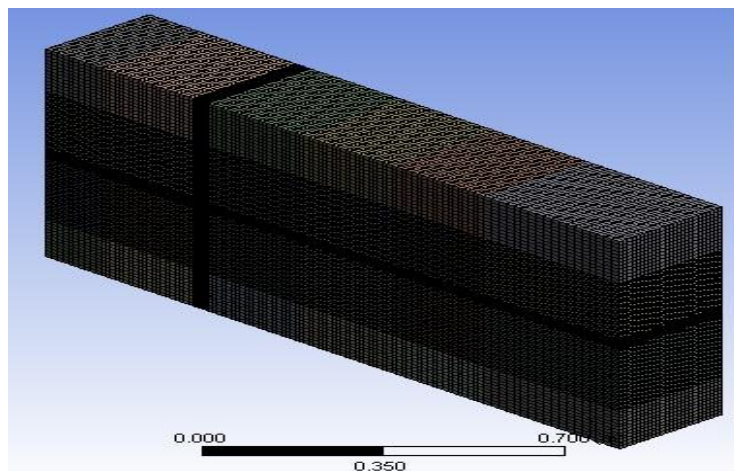


Fig. 5.1(b) 3D computational grid

5.2.1 Computational Domain and Mesh

A domain $40d$ long and $20d$ wide was selected for numerical simulation after conducting domain independence study. Figure 5.1 shows the two-dimensional view of the domain. The splitter plate of length $1d$ and thickness $0.1d$ was used as the passive device. Boundary conditions applied were constant inlet velocity and atmospheric pressure outlet. The simulations have been carried out with different grid sizes (coarse to fine) to ensure domain and grid independencies. Domain and grid sizes were finally selected to ensure accurate capture of flow conditions. The studies on grid independency showed some dependency on the flow parameters on the grid resolution. The flow parameters were found to attain steady values in all runs beyond a grid cell size of approximately 1 million cells.

5.2.2 Discretization method

The governing equations have been discretised using the finite-volume scheme on a fixed Cartesian-staggered grid with non-uniform grid spacing. The grids in the region of the embedded boundaries were sufficiently fine to achieve reasonable accuracy. The temporal discretisation was made in conformity with the fully implicit scheme and PISO (Pressure Implicit with the Splitting of Operators) procedure was applied to calculate the flow variables.

5.2.3 Boundary Conditions

The inlet conditions were mainly specified by velocity inlet and outlet conditions by pressure outlet. At the bottom boundary, ‘symmetry’ boundary condition was applied. Table 5.1 gives the inlet conditions for the numerical simulation using passive devices.

Table 5.1 Flow properties

Property	P_{∞} (Pa)	ρ_{∞} (kg/m³)	U_{∞} (m/s)	Reynolds Number (Re)
Magnitude	101300	1.225561	8.034	22000

5.3 RESULTS AND DISCUSSION

In this section, the results are analysed for Reynolds number of 22000 for two different cases; (1) for a square cylinder without any attachment and (2) for a square cylinder with detached splitter plate of constant thickness at varying gap distances (G) from trailing edge of a square cylinder.

5.3.1 Flow over the square cylinder.

Initially simulations were performed for the square cylinder with $Re = 22000$. The primary aim was to characterise the flow structure around the cylinder and to obtain the flow variables such as static pressure and velocity near the cylinder and in the wake region. Moreover, focus is made on vortex shedding pattern and vortex shedding frequency.

Figure 5.2 shows the variation of pressure in the wake region of the cylinder. The trends in variation of coefficient of pressure indicate that the domain size, mesh resolution and other essential parameters in the numerical scheme have been adequately chosen to capture the complex wake behaviour.

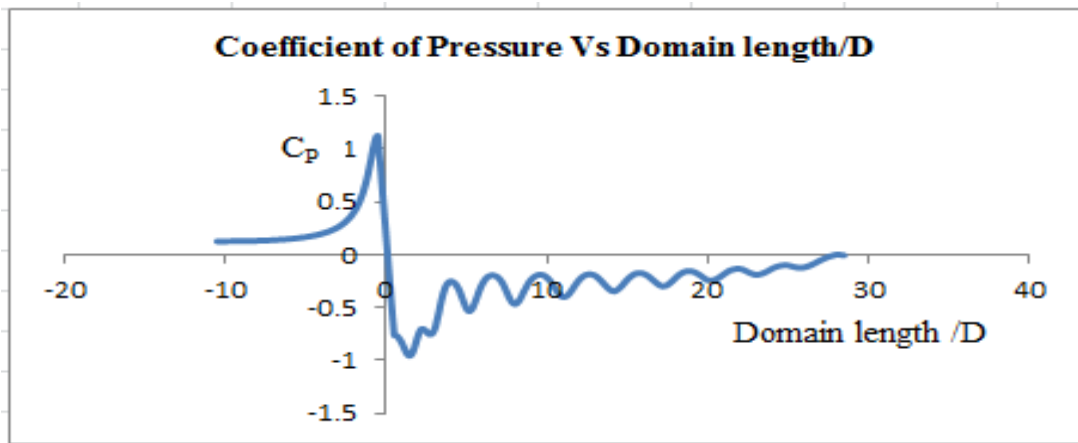


Fig. 5.2 Variation of coefficient of pressure with domain length

5.3.2 Flow over the square cylinder with and without detached splitter plate

The simulations were performed for a square cylinder with and without detached plate. The length L of the plate was taken as d and thickness $t = 0.02d$ (d is the length of one side of the square cylinder) at $Re = 22000$ to identify the changes in the flow characteristics in the wake region of the cylinder. Embedding the splitter-plate in the downstream of the cylinder could alter the flow in the wake region till a gap distance $G = 4d$. At this gap distance, the plate interrupts the vortex shedding phenomenon to a significant level, as shown in Figure 5.3. The splitter-plate limits the formation space of the vortices and suppresses vortex shedding effectively.

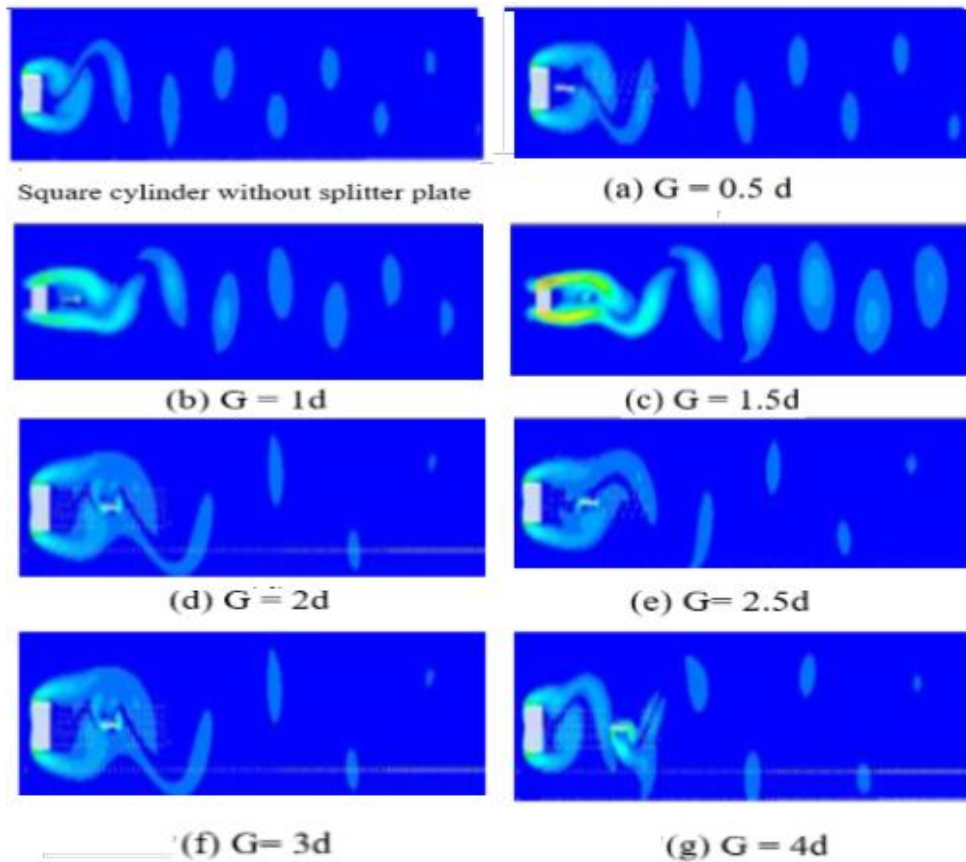


Fig. 5.3 Velocity contours at different amplitudes of oscillations

On analysing the flow field, it is observed that the flow past a square cylinder with a splitter plate highly interrupts the vortex shedding phenomenon. The interaction between the top and bottom fluid layers is notably interrupted. It can be deduced that the splitter plate effectively delays the formation of vortices for a gap distance $G = 1d$ and $1.5d$. The vortices behind the splitter plate are found to be weaker, and their strength reduces as they move away from the trailing edge of the square cylinder. The computed drag forces have a reduction in magnitude when compared with that of a square cylinder without a splitter plate.

When the splitter plate gap distance is in between $G = 2d$ and $G = 2.5d$, the magnitude of drag forces is seen to reduce considerably. As the value of drag force at

$G = 2.5d$ is found to be the minimum in the present analysis, the critical gap distance (G_{cr}) was selected as $2.5d$.

However, if the splitter plate gap distance is maintained at $G = 3d$ and $G = 4d$, the secondary vortex cores are formed inside the gap between the trailing edge of the square cylinder structure and the splitter plate. The gap distance is seen to be highly influential in increasing the magnitude of the drag force as it allows the interaction between the fluid layers from the top and bottom of the wake. Another vortex core is formed at the leading edge of the splitter plate for an increased gap distance of $G=4d$ as seen in Figure 5.3(g). Also, the change in the splitter plate position has a significant role on the pressure distribution downstream of square cylinder.

The values of coefficient of drag (C_D) is computed for different splitter plate distances (G) from the trailing edge of the square structure and plotted, as shown in Figure 5.4. From the graph it was evident that the coefficient of drag is reduced considerably by placing the splitter plate in the downstream of the flow. A gradual decrease in drag is observed for the splitter plate up to a distance of $G = 2.5d$; beyond which there is an increase in the value of drag; and thereafter it gradually reaches a value which is similar to one without a splitter plate. Hence the splitter plate distance of $G = 2.5 d$ is chosen as critical gap distance G_{cr} and is very crucial in the analysis of vortex shedding phenomenon.

Besides, it can be deduced that beyond this critical gap distance the splitter plate has no significant effect on the suppression of vortex shedding. It is mainly due to the formation of secondary vortex regime that cannot be prevented by the splitter plate. If the distance increases beyond the critical value, the secondary vortices begin to form well within the gap distance.

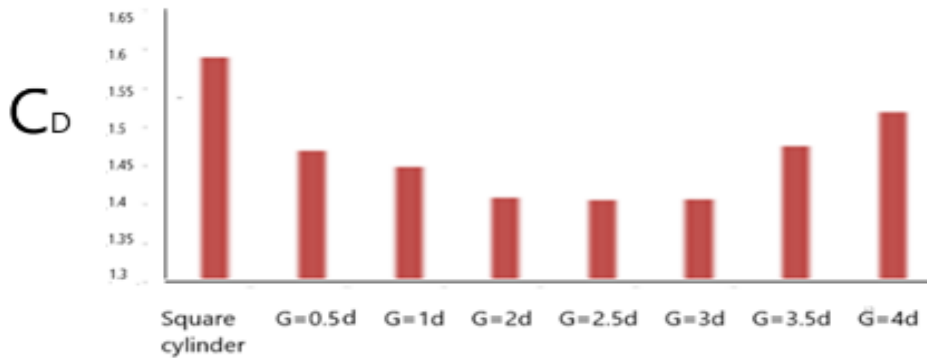


Fig. 5.4 Variation of coefficient of drag C_D with splitter plate

A discussion regarding the similarity between gap distances and the length of splitter plate seems to be valuable at this moment. In the present study, a detached splitter plate of constant length (D) and thickness at varying gap distances (G) from trailing edge of a square cylinder (of side length D) was carried out numerically. It was observed that the splitter plate is highly effective in interrupting the regular vortex formation, which in turn suppresses the vortex shedding phenomenon and thereby reducing flow-induced forces. An optimum gap distance known as critical gap distance ($G_{cr} = 2.5D$) between the splitter plate and the square cylinder, beyond which splitter plate has no significant effect on the development of vortex shedding phenomenon.

Li *et al.* (2014) have carried out numerical simulations on splitter plates with length varying from $0D$ to $6D$, where D is the side length of the square cylinder. It was reported that the wake interactions with shear layers are inhibited by the splitter

plate. When length of the splitter plate is varied systematically, initially the free shear layers are convected downstream and then the shear layers start to roll up and move towards the trailing edge. On further increase in length, a secondary vortex is clearly observed in the trailing edge and finally the free shear layers reattach to the splitter plate and thereby blocking the interaction between the shear layers. It may be emphasised that a similar effect was attained when the gap distance G was varied from $0.5D$ to $4D$.

Mittal (2003) has conducted experimental studies by varying the length of the slip splitter plate in the wake of a cylinder. When the plate was lengthened a slow reorganization of the near wake augmenting the vortex formation length and eventually, the vortex shedding is completely suppressed. The shortest length required to suppress vortex shedding is two cylinder diameters and must be located in the latter part of the wake bubble where the vertical velocity component changes direction. The above observation is in reasonable agreement with the present predictions of critical gap distance G_{cr} . It is clearly evident from C_D vs Gap distance (G) plot that the coefficient of drag reduces as G approaches $G_{cr} = 2.5D$ and there after it increases.

5.4 SUMMARY

An investigation on the suppression of fluid forces around a square cylinder was conducted by employing a passive device. The formation of vortex shedding and the associated changes in flow parameters were analysed along the flow field with and without the detached splitter plate at various gap ratios (G/d). It was observed that the splitter plate is highly effective in interrupting the regular vortex formation, which in

turn suppresses the vortex shedding phenomenon and there by a reduction in flow-induced forces. There is an optimum gap distance known as critical gap distance (G_{cr}) between the splitter plate and the square cylinder, beyond which splitter plate has no significant effect on the development of vortex shedding phenomenon.

CHAPTER - 6

SUPPRESSION OF VORTEX INSTABILITIES USING STRAIGHT FINS

6.1 INTRODUCTION

The frequency of the vortex induced vibration of a bluff body is usually reduced by attaching different passive devices on the structure. This chapter presents a numerical investigation of the reduction of vortex instabilities by using straight fins on the surface of the structure. The analysis focuses on the effectiveness of fins in diminishing the vortex instabilities in the wake of a structure when a stream of water flows past it. The evaluation was performed after determining the flow parameters such as Strouhal number drag and lift forces. The flow was considered to be incompressible, unsteady and turbulent with a subsonic Mach number less than 0.3. A three-dimensional computational domain was used for the simulation and the unsteady Reynolds Averaged Navier Stokes equations coupled with SST $k-\omega$ turbulence equations were solved using ANSYS CFD code.

6.2 COMPUTATIONAL DOMAIN

The entire flow domain has been discretised using the finite volume scheme with fine non-uniform grids for capturing the vortex phenomenon with reasonable accuracy by implementing the PISO algorithm along the domain.

A flow domain, as shown in Figure 6.1 of length $40d$ and width $20d$, where $d = 0.04$ m was employed for the simulation. Boundary conditions were applied, and numerical simulation was conducted to ensure the domain and grid independencies. The grid independence study showed that the lift forces predicted was approximately

the same in all runs beyond a grid size of approximately 0.4 million cells and hence all the 3D calculations were performed with a grid size of approximately 0.4 million cells.

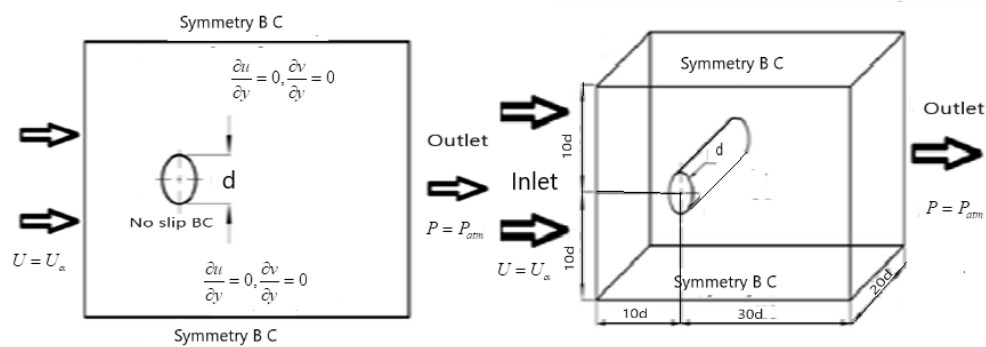


Fig. 6.1 Computational domain of fluid flow with boundary conditions

6.3 RESULTS AND DISCUSSION

In the present study, simulations and analysis of 3 different cases, one with a bare circular cylinder and two with circular cylinder fitted with straight fins at different fin numbers and fin orientations are included.

6.3.1 Flow over a circular cylinder without attachments

As a preliminary work, simulations of the flow over a bare circular cylinder were carried out at Reynolds numbers of 40 and 100. The objective of this analysis was to study the flow structure, pressure and velocity variations near the cylinder and along the wake region at different velocities. A dimensionless frequency known as Strouhal number was computed to investigate the range of frequency over which the vortex shedding occurs.

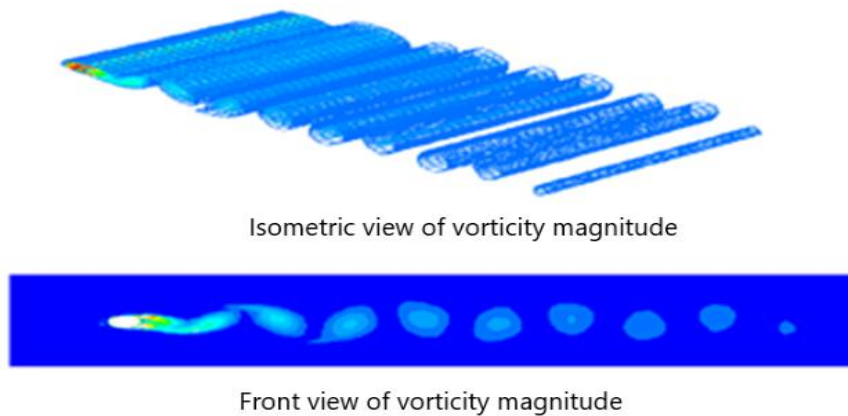


Fig. 6.2 Contours of vorticity magnitude

As the flow moves over the circular cylinder, due to an increase in the pressure of the fluid, an adverse pressure gradient is induced, followed by the boundary layer separation from the surface of the cylinder. As a result of this, fluid begins to detach alternatively from the top and bottom surface of the cylinder continuously, leading to both drag and lift forces acting on the structure. This alternate shedding of vortices from either side of the body in the downstream direction is shown by the contour of vorticity magnitude in Figure 6.2.

The changes in pressure crop up with the formation of vortices in the vicinity of the body. At stagnation point, the flow comes to rest and pressure reaches the maximum value, as shown in Figure 6.3(a). Flow separation occurs when shear stress cannot overcome the adverse pressure gradient. Flow separation occurs where wall shear stress is zero, as shown in Figure 6.3(b). If the flow takes place at laminar conditions, the variation in the wall shear stress along the surface is very less. When the Reynolds number is increased to 100, the flow under investigation becomes more turbulent and display significant variation along the surface of the cylinder. The flow is unsteady and therefore the quantities obtained are instantaneous values. The graph

clearly shows that when the wall shear stress approaches zero, the flow separation commences with the initiation of vortex shedding.

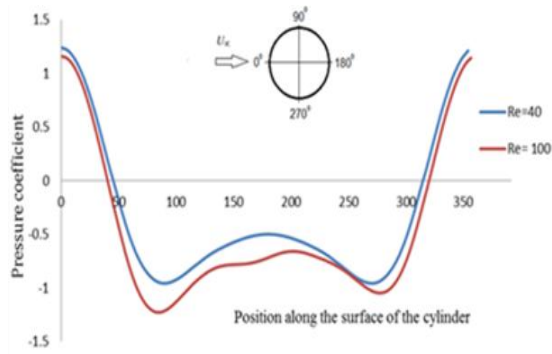


Fig. 6.3(a) Pressure coefficient along cylinder surface

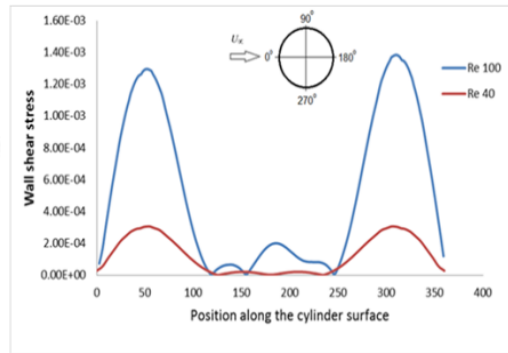


Fig. 6.3(b) Wall shear stress along cylinder surface

6.3.2 Flow over the circular cylinder with fins

The bare cylinder with different fin configurations and fin orientations were examined numerically. The fin height taken was $0.1d$ for all cases. The number of fins or fin count provided in the circular cylinder includes 3, 4, 6, and 8, which are equally spaced on the periphery of the cylinder, as shown in Figure 6.4.



Fig. 6.4 Geometry of cylinders with fins

6.3.3 Effect of fin count

The addition of the fins is found to enhance the process of flow turbulence. The fact observed was that the fins increase the correlation length and the amplitude

of velocity fluctuation at the vortex shedding frequency. The effect of fins on the vortex shedding characteristics around the circular cylinder was investigated by changing the number of fins on the periphery of the cylinder. The contours of vorticity magnitude of different fin arrangements (Figure 6.5) showed that vortex shedding occurs in the wake of cylinder fitted with fins but with different magnitudes. Finned cylinders have a larger mean velocity deficit than bare cylinders. Hence larger velocity gradients have been observed in the wake of finned cylinders confirming that the wake behaviour is fundamentally different from bare cylinders. The increase in fin count increases the amplitude of velocity fluctuations inducing a non linear nature of flow in the wake.

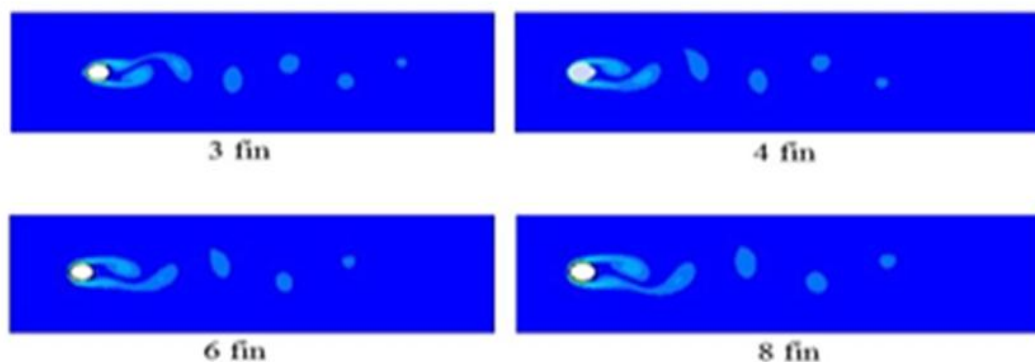


Fig. 6.5 Contours of vorticity at different orientations

The Strouhal number with the different fin count was compared with that of a bare cylinder in Figure 6.6 and Table 6.1. It is evident that the decrease in Strouhal number is only marginally with increase in fin count.

Table 6.1 Strouhal Number variation with fin count

No. of fins	% reduction in Strouhal number
3	0.29
4	2.05
6	3.28
8	4.1

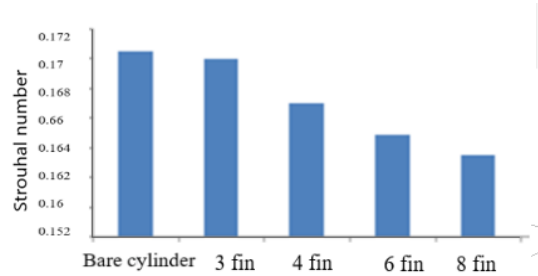


Fig. 6.6 Percentage reduction in Strouhal number with fin count

The predictions showed marginal decrease in Strouhal number with the increase in fin count in the range of Re considered. A decrease in Strouhal number indicates a decrease in vortex shedding frequency and in turn a reduction of approximately 4% was attained by providing eight fins on the periphery of the cylinder.

6.3.4 Effect of fin orientation

The fins also increase the nonlinear nature of the flow in the wake, as proved by a remarkable increase in the turbulence of fluid flow. However, the correlation length in the wake of the cylinder with fins is found to change with fin orientation around the circular cylinder. This phenomenon seems to be related to an irregular wavy pattern induced by the fin distribution along the cylinder axis.

Two cylinders with different fin orientation, as shown in Figure 6.7 were investigated. The fin count was 4, fin height $0.1d$ and the angle between the two fins was 90° .

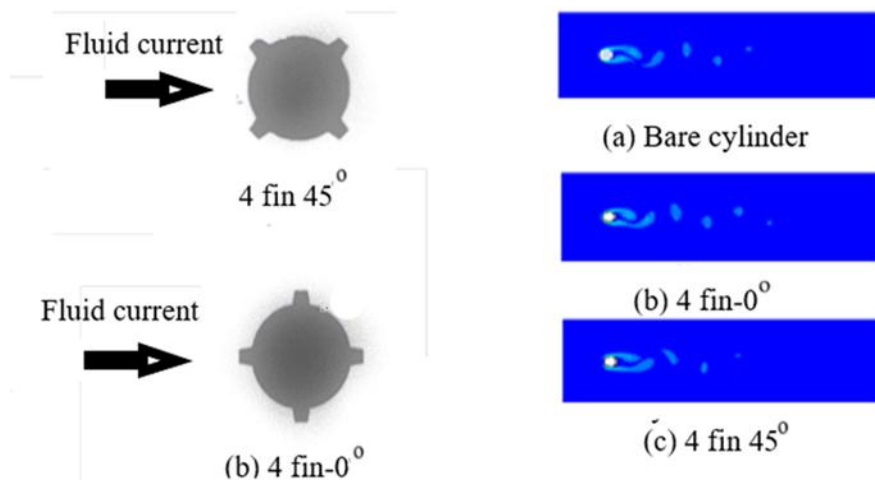


Fig. 6.7 Vorticity contours for different fin orientations

Figure 6.7 depicts typical vortex structures behind the cylinders with and without fins demonstrating the evidence of fin effects. For 4 fin-45° orientation, the auxiliary fin arrangements decrease the lateral spacing of the first large vortex. The lift force on the cylinder provided with 4fin-0° orientation is higher than that of the bare cylinder.

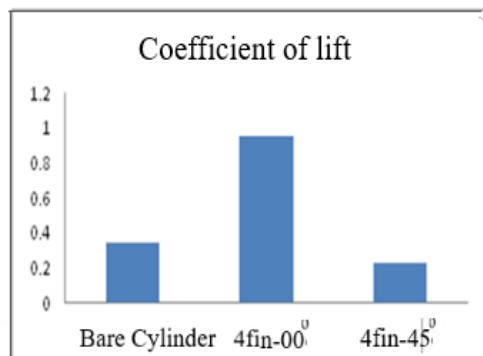


Fig. 6.8(a) Coefficient of lift at different fin orientations

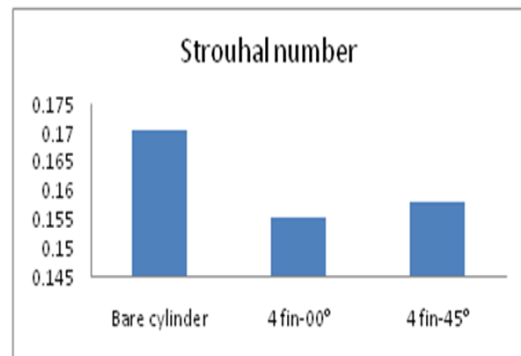


Fig. 6.8(b) Strouhal number variation with fin orientations

However, the 4fin-45° orientation decreases the lift force on the cylinder. Both fin arrangements seem to be effective in reducing the Strouhal number (Figure 6.8). It

may be inferred that the fins with 0° orientations are more effective in reducing the Strouhal number and vortex induced vibration.

When the fin count increases, more and more rotating masses of fluids interact with each other and delay the formation of vortex shedding. This phenomenon reduces the Strouhal number and the same cylinder with different fin orientations can provide better flow characteristics. The result indicates that the effectiveness of straight fin on vortex shedding suppression depends primarily on the fin orientation.

6.4 SUMMARY

Numerical investigation of the flow around a circular cylinder with straight fins was conducted to analyse the flow characteristics around a bluff body in a subsonic flow. As a passive vortex control method, the straight fins are found to be effective in suppressing the vortex induced vibrations of the structures. The modification in the design by varying fin count and orientation provided valuable information on vortex shedding phenomenon. The vortex shedding and Aeolian vibrations were reduced by the use of straight fins fitted on the cylinder surface. Although the change in reduction of VIV by increasing the number of fins is marginal, selection of proper fin orientation seems to be more important.

The study on straight fins on structures infers that the lift force gets reduced at the expense of increase in drag force and the order of its increase has to be evaluated further. The study is limited to low and medium Reynolds numbers and confined to incompressible fluid flows alone.

CHAPTER - 7

FLUID FLOW OSCILLATIONS IN THE WAKE OF A CYLINDER WITH HELICAL STRAKES

7.1 INTRODUCTION

Heavy winds blowing across tall structures can cause severe structural damages, leading to substantial challenges in their design and construction. In this chapter, the study of fluid flow oscillations in the wake of the cylinder due to air currents and the possible suppression of vortex induced vibrations by using helical strakes were performed. The effect of passive methods envisioned in the reduction of VIVs was analysed using computationally less expensive Reynolds Averaged Navier Stokes simulations. The turbulent behaviour of subsonic flows around the cylindrical structures was accurately captured and analysed with the help of computational fluid dynamics. The flow instabilities were obtained by measuring the variations in flow parameters such as Strouhal frequency, drag, and lift coefficients. The investigation offers valid information that helps to prevent the premature collapse of tall structures due to crosswind currents. By reducing the probability of occurrence of intense vortex shedding, the safety of tall structures and people living nearby could be ensured.

7.2 COMPUTATIONAL DOMAIN AND MESHING STRATEGY

The horizontal and vertical extents of the two-dimensional domain were $40d$ and $20d$ respectively, where d is the diameter of the circular cylinder. In three dimensional domain, the width corresponds to the length of the circular cylinder ($L = 0.4$ m).

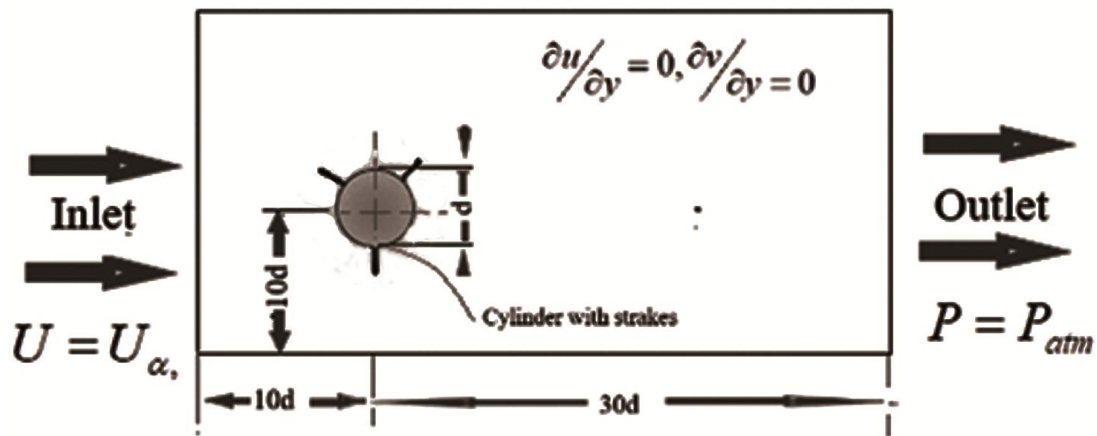


Fig. 7.1 Flow domain for a circular cylinder

The two-dimensional view of the domain and boundary conditions are shown in Figure 7.1. Numerical simulations were carried out to ensure the domain and grid independence studies. The grid size used for the present 3D numerical simulation was 1 million. Mesh refinement near the no-slip surfaces is such that the area weighted wall y^+ is less than 10. The volume weighted average of cell equi-angle skew is 0.3 and maximum value is 0.5. Furthermore, second order accurate discretization has been used for all the variables. Calculations were carried out till the residuals for all the equations were less than 10^{-6} . The full domain has been divided into 27 volumes and these volumes have been discretized using a hybrid mesh. Hexahedral mesh with 0.6 million cells have been used to mesh the region surrounding the cylindrical surface. An additional 0.4 million tetrahedral cells have been used to discretize the regions surrounding the helical strakes. These fine meshes of approximately $50 \mu\text{m}$ in the strake surface have been created in a view to capture the vortex interaction regions of the flow.

7.2.1 Boundary conditions

The domain inlet and outlet were defined with boundary type ‘velocity inlet’ and ‘pressure outlet’ respectively. At the axis of the domain, ‘symmetry’ boundary condition was applied. Table 7.1 provides the inlet conditions

Table 7.1 Flow properties

Property	$P_{\infty} (Pa)$	$\rho_a (kg/m^3)$	$U_{\infty} (m/s)$
Magnitude	101300	1.22555	8.034

7.3 RESULTS AND DISCUSSION

The numerical simulations were carried out to study the development of vortex flow instabilities in the wake of the circular cylinder fitted with and without helical strakes. The results are discussed for the above cases by analysing the parameters such as coefficient of lift (C_L), coefficient of drag (C_D) and Strouhal number (St)

7.3.1 Flow characteristics across a cylinder without strakes at $Re=22000$

The numerical simulation of fluid flow past a bare circular cylinder at Reynolds number of 22000 was conducted to study the variation of properties in the flow field. The trends of the aerodynamic quantities such as coefficient of lift and coefficient of drag are shown in Figure 7.2.

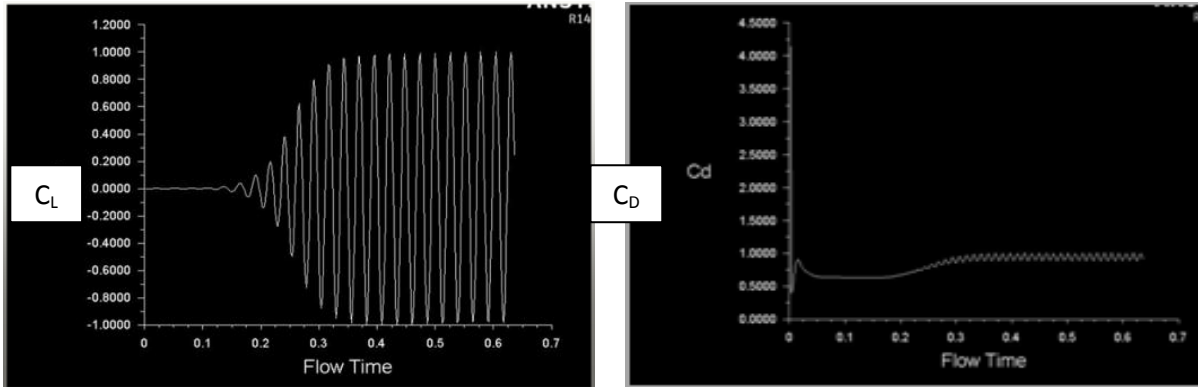


Fig. 7.2 Coefficient of lift and coefficient of drag

Numerical simulations were conducted with a flow velocity of 8.034 m/s. Figure 7.2 shows that the fluid flow oscillations attain steady conditions in the wake of the cylinder inducing a structural vibration perpendicular to the flow direction. It also displays a drag force on the cylinder, which has a slight variation in the initial stages and attains a near-constant value at a later stage.

Figure 7.3 shows the variation in pressure distribution throughout the domain. As expected, a low-pressure zone was formed in the wake of the cylinder. Due to the significant pressure drop across the cylinder, the fluid undergoes oscillations due to shear instabilities. The fluid tends to get separated from the top and bottom surfaces of the cylinder alternatively inducing shedding of vortices from either surface.

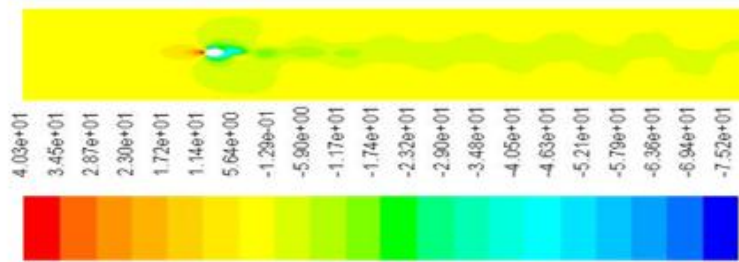


Fig. 7.3 Mean pressure distribution along the central plane

Figure 7.4 shows well-developed vortices that get detached from either surface of the cylinder alternatively. The vortices slowly disintegrate into smaller eddies and ultimately diffuse into the medium by increasing the internal energy of the fluid. Since the vortices resemble the footsteps in the street, this pattern is often termed as Von Karman vortex street.

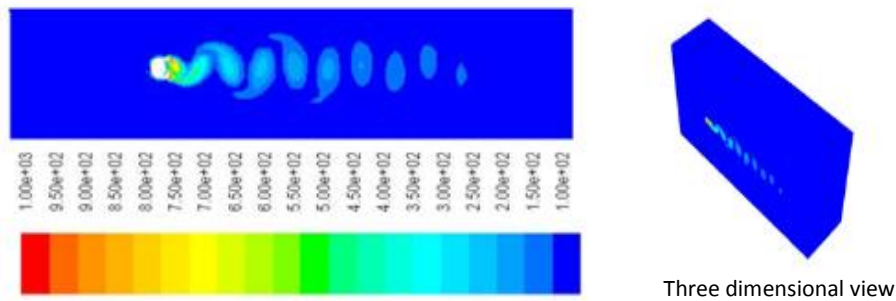


Fig. 7.4 Contours of vorticity magnitude in the central plane

The distribution of static pressure (Figure 7.5) shows the formation of a low-pressure zone in the wake of the cylinder. When the flow strikes the cylinder, the pressure attains a maximum value; but immediately undergoes a substantial drop in the wake of the cylinder. The velocity profile displays that the velocity is reduced to zero on striking the cylinder and abruptly regains magnitude towards the exit of the domain.

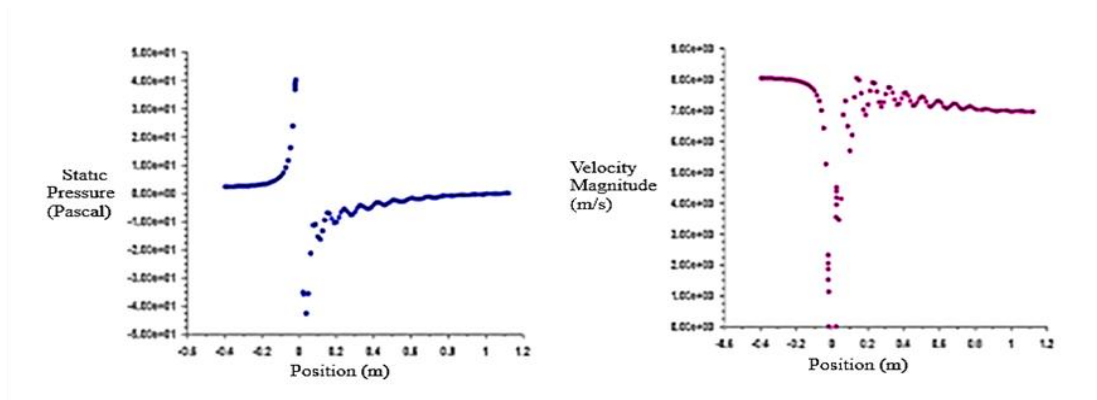


Fig. 7.5 (a) Distribution of Static pressure along central plane

Fig. 7.5 (b) Velocity magnitude along central plane

The Strouhal frequency was computed with the help of Fast Fourier Transform (FFT). The Strouhal number, the nondimensional form of Strouhal frequency was determined based on the diameter of the structure and inlet velocity of the flow. Figures 7.6(a) and (b) show the nature of Strouhal frequency and Strouhal number during the fluid flow. Assi *et al.* (2009) reported a C_L value of 1.03 for bare cylindrical structures whereas the present study gives a reasonable agreement of $C_L = 0.9$.

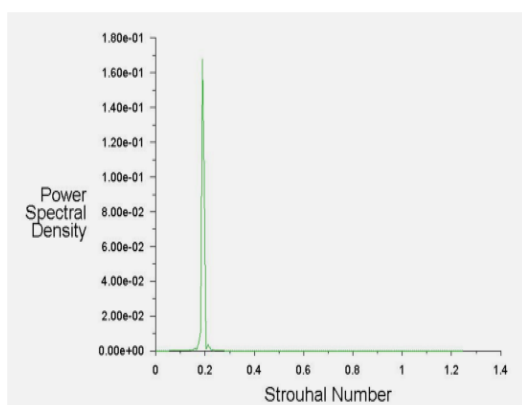


Fig. 7.6(a) Strouhal frequency

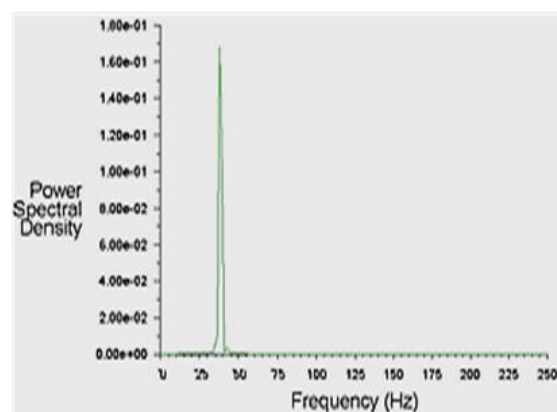


Fig. 7.6 (b) Strouhal number

The magnitudes of drag, lift, C_L , C_D , Strouhal frequency and Strouhal number are presented in Table 7.2.

Table 7.2 Flow conditions for fluid flow past a circular cylinder without strakes

Drag (N)	Coefficient of drag	Lift (N)	Coefficient of lift	Strouhal frequency (Hz)	Strouhal number
0.567	0.896	-0.108	-0.172	39	0.20

7.3.2 Flow over circular cylinder with triple start helical strakes at $Re=22000$

3D simulations were performed for a circular cylinder fitted with helical strakes of different pitches and heights. Pitches of $5d$, $10d$ and $15d$ and heights of $0.05d$, $0.1d$, and $0.15d$ were used in the numerical simulations. A triple start helical strake was attached as a passive device on the surface of a circular cylinder, as shown in Figure 7.7. Figure 7.8 shows the velocity vector at three different 'z' planes taken along the length of the circular cylinder fitted with helical strakes during the airflow.

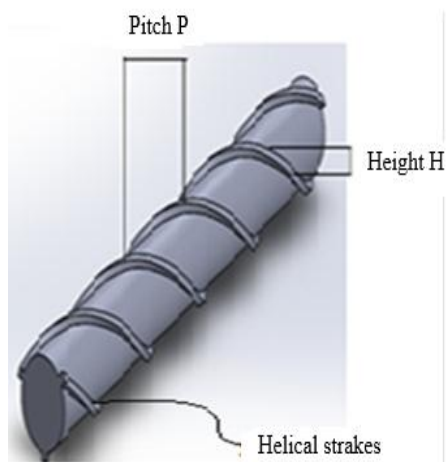


Fig. 7.7 Circular cylinder fitted with triple start helical strakes

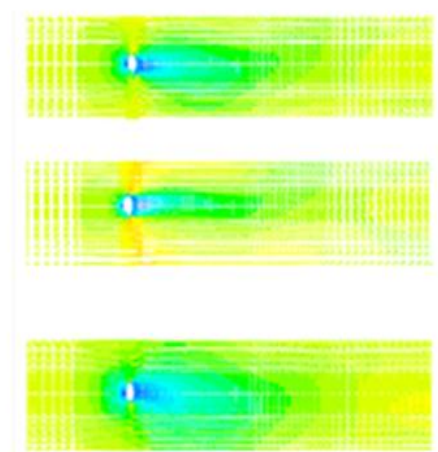


Fig. 7.8 Velocity vectors at different z planes

When the fluid flows past the cylinder with helical strakes, the flow breaks at the edges of the strakes generating vortices at different points along the cylinder surface. These vortices formed around the structure are found to be out of phase with one another and leads to partial cancellation of the forces at different span-wise positions. Lift force developed with strakes is much smaller than that of a bare cylinder.

The helical pattern of the projecting fin induces a span-wise motion for the fluid while it flows around the cylinder with strakes. The swirling motion of fluid in the wake region disrupts the span-wise vortex formation in the downstream. The strength of these swirls induces a partial cancellation of vortex formation at different points which in turn becomes highly instrumental in the reduction of the vortex induced vibration. The flow characteristics past a cylinder fitted with helical strakes display significant variation from that of the fluid flow past a bare cylinder. Due to the tremendous interaction between the rotating masses of fluid around the cylinder, the flow separation and vortex shedding frequency are minimised. The pitch and height of the strakes have a significant role in determining the intensity of fluid flow oscillations at the wake of a cylinder, as shown in Figure 7.9. A decrease in the pitch of the strakes causes a corresponding reduction in the vortex induced vibrations. Also, a significant effect was observed by experimenting with the height of strake. Vortex shedding was found to reduce with an increase in the height of the strakes. A close interaction between the two shear layers induces an oscillating wake for a bare cylinder. If the cylinder is provided with helical strakes, the strake height and pitch would control the shear layer interaction that tends to move farther downstream from the cylinder body, than the flow over a bare cylinder.

For a cylinder with strakes, the two shear layers do not interact with each other, resulting in the absence of the oscillating wake in the downstream region of the cylinder. This fact is evident from the reduction in the values of Strouhal number computed for the cylinder with helical strakes.

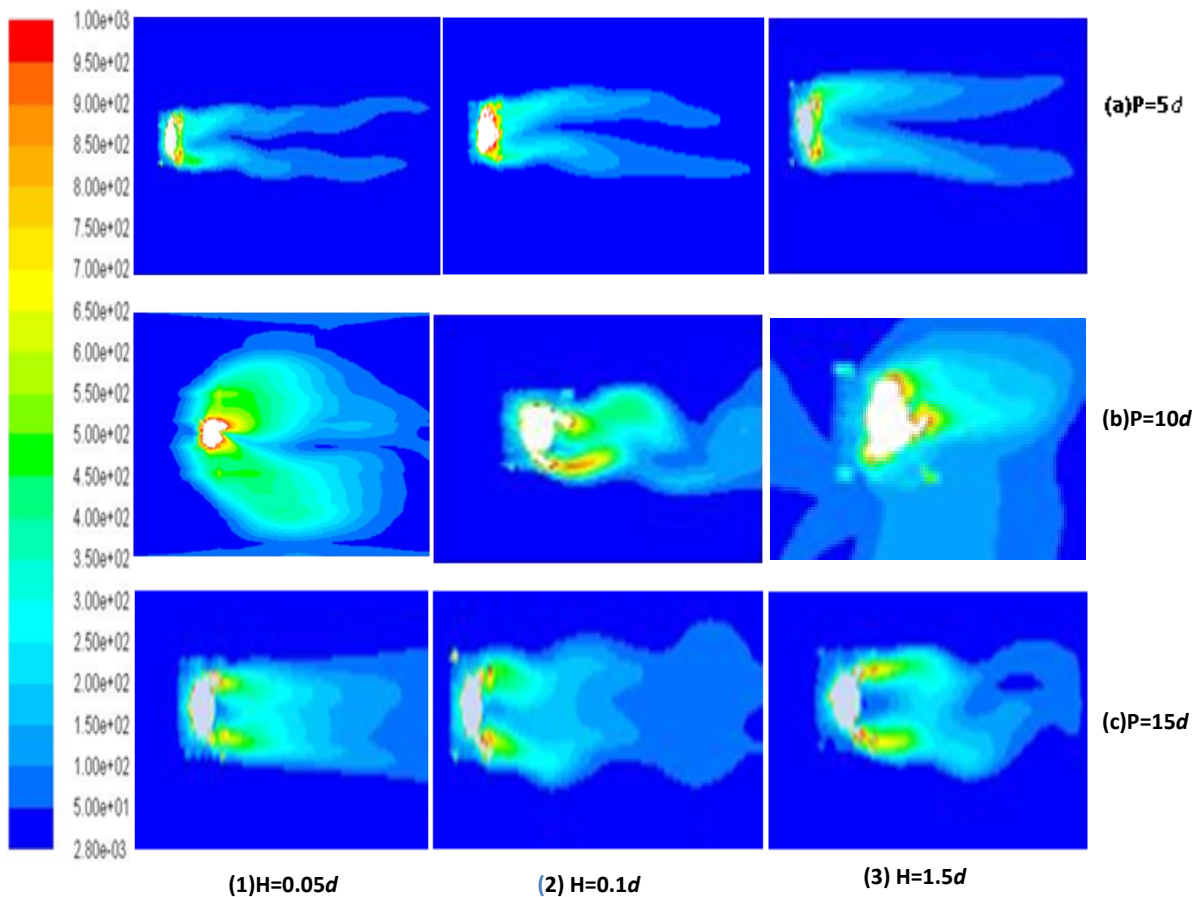


Fig. 7.9 Contours of vorticity magnitude at (a) pitch = $5d$
 (b) pitch = $10d$ and (c) pitch = $15d$

The investigation on fluid flow past a circular cylinder with helical strakes reveals that a decrease in lift force occurs at the expense of an increase in drag force.

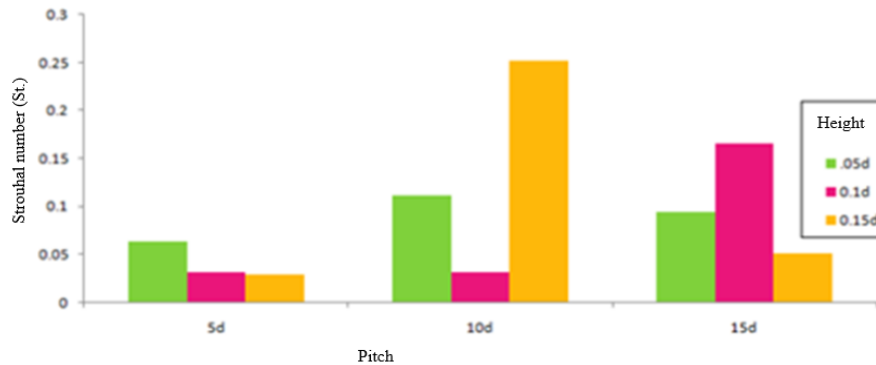


Fig. 7.10 Strouhal number variation with different pitches

Figure 7.10 shows that fluid flow oscillations vary significantly with different dimensions of the strake. It is evident from Table 7.3 (a) and (b) that the helical strake with height $0.15d$ and pitch $5d$ is found to be most effective in suppressing the vortex induced vibrations. When the pitch is small, the helical strakes are highly effective in disturbing the formation of vortex shedding, and the fluid flow becomes more and more turbulent. The interaction of fluid masses from the top and bottom layers in the immediate wake of the structure are barred by the strakes. Hence the vortex shedding and associated vortex induced vibrations are reduced to low values. It is also apparent that the increase in strake height also contributes to the reduction of vortex induced instabilities. It can slash the formation of vortices in the wake and prevent them from interacting from either side.

Moreover, the formation of different out of phase fluid layers all over the structure, which is very close to each other are highly instrumental in reducing the vortex induced vibrations. The helical strakes have seen to be much more superior to other passive devices like splitter plates and shrouds in disturbing the fluid flow and thereby reducing the vortex induced instabilities in the wake of the structure. A significant reduction in Strouhal frequency of 85% was obtained with the use of helical strakes. However, when compared

with flow parameters for a bare cylinder, the drag force is slightly increased for the cylinder with strakes. The same was reported by Huang (2011) in his experimental study with helical grooves. Huang claimed that the surface protruding from VIV suppression devices could reduce vibration, but only at the cost of increasing the drag. The main disadvantage of strakes is this increase in inherent drag that is developed during the flow past any structure fitted with protrusions.

Table 7.3 (a) Flow parameters for fluid flow over a bare cylinder

Bare cylinder

Reynolds Number	C_L	C_D	St
22000	-0.172	0.896	0.2

Table 7.3 (b) Flow parameters for fluid flow over a cylinder with strakes

Cylinder fitted with helical strakes

Reynolds number	Pitch	Height	C_L	C_D	St
22000	5d	0.05d	-0.039	1.05	0.063
		0.1d	-0.059	0.195	0.031
		0.15d	-0.031	1.33	0.029
	10d	0.05d	0.007	1.108	0.111
		0.1d	0.01	1.492	0.031
		0.15d	0.65	4.8	0.252
	15d	0.05d	-0.016	0.946	0.094
		0.1d	-0.06	1.334	0.165
		0.15d	-0.085	1.54	0.051

The reduction in oscillations was augmented by the interaction of fluid masses in different turbulent layers formed by the slicing of the fluid layers due to the strakes. Within a turbulent boundary layer, the fluid has more kinetic energy than in a laminar flow. As a result, the adverse pressure gradient takes longer to arrest the flow and the point of separation moves back to the rear of the cylinder. It was perceived that the strakes with smaller pitch lengths and larger heights are highly effective in increasing the turbulence. Since the increase in turbulence is higher when compared to any other passive device, the helical strakes are considered as the most effective passive method of VIV reduction. Huang (2011) has claimed a VIV reduction of 64% in his experimental works by using a passive device known as helical grooves on the surface of the cylinder. However, in the present work, a better VIV reduction of 85% is attained by using helical strakes of optimum design based on pitch and height. Helical grooves are advantageous over helical strakes by the fact that it can reduce the drag loading up to 25%. The exact phenomena of VIV control by helical strakes need further theoretical understanding in this field.

7.4 SUMMARY

Computational study of a subsonic flow of air past a circular cylinder with and without helical strakes has been performed using Reynolds Averaged Navier Stokes calculations with Shear Stress Transport $k-\omega$ turbulence model. The numerical predictions provided valuable information on changes in various flow parameters. The Strouhal frequency was seen to reduce appreciably by fitting helical strakes on the surface of cylindrical bodies. A reduction in VIV of approximately 85% was made possible by employing the helical strakes. The investigation revealed that the effectiveness of strakes would be highest at an optimum pitch and height. It was detected that the use of helical strakes in the fluid flow had increased the drag marginally due to the obstruction in the flow

affecting its smooth movement around the structure, inducing a force in the direction of flow. This phenomenon is known as drag crisis which may have to be further investigated for the complete analysis of fluid flow characteristics. The primary application of helical strakes lies in the reduction of Strouhal frequency and subsequent damages on different offshore and onshore structures.

CHAPTER - 8

EFFECT OF ACTIVE AND COMPOUND METHODS ON VORTEX DYNAMICS IN THE FLOW FIELD

8.1 INTRODUCTION

Bluff structures are prevented from disastrous failure by using suitable passive devices when constant wind currents blow across them. Passive methods are recognised to be very effective in reducing Aeolian vibrations of structures. Apart from this, the 'Active method' of providing external excitations to the structure was in practice for the suppression of vortex shedding and associated instabilities. In the 'Active method', energy is to be supplied externally to produce the suppression of VIV. Two different methods can be employed. In the first method, the oscillations could be imparted to the bluff structure itself. In the second one, oscillations are given to a splitter plate provided in the wake of the structure. The second method combines the effect of both 'Passive' and 'Active' methods, hence termed as the 'Compound method'. Both methods were employed and calculations were carried out to analyse the flow instabilities accurately by measuring the flow parameters like Strouhal frequency, drag and lift forces. The flow was considered to be unsteady, incompressible and turbulent in the flow field. Unsteady Reynolds Averaged Navier Stokes (*RANS*) equations coupled with SST $k-\omega$ turbulence model was used for numerical simulation. The flow oscillations in the wake were investigated for different amplitudes of oscillations provided either to the structure or the splitter plate. The numerical simulation was carried out using dynamic meshing facility of the CFD

software where amplitudes of oscillations were conveyed by writing codes for user defined functions.

8.2 FLOW DOMAIN FOR ACTIVE METHOD

8.2.1 Computational domain

A rectangular domain was used with a length of $40d$ and a width of $20d$ after conducting domain independence study. Figure 8.1 shows the two-dimensional view of the domain. The centre of the square cylinder has the coordinates $x = 10d$ and $y = 10d$.

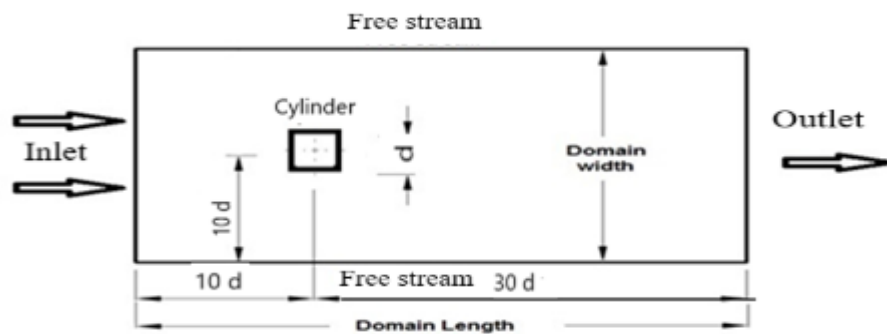


Fig. 8.1 Domain of fluid flow with boundary conditions

The grid independence study was conducted based on drag coefficient and its faster recovery was observed when the grid resolution increased up to 0.1 million cells as shown in Figures 8.2(a) and (b). Hence a grid size of approximately 0.1 million cells was chosen for the present 2D simulations.

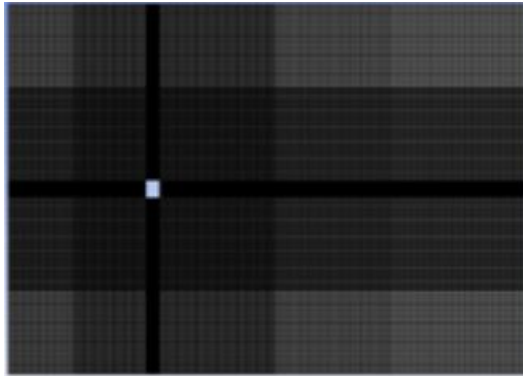


Fig. 8.2(a) Domain of fluid flow with mesh

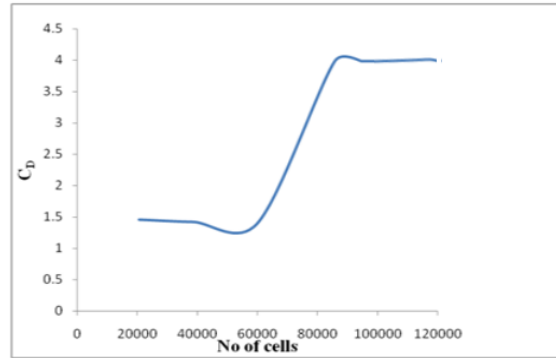


Fig. 8.2(b) C_D versus Cell count

8.2.2 Boundary Conditions

The inlet was specified by velocity inlet, outlet by pressure outlet and axis by symmetry boundary conditions. No-slip condition has been applied at the cylinder wall. Table 8.1 tabulates the flow parameters.

Table 8.1 Flow properties

Property	P_∞ (Pa)	ρ_∞ (kg/m ³)	U_∞ (m/s)	Re
Magnitude	101300	1.225561	8.034	22000

8.3 RESULTS AND DISCUSSION

8.3.1 Flow over a stationary square cylinder

The primary aim of simulating flow over a stationary square cylinder at $Re=22000$ is to obtain the flow variables in the downstream region. It also aims to estimate the frequency of vortex induced vibration downstream of the structure. Figure 8.3 depicts the vorticity contours obtained in the simulation.

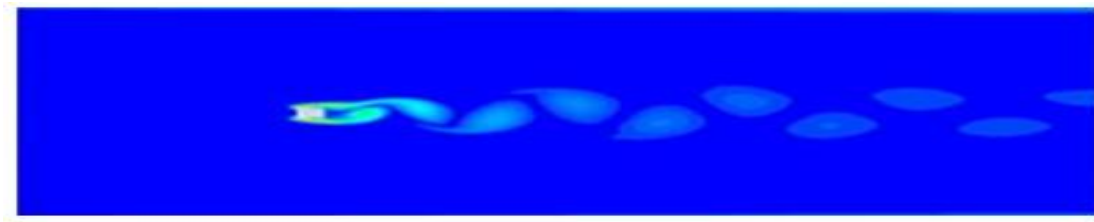


Fig. 8.3 Contours of vorticity magnitude

The coefficient of drag and lift shown in Figures 8.4(a) and(b) depicts a regular pattern and signifies the presence of a distinct vortex shedding in the wake of the structure

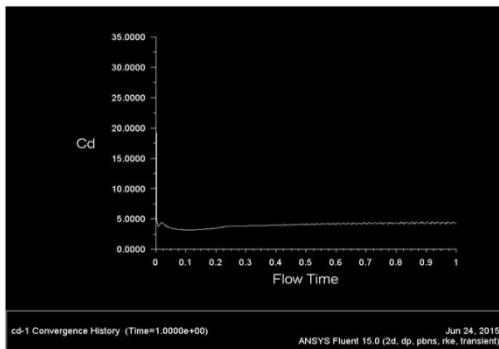


Fig. 8.4 (a) C_D with flow time

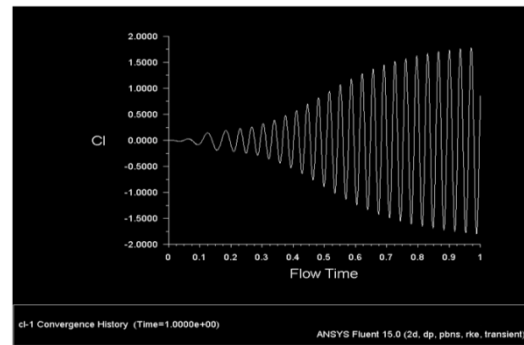


Fig. 8.4 (b) C_L with flow time

8.3.2 Flow over oscillating square cylinder at different amplitudes

Simulations were performed for an oscillating square cylinder with same Reynolds number of 22000 to identify the changes in the flow characteristics in the wake region of the cylinder. Dynamic meshing was engaged and changes in the amplitude of oscillation were applied by writing codes for user defined functions. Usually, the time step size are computed based on the widely accepted Strouhal number in the literature and Strouhal frequency is obtained from existing relations. The reciprocal of twice the Strouhal frequency is taken as the time step. In the present case, the frequencies of interest are below 1000 Hz and the time step was calculated based on the above frequency. At least 2 points are essential to represent a wave

properly. The time step for the present calculation was calculated as 5×10^{-4} . Initially, steady state calculations were run till the overall mass balance in the domain was maintained. At this point, unsteady calculations were started. The time step size was $500 \mu\text{s}$ and the calculations were run till there was no change in the predicted values of properties. The number of iterations was given as 20 per time step and the converged solutions were obtained in approximately 10,000 time steps.

The ‘appropriate’ time step for a given grid and solution should be the one that is stable, yet gives results to desired accuracy. A too large time step would result in a lower temporal accuracy, reflected in the results or worse could cause stability issues. A very small time step is undesirable, purely because we spend more time than required in actually getting the solution. The choice for the ‘optimum’ or ‘appropriate’ time step is difficult to decide though in some cases available information (such as frequency of vortex shedding etc.) could help us make a good decision. In an unsteady flow simulation, both the spatial and temporal accuracies are important. Although spatial accuracy would resolve the flow features better and since the problem is time--dependent, the temporal accuracy would have its effect on the simulation.

Amplitude ‘*a*’ of oscillation ranging from 0.01 m to 0.04 m and frequency of 1 Hz. were applied for providing oscillation to the square structure. Dynamic meshing option of the software was used for providing the oscillation for the cylinder. The oscillatory movement of the cylinder interrupts the vortex formation and is evident from Figure 8.5.

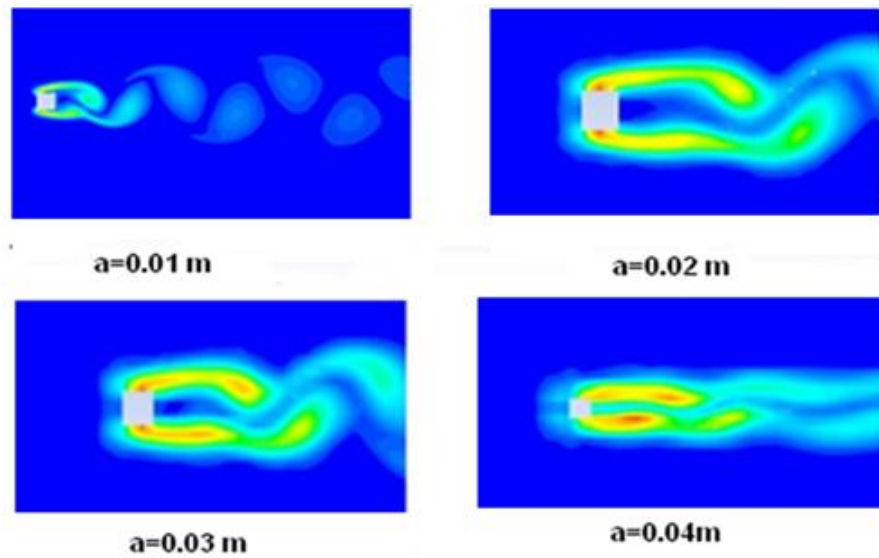


Fig. 8.5 Contours of vorticity magnitude at different amplitudes of oscillation for the cylinder

The vorticity contours showed tremendous modifications in the wake of the cylinder at different amplitudes. This variation is obviously due to the oscillatory action imparted to the square cylinder. The oscillation of the cylinder affects the formation of flow separation and subsequent vortex shedding. As the amplitude increases, vorticity contours are more and more diffused, resulting in more turbulence in the wake of the cylinder.

8.3.2.1 Effect of drag

One of the main parameters that can exhibit the vortex instabilities of a structure is its drag force. The velocity and the area of the projection of the structure affect the value of the drag force in the wake of the structure. Coefficient of drag (C_D) was used for representing the drag force.

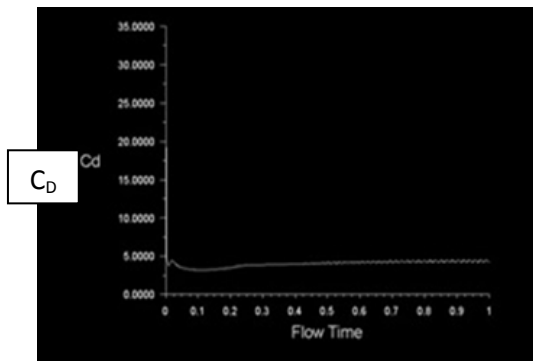


Fig. 8.6(a) C_D with flow time for a stationary cylinder

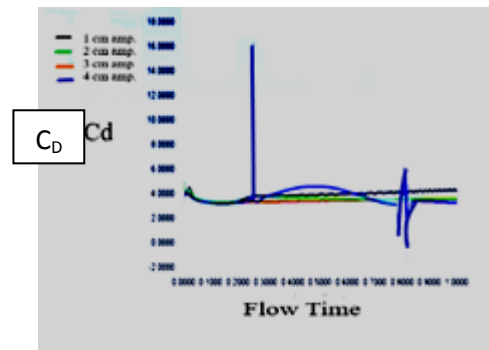


Fig. 8.6(b) C_D with flow time at different amplitudes of oscillations

Figures 8.6(a) and (b) shows the effect of C_D on the stationary and oscillating square cylinder. For the stationary square cylinder, the C_D obtained is 4.25, and the same for the oscillating square cylinder at different amplitudes were relatively low. The information indicates that the value of C_D gets reduced when oscillation is applied to the square cylinder. The value of coefficient of drag is low for the amplitude of 0.03 m and is found to be very high for the amplitude of 0.04 m. The value of C_D for the oscillating cylinder with amplitude of 0.03 m is 3.25 and is seen to be less than the value for the stationary cylinder.

8.3.2.2 Effect of Lift

Coefficient of drag does not adequately describe the instability of the structure and provides only the component of force in the flow direction. Lift force on the structure can provide more information the changes of fluid flow characteristics as shown in Figures 8.7(a) and (b).

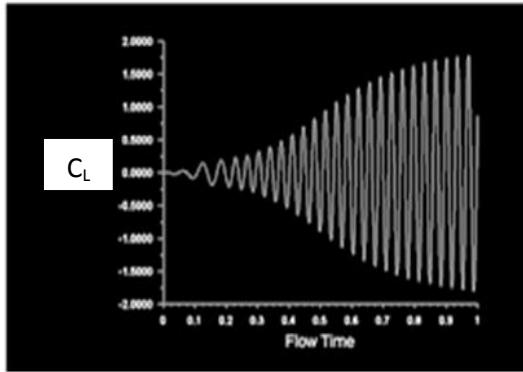


Fig. 8.7(a) C_L with flow time
(Non-oscillating case)

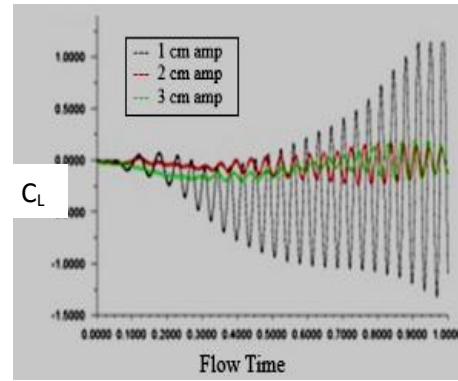


Fig. 8.7(b) C_L with flow time
(With oscillation amplitudes)

The value of C_L for the stationary square cylinder is 0.856 and the same for the oscillating square cylinder for 0.01m amplitude and frequency of 1Hz. is -1.082. It indicates that the value of the coefficient of lift gets reduced when the structure is put on oscillations. In the investigation of oscillating square cylinder method, the favourable value for the amplitude of oscillation is 0.03 m. For higher values of amplitudes beyond 0.3 m, C_L recorded abnormal values and hence discarded.

8.3.2.3 Variation of Strouhal number with amplitude of oscillations

The vortex shedding frequency for stationary cylinder was 30.86 Hz. and same for oscillating square cylinder having 0.01m amplitude was 28.75 Hz. This clearly indicates that the vortex shedding is suppressed by the above method. For amplitudes of 0.02 m and 0.03 m, the value of Strouhal frequency attained were 27.38 Hz and 26.13 Hz respectively. The Strouhal number obtained for the stationary cylinder was 0.16 and that obtained for the oscillating square cylinder was 0.143 m at 0.01 m amplitude. This further decreased with increase in amplitudes of oscillations as shown in Figures 8.8(a) and (b).

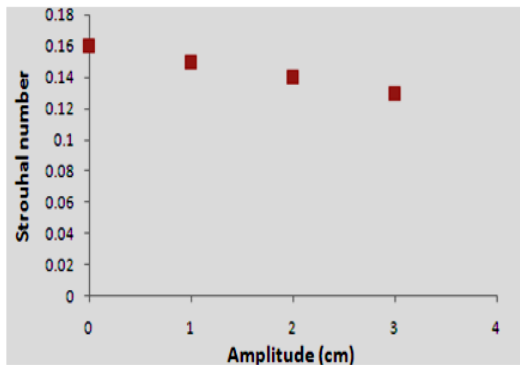


Fig. 8.8(a) Strouhal number with different amplitudes of oscillations

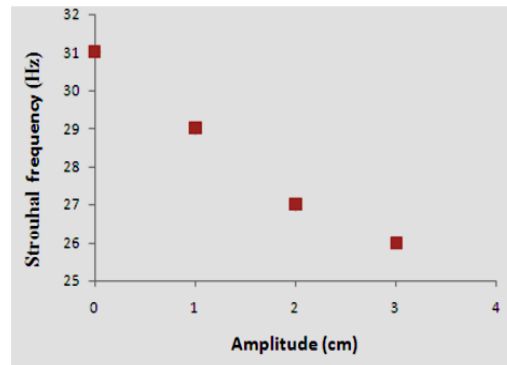


Fig. 8.8(b) Strouhal frequency with amplitudes of oscillations

The Strouhal number obtained for 0.02 m and 0.03 m amplitudes are 0.136 and 0.130 respectively. This trend in reduction of Strouhal number clearly indicates that the vortex shedding could be suppressed by this active method.

8.4 COMPARISON OF PASSIVE AND ACTIVE METHODS

Three-dimensional numerical simulations for fluid flow over a stationary square cylinder with an oscillating splitter plate in the wake at $Re=22000$ were carried out. Dynamic meshing was used to provide oscillations to the splitter plate in the wake. The flow characteristics were determined and compared with that of stationary and oscillating cylinders at the same Reynolds number.

8.4.1 Gridding strategy

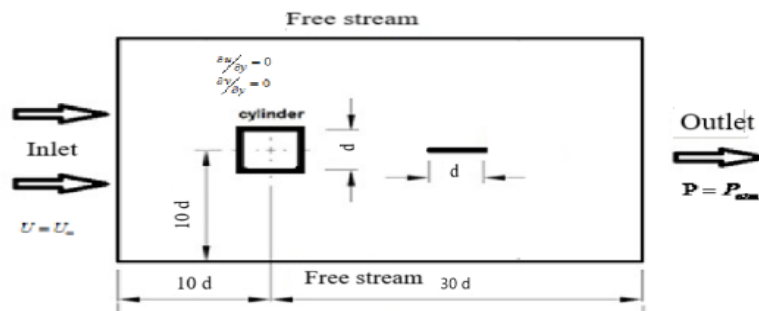


Fig. 8.9 Domain of fluid flow with boundary conditions

A domain $40d$ long and $20d$ wide was selected for simulation after conducting proper domain independence study. The splitter plate of length $1d$ and thickness $0.1d$ was used as the passive device. Appropriate boundary conditions were applied as in the previous cases. The grids were selected in such a way that the fluid parameters can be captured accurately.

9.4.2 Boundary Conditions

Computational domain indicating the boundary types and boundary conditions are shown in Figure 8.9. Table 8.2 provides the flow properties for the simulations.

Table 8.2 Flow Properties

Property	$P_{\infty}(Pa)$	$\rho_a(kg/m^3)$	$U_{\infty}(m/s)$
Value	101300	1.2255561	8.034

8.5 RESULTS AND DISCUSSION

The investigation for the fluid flow instabilities behind the structure was treated as three independent cases. Numerical simulation of fluid motion past a stationary cylinder was carried out first, followed by simulation for a cylinder with a stationary splitter plate in the wake. Then compound method (combination of active and passive methods) was employed by simulating a cylinder with an oscillating splitter plate in the wake at different amplitudes of oscillation and the results were compared with the earlier two cases.

8.5.1 Case 1: Cylinder without splitter plate in the wake – Baseline simulation

Numerical simulations were conducted with a flow velocity of 8.034 m/s. Figure 8.10 (a) shows that the fluid flow oscillation remains steady in the wake of the cylinder and undergoes a structural vibration perpendicular to the flow direction.

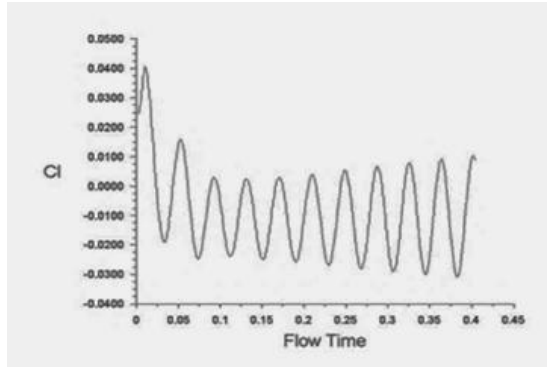


Fig. 8.10(a) Coefficient of lift with flow time

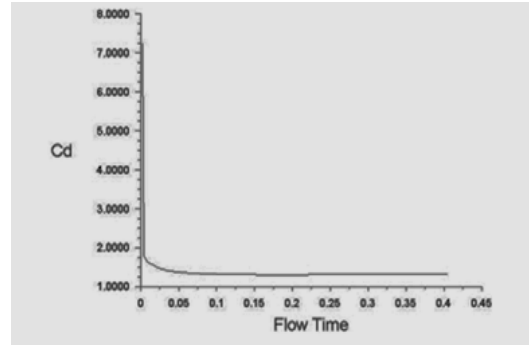


Fig. 8.10(b) Coefficient of drag with flow time

Figure 8.10 (b) indicates that the drag force on the cylinder due to the flow, varies in the initial stages and later attains a steady condition with in a short duration of time. Table 8.3 delivers the flow conditions over a cylinder without a splitter plate in the wake.

Table 8.3 Flow Parameters for a Stationary Cylinder

Drag Force (N)	Coefficient of drag	Lift force (N)	Coefficient of lift	Strouhal frequency (Hertz)	Strouhal number
1.038	1.313	0.004	0.005	26	0.152

Figure 8.11 clearly demonstrates the formation of distinct vortices in the wake of the cylinder. The Strouhal frequency is found to be agreeing well with the experimental works reported in the literature. The fact observed is that Strouhal number changes marginally with variation in Reynolds number.

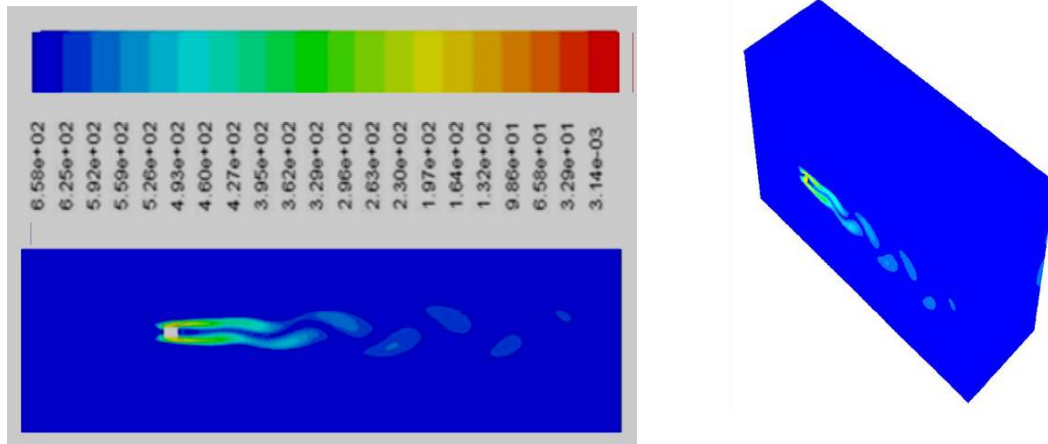


Fig. 8.11 Contours of vorticity magnitude in 2D and 3D

8.5.2 Case 2: Cylinder with a splitter plate in the wake – Passive method

A splitter plate was provided as a passive device in the rear of the cylinder to study the changes in the flow oscillations. Splitter plate of length $1d$ and thickness $0.1d$ was used for this investigation. The introduction of the splitter plate disturbs the fluid conditions in the wake noticeably. Since the upper layers of fluid is prevented from any interaction with bottom layers, drag and lift forces are modified significantly. A decrease in Strouhal frequency was detected and a reduction in VIV was attained.

The computations were carried out with the same fluid velocity at inlet and atmospheric pressure at the outlet as in the earlier cases. Figures 8.12(a) and (b) show the variations in lift and drag forces with the introduction of a stationary splitter plate in the wake. The new flow constraint is seen to influence the lift forces significantly.

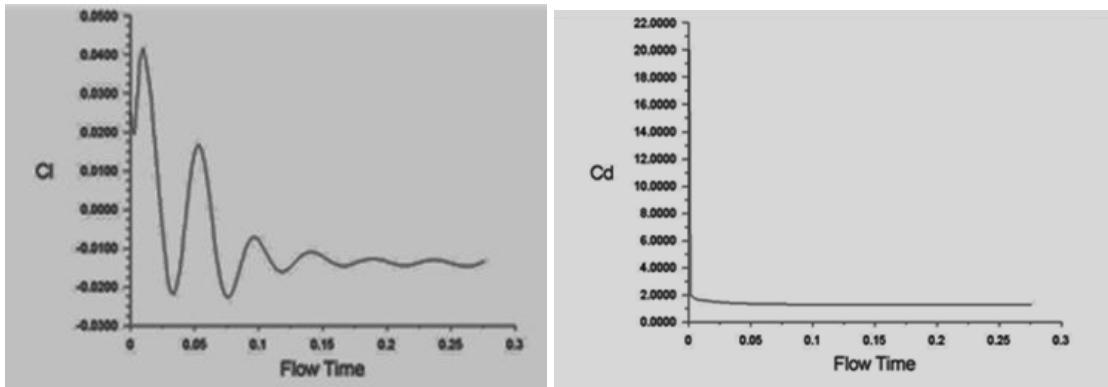


Fig. 8.12(a) Coefficient of lift with time Fig. 8.12(b) Coefficient of drag with time

The vorticity contours plotted in Figure 8.13 show that significant disturbances are created in the wake of the cylinder by the introduction of the splitter plate. These flow disturbances contribute to the reduction of VIV acting on the cylinder.

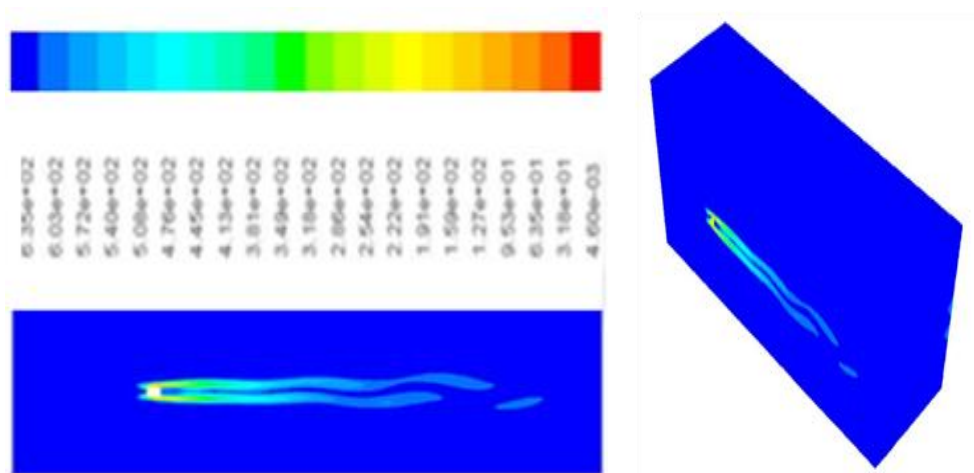


Fig. 8.13 Contours of vorticity magnitude in 2D and 3D

Table 8.4 provides flow parameters for flow past the cylinder with a splitter plate in the wake. With the introduction of the splitter plate in the wake, the Strouhal frequency has decreased to a low value. The presence of the splitter plate prevents the fluid masses from getting detached from either side of the cylinder due to fluid layer interactions. This causes alterations in flow conditions in the wake resulting in the reduction of VIV acting on the cylinder, and thereby a low Strouhal number.

Table 8.4 Flow parameters for a stationary splitter plate

Drag Force (N)	Coefficient of drag	Lift force (N)	Coefficient of lift	Strouhal frequency (Hertz)	Strouhal number
1.00	1.265	-0.0104	-0.013	17	0.10

8.5.3 Case 3: Cylinder with an oscillating splitter plate– Compound method

The compound method for the suppression of VIV effectively combines the use of the passive device in the wake and providing oscillations to the same, making it an active method. The investigation was carried out by employing the compound method with the same flow conditions. Oscillations with amplitude ranging from 0.0025 m to 0.02 m and frequency of 1 Hertz were applied to the splitter plate. The oscillating splitter plate was highly effective in disturbing the fluid layers on both sides of the wake region. Hence the generation of distinct vortices and their detachment from either side of the structure is reduced by an unusual level. This effect leads to the reduction in VIV and is asserted by the numerical investigation. The vorticity magnitude contours shown in Figure 8.14 depicts the change in flow conditions in the wake of the cylinder. When the amplitude is increased to larger values, the entire fluid flow in the domain gets disturbed, and the Strouhal frequency increases to a much larger value that exceeds the value obtained for a bare cylinder placed in the same flow conditions.

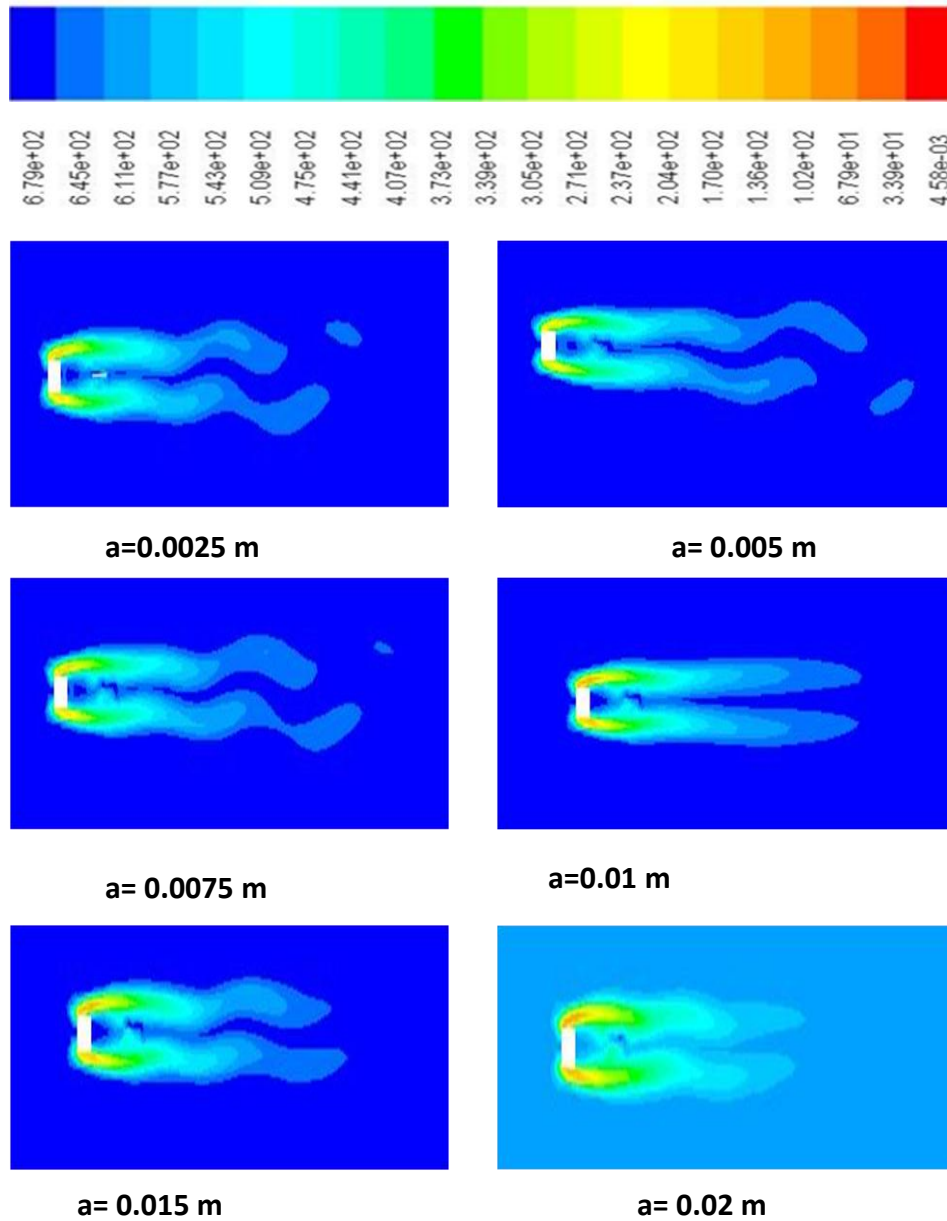


Fig. 8.14 Vorticity magnitude contours at different amplitudes of oscillation

At low amplitudes of oscillation, the investigation showed a significant effect on the reduction of vortex induced vibration whereas at high amplitudes of oscillation, reverse trends in fluid flow characteristics was observed as tabulated in Table 8.5. At low amplitudes, the presence of the splitter plate in the wake prevents the fluid layers from interactions in the downstream direction. Observations revealed that mild oscillations of the plate disturbs the flow in a controlled manner and hence

instrumental in attaining low VIV. However, with further increase in amplitude, the fluid layers get disturbed to extraordinary levels. These interactions of turbulent wake with the cylinder have high intensity which attributes to the increase in VIV.

Table 8.5 Flow parameters at different amplitudes of oscillation

Reynolds Number	Amplitude (m)	C_L	C_D	St
22000	0.0025	-0.018	1.307	0.095
	0.005	-0.0198	1.398	0.075
	0.0075	-0.0188	1.309	0.042
	0.01	-0.017	0.296	0.052
	0.015	-0.0165	1.317	0.15
	0.2	-0.0197	1.323	0.17

The changes in Strouhal number with amplitude of oscillation are shown in Figure 8.15. The amplitude was varied between 0.0025 m to 0.02 m. The study confirmed a decreasing trend in Strouhal frequency with escalating amplitudes of oscillation up to a certain limit. It is definitely due to the presence of a splitter plate which has mild oscillation and placed in the rear of the cylinder. Fluid layers detaching from both sides of cylinder prevent them from interacting with each other due to the presence of this oscillating member. Hence the vortex formation seems to decrease, and a corresponding reduction in Strouhal frequency was registered. However, if the amplitude of oscillation is increased beyond a certain limit, a gradual increase in Strouhal frequency is observed. The oscillating plate is instrumental in producing a highly turbulent wake, and fluid layers from both sides interact behind

the splitter plate. The flow parameters in the entire domain are influenced by this phenomenon and sharp variations in the flow parameters in the rear of the cylinder are observed.

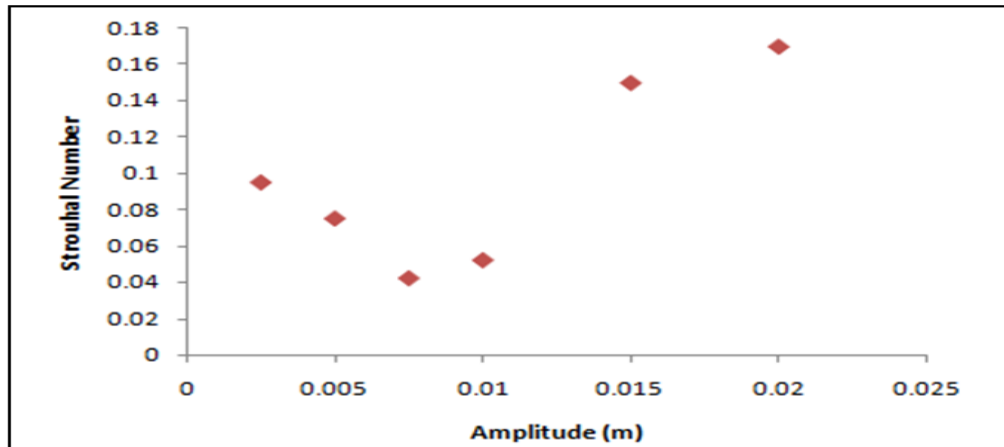


Fig. 8.15 Strouhal number with different amplitudes of oscillation

8.6 SUMMARY

Numerical study on flow past both stationary square cylinder and the oscillating square cylinder has been carried out to get an insight into the effect of oscillation provided to the structure to suppress the vortex induced vibrations. It is observed that the oscillation of the square cylinder considerably suppresses the vortex shedding phenomenon. Simulations were performed for the oscillating square cylinder at different amplitudes of oscillation provided to the structure. Strouhal frequency is found to reduce with increase in amplitudes of oscillation. Beyond certain amplitude, both the coefficient of drag and coefficient of lift shows some unrealistic values. Hence amplitudes less than 0.03 m are considered to be a favourable value of oscillation that could prevent the structure from VIV.

Fluid flow characteristics due to shear layer instability during a flow past a structure with and without stationary and oscillating splitter plate were also investigated. The compound method, which combines the effect of both passive and active controls for the suppression of vortex induced vibration, was employed. The oscillating splitter plate placed in the wake effectively interrupts the formation of vortex shedding and the wake becomes more and more turbulent. A reduction in Strouhal frequency along with diminished vortex shedding phenomenon was observed due to forced oscillations of the splitter plate. The fluid layers getting detached from both sides of the cylinder were prevented from interacting with each other in the wake region. At low amplitudes of oscillations, this method reduces the Strouhal frequency to a much lesser value and this control measure is found to be effective in the suppression of VIV. However, at higher amplitudes, the simulation recorded strong vibrations initiated by the highly turbulent wake. Since the compound method resulted in substantial reduction in the Strouhal frequency, this method is found to be superior to both active and passive methods when enacted separately. The advantage of passive method is that it can be permanently fixed on the surface of the structure, without any aid of external energy for its functioning and provides reasonable reduction in vortex induced forces. Although active method requires external energy for its proper functioning, better results are obtained when it is used in conjunction with passive devices. Hence the concept of compound method may be highly effective in preventing the damage to tall structures and underwater applications that is subjected to hefty fluid loads across them.

CHAPTER - 9

AN INVESTIGATION ON REDUCTION OF VORTEX INDUCED LOADS ON TALL CHIMNEYS AND MARINE RISERS

9.1 INTRODUCTION

Tall chimneys, when subjected to hefty wind loads across them, undergo structural failure catastrophically. Similar is the case of deep marine risers subjected to harsh ocean currents. The complex vortex dynamics in and around towering cylindrical structures is a critical challenge for the designers. As the formation and development of VIVs cause severe safety issues to the entire industrial setup, the reduction of shear layer instability emerged as an area of intense research. Constant and harsh currents that flow across long cylindrical structures often lead to the initiation of vortex shedding phenomenon around them. These structures were then subjected to both drag and lift forces. The lift force on the structure is instrumental in the development of structural vibrations across the flow direction. In due course, when the vortex shedding frequency comes in resonance with the natural frequency, the structure vibrates violently that can challenge the safety and life of the structure.

The numerical investigation on structures with and without structural modifications can impart precise information of the alterations in fluid flow characteristics around them. The reduction and control of VIVs are essential to save marine risers and tall chimneys against all odd currents. A computationally, less expensive RANS simulation was used to estimate the changes in flow characteristics. The flow was presumed to be predominantly turbulent and incompressible in the flow field. Shear Stress Transport (*SST*) $k-\omega$ turbulence model was used to capture the

turbulent characteristics accurately and the simulation carried out using CFD software. The response of the structure to fluid currents was probed for same velocity on a bare structure and one fitted with the passive device.

9.2 COMPUTATIONAL FLOW DOMAIN FOR A CHIMNEY

9.2.1 Chimney

A chimney with an overall height of 180 m, as shown in Figure 9.1 was considered for analysis under wind loads. Outer diameter (d) of the shell was constant and was equal to 10 m. A triple start helical strake was mounted on the chimney to a length of 60 m from the top, to counter undesired wind loads. The section of chimney length chosen for analysis was 20 m. A strake of pitch $2d$, height $0.1d$, and thickness $0.01d$ was used to control crosswind vibrations.

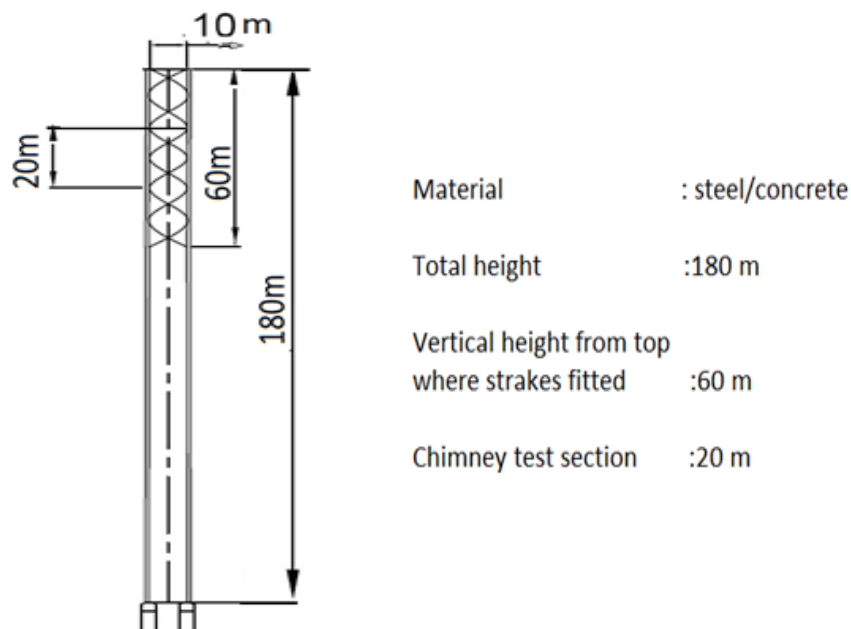


Fig. 9.1 Chimney

9.2.2 Simulation Parameters

Three dimensional numerical simulations were performed on a chimney with and without triple start helical strakes. The diameter (d) and length (L) of the cylindrical chimney were 10 m and 180 m respectively. The helical strakes of constant pitch and height were used for numerical simulation in this investigation. Since the Mach number was less than 0.3, the fluid flow was presumed to be incompressible.

9.2.3. Computational domain and mesh

A domain of length $40d$ and width $10d$ was used as flow field as shown in Figure 9.2 after domain independence study. The height of the section of the chimney taken for analysis is $h = 2d$. Numerical simulations were conducted to determine the optimum domain size and number of grids required in the domain. It was observed that the magnitude of lift force has a constant value for the number of cells beyond 0.8 million and hence, a grid of 0.8 million cells was selected for the present computational study.

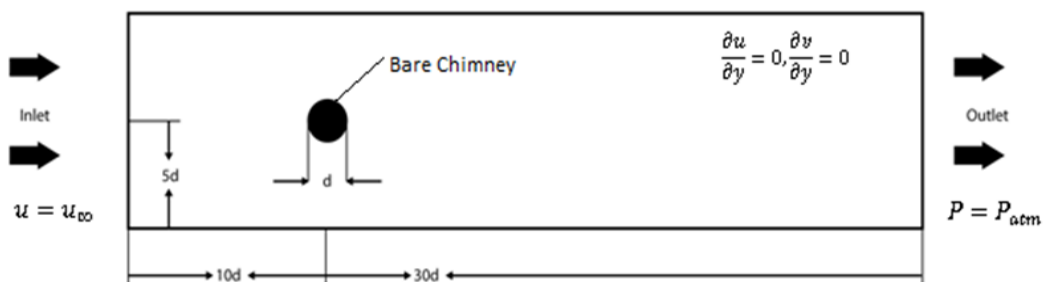


Fig. 9.2 Computational domain for a chimney without strakes

9.2.4 Boundary Conditions

Boundary conditions of ‘velocity inlet’ and ‘pressure outlet’ were applied at the inlet and outlet respectively. Table 9.1 specifies the inlet conditions for both cases.

Table 9.1 Flow properties

Property	$P_{\infty} (Pa)$	$\rho_a (kg / m^3)$	$U_{\infty} (m / s)$
Magnitude	101300	1.225	10

9.3 RESULTS AND DISCUSSION

9.3.1 Flow characteristics across a chimney without strakes

Numerical simulations were carried out to study the flow parameters for a wind current past a bare chimney. The effect of wind loads on the chimney was examined in terms of dimensionless Strouhal number. VIV increased marginally with increase in wind speed. The predictions are in reasonable agreement with the experimental measurements reported in the literature.

Simulation details:

- Velocity = 10 m/s
- Characteristic length = 10 m
- Numerical simulation: 3D, Transient, RANS
- Turbulence model: *SST k- ω*

- Condition : Free stream.
- Outlet Pressure: Atmospheric pressure.

A flow velocity of 10 m/s was used in the numerical simulation. Figure 9.3(a) shows that the flow oscillations have a definite pattern in the wake of the cylinder inducing a structural vibration perpendicular to the flow direction. Figure 9.3(b) indicates a drag force on the cylinder, which has a huge variation in the initial stage and attains a steady level and a definite pattern at later stages.

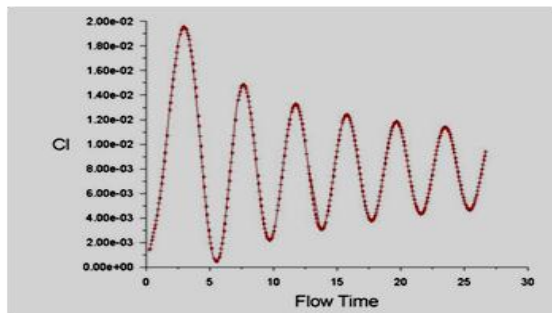


Fig. 9.3(a) Coefficient of lift with flow time

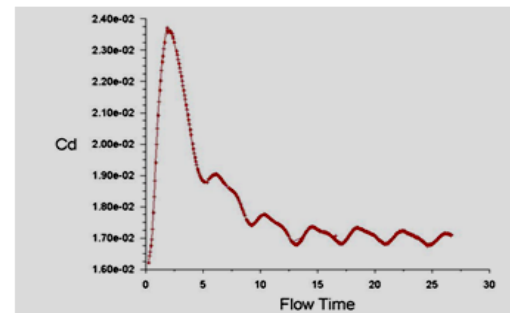


Fig. 9.3(b) Coefficient of drag with flow time

Figure 9.4 shows the variation in pressure distribution throughout the domain. A low pressure zone formed in the wake of the cylinder has resulted in the flow separation from the structure and initiation of vortex shedding. The fluid undergoes oscillations resulting in shear instabilities due to the enormous pressure drop in the wake of the cylinder. As the fluid becomes slower and slower, the fluid layer near the chimney tends to get separated from the top and bottom surfaces of the cylinder alternatively, inducing VIV of the structure. The presence of an adverse pressure gradient contributes to this effect. The distribution of static pressure illustrates the formation of a low pressure zone in the wake of the cylinder. When the flow strikes

the cylinder, the pressure attains a maximum value but immediately undergoes a substantial drop in the wake of the cylinder. The pressure plot shown in Figure 9.4 clearly indicates that immediately after the chimney, there is an abrupt change in the pressure resulting in a highly turbulent wake.

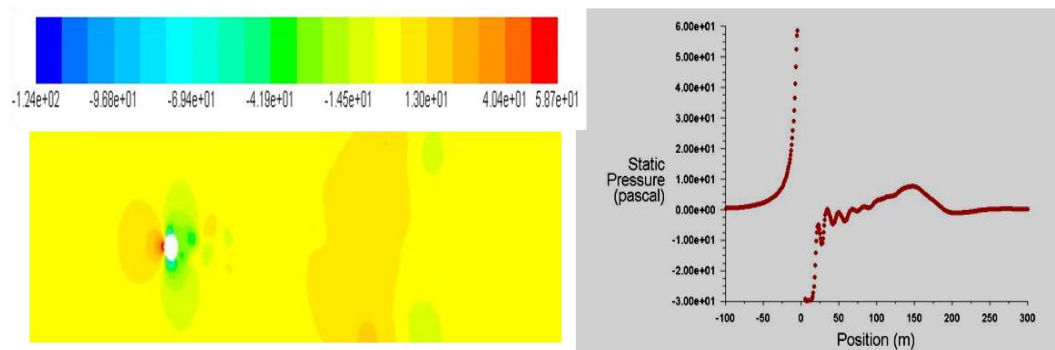


Fig. 9.4 Pressure distributions in the central plane

Figure 9.5 shows the velocity variations in the central plane. The wind on striking the chimney attains a stagnation condition, and it restores its velocity only towards the end of the domain. The velocity profile clearly confirms that the velocity has reduced to zero on striking the cylinder and regains magnitude towards the exit of the domain. Similar to the pressure distribution, abrupt velocity fluctuations are also seen in the wake of the cylinder. The formation of vortices from the sides of the chimney is mainly responsible for the velocity fluctuations.

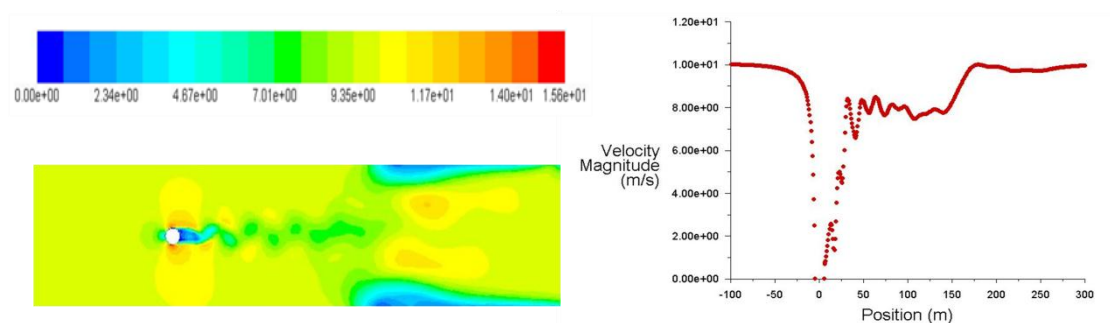


Fig. 9.5 Velocity distributions in the central plane

Figures 9.6(a) and (b) show vortex shedding phenomenon where distinct vortices are getting detached from both surfaces of the cylinder alternatively. The vortices formed resembles Von Karman vortex street. Initially, large vortices are produced and as it moves away from the chimney slowly disintegrates into smaller vortices and finally diffuses into the medium due to an increase in the internal energy of the fluid.

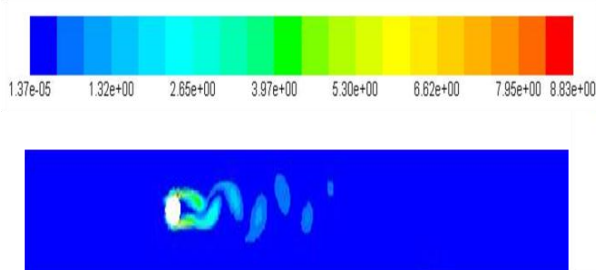


Fig. 9.6(a) Contours of vorticity magnitude

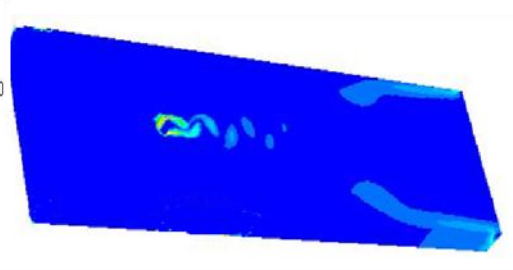


Fig. 9.6(b) 3D view

The Strouhal frequency and Strouhal number are presented in Figures 9.7 (a) and (b). The Strouhal frequency is computed with the help of Fast Fourier Transform (FFT) and Strouhal number is estimated based on the diameter of structure and inlet velocity of the flow. The Strouhal number is estimated as 0.24 corresponding to a wind velocity of 10 m/s. This value is in reasonable agreement with the experimental data for circular cylinders of smaller diameters available in the literature.

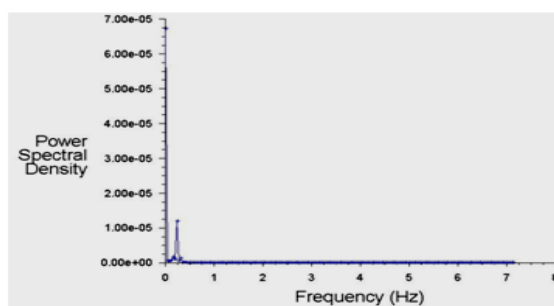


Fig. 9.7(a) Strouhal frequency

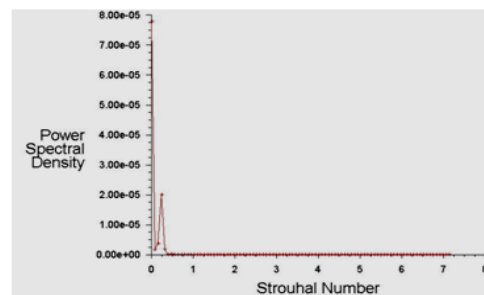


Fig. 9.7(b) Strouhal number

The different parameters in the flow field for flow past a bare chimney is tabulated in Table 9.2. The Strouhal number was marginally higher than the experimental values available in the literature for fluid flow past a cylinder of smaller dimensions. The increased velocity and increased rate of the detachment of vortices from the structure might have contributed to this high value of Strouhal number. If this value is close to the natural frequency of the structure, the structure may collapse eventually. Hence the suppression of VIV becomes the significant challenge for the engineers to design tall chimneys. Many researchers in this field have suggested that surface protrusion devices can suppress these vortex shedding and reduce the magnitude of VIV. One of the passive devices that can reduce VIV is helical strakes that can be attached on the outer surface of the chimney.

Table 9.2 Flow characteristics across a circular chimney without strakes

Drag (N)	Coefficient of drag	Lift (N)	Coefficient of lift	Strouhal frequency (Hz)	Strouhal number
6616.67	0.017	1472.37	0.0038	0.24	0.24

9.3.2 Flow over chimney with triple start helical strakes at a velocity of 10 m/s

3D numerical simulation was performed for a tall chimney fitted with helical strakes on one-third of its entire length. Triple start helical strakes of $2d$ pitch and $0.1d$ height were used in all simulations. The chimney section of length $2d$ with strakes was chosen for analysis.

Simulation details:

- Velocity = 10 m/s
- Outer diameter = 10 m
- Strakes: Triple start helical, pitch $2d$, height $0.1d$ and thickness $0.01d$
- Numerical simulation: 3D, Transient, RANS
- Turbulence model: SST $k-\omega$
- Condition: Free stream
- Outlet Pressure: Atmospheric pressure

Figure 9.8 shows the cross-sectional view of the domain. The domain is the same as the domain for a bare chimney except for the inclusion of the chimney with triple start helical strakes in place of the bare chimney. The numerical simulation was carried out with the same boundary conditions,

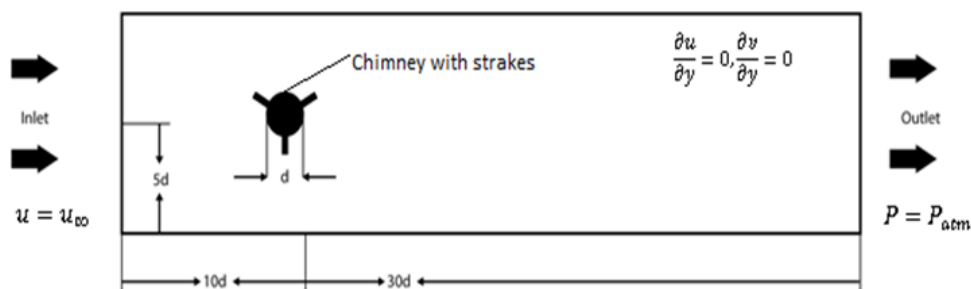


Fig. 9.8 Computational domain for a chimney with strakes

The variation in the flow field was probed by observing various flow parameters. When the fluid flows past the cylinder with helical strakes, fluid layer

close to the cylinder surface was disturbed by the helical fins protruding from the chimney surface to a large extent. Small vortices formed around the structure close to the strakes are found to be out of phase with one another and leads to partial cancellation of the forces at different span-wise positions. It could be observed that small vortices formed near the strakes on the chimney surface are not significant and the lift forces developed with strakes are much smaller than that of a bare chimney.

The helical pattern of the strakes induces a span-wise motion for the fluid while it flows around the chimney surface. This flow produces a swirling motion for the fluid in the rear of the chimney and disrupts the span-wise vortex shedding within a small extent. It was noted that the strength of these swirls is instrumental in the partial cancellation of vortex formation at different points. The flow characteristics past a chimney fitted with helical strakes show significant variation when compared with that of fluid flow past a bare chimney. There is tremendous interaction between the rotating masses of fluid around the chimney leading to a significant reduction of the flow separation and vortex induced vibration.

Figure 9.9 indicates that the values of the coefficient of lift and drag observed with strakes are generally different from that of a chimney without strakes. The magnitudes of C_L and C_D are undergoing abrupt changes when the fluid flows past the chimney with strakes. The nature of the curve has an entirely different pattern when compared to that of a bare chimney

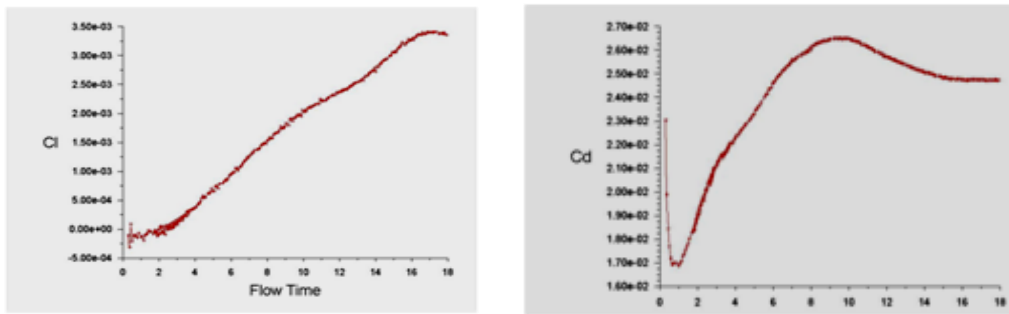


Fig.9.9 Coefficient of lift and drag with flow time

Figure 9.10 describes the pressure distribution in the central plane of the chimney flow field. The formation of a well defined low pressure zone is prevented in the wake of the structure by the presence of strakes. Pressure plot demonstrates that the pressure regains the original magnitude smoothly in the wake region in contrast to abrupt changes observed for a chimney without strakes.

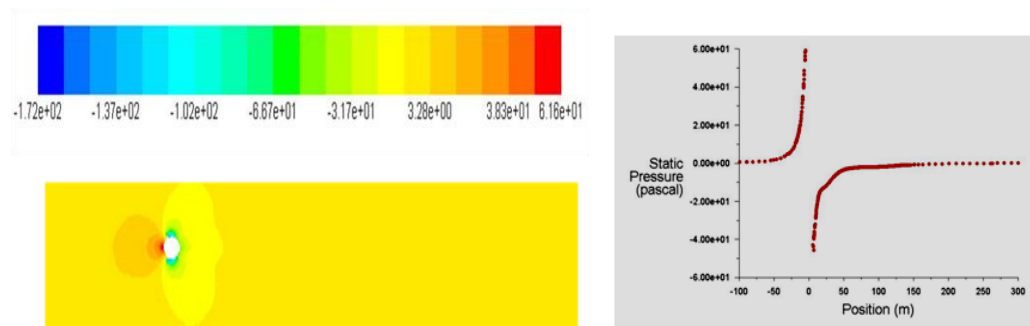


Fig. 9.10 Pressure distribution in the central plane

Figure 9.11 shows the velocity distribution in the central plane for fluid flow past a cylindrical chimney structure with strakes. The velocity plot depicts that restoration of velocity is smooth in the wake due to the presence of strakes.

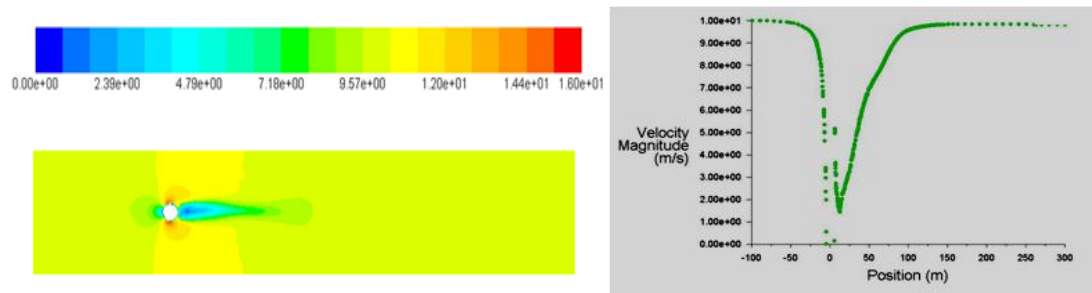


Fig. 9.11 Velocity distribution in the central plane

The contours of vorticity magnitude shown in Figures 9.12(a) and (b) clearly illustrate the absence of distinct vortex shedding pattern during the fluid flow past a chimney with strakes. The small localised vortices found around the strakes have a relatively small contribution to the formation of VIV.

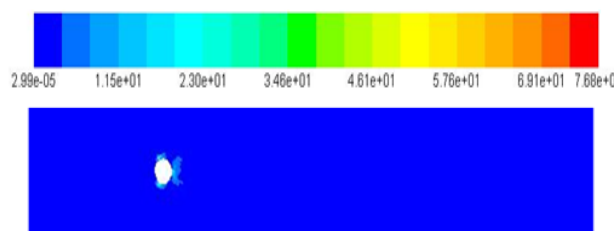


Fig. 9.12(a) Contours of vorticity magnitude in central plane



Fig. 9.12(b) 3D view

The resultant Strouhal number and Strouhal frequency were shown in Figures 9.13 (a) and (b) respectively. The Strouhal frequency estimated with the help of Fast Fourier Transform shows that there is a significant reduction in the frequency of VIV when compared with that of a bare chimney. The reduction in these parameters is due to the existence of the helical strakes 360° around the chimney.

Since the effect of helical strakes is omni-directional, the partial cancellation of vortices formed around the circumference, occurs all along the length

of the strakes. It results in the suppression of vortex shedding from all the sides of the chimney. The vortices formed in one plane tend to get cancelled by the other vortices formed in another plane. As a result, the strength of vortices detaching from the chimney surface diminishes, and the VIV was found to reduce significantly. The smaller vortices formed all along the length of strakes contributes less momentum in the formation of vortex shedding. This phenomenon results in the reduction of Strouhal frequency and VIV.

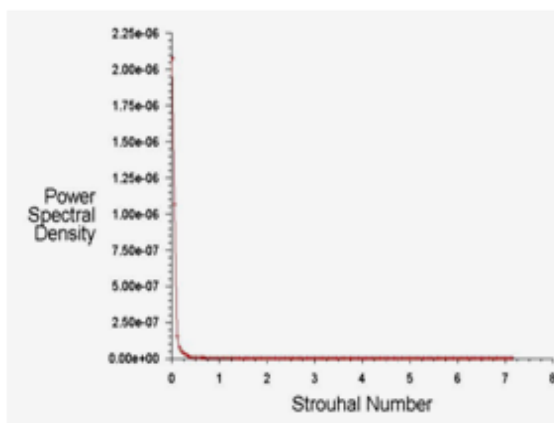


Fig. 9.13(a) Strouhal number

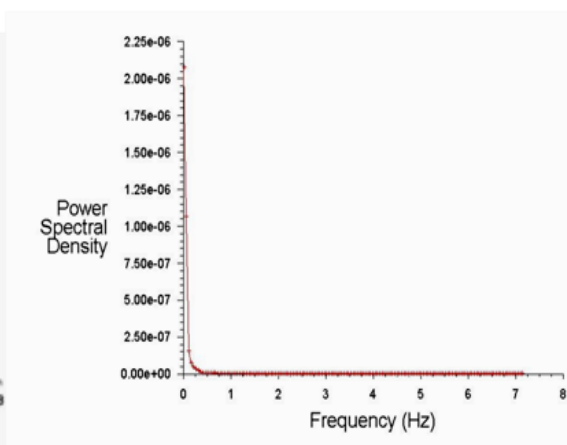


Fig. 9.13(b) Strouhal frequency

The flow parameters for fluid flow past a chimney with helical strakes were shown in Table 9.3. There is a significant reduction in lift along the flow field when compared with that of a bare chimney. The coefficient of lift also marked a decreasing trend. Both Strouhal frequency and Strouhal number registered sharp decline in magnitude. There is no drag crisis as reported by Huang (2011), and an increase in drag was not observed. The decrease in magnitude of Strouhal frequency ensures reduction in VIV to a much lesser value by the presence of helical strakes. Since the effect of helical stakes is omni-directional, it can disturb the fluid flow all along the length in all the planes around the structure. The partial cancellation of momentum of

fluid masses, leaving the structure happens simultaneously, and the frequency of vortex shedding reaches a minimum value. A reduction in Strouhal number of approximately 78.33% was attained with the presence of strakes.

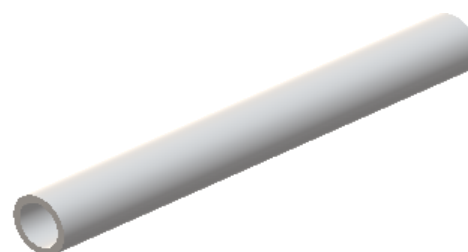
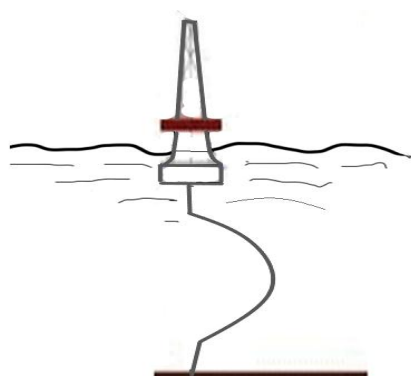
Table 9.3 Flow characteristics across a circular chimney with strakes

Drag (N)	Coefficient of drag	Lift (N)	Coefficient of lift	Strouhal frequency (Hz)	Strouhal number
6509.31	0.025	1275.89	0.0033	0.052	0.052

9.4 COMPUTATIONAL DOMAIN FOR A MARINE RISER

9.4.1 Marine Riser

A marine riser with 0.4 m diameter and height 100 m, as shown in Figure 9.14 was considered for analysis with loads due to ocean currents on them. Outer diameter (d) of the riser is constant. A suitable modification of structure can reduce damage due to constant ocean currents by preventing vortex shedding. The structure modified with dimples on the surface provided all along its length was used in this investigation.



Material: Steel, Aluminium, Titanium
 Length: 100 m – 3000 m
 Diameter: 0.4 m- 0.8 m

Fig. 9.14 Marine riser

9.4.2. Domain and mesh selection

A domain of length $40d$ and width $10d$ was used for calculations as shown in Figure 9.15 after conducting domain independence study, where d is the diameter of the circular cylinder. The height of the section of the marine riser taken for analysis is $h = 0.5$ m. Numerical simulations were conducted to determine the optimum domain size and number of grids required in the domain. It was observed that drag force has a constant value for the number of cells beyond 1.16 million, and hence a grid of approximately 1.2 million cells was chosen for the present computational study.

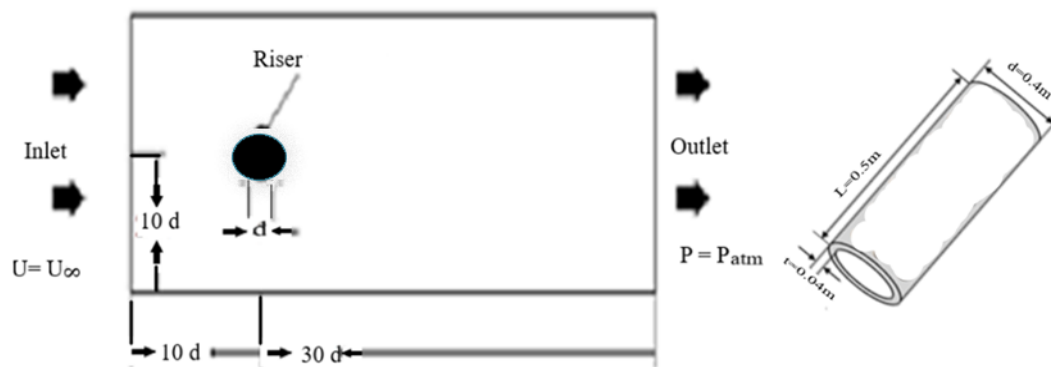


Fig. 9.15 Computational flow domain for a bare marine riser

9.4.3 Boundary Conditions

Boundary conditions were suitable assumed at inlet and outlet of the domain.

Table 9.4 shows the flow properties for both cases.

Table 9.4 Fluid flow properties

Property	$P_{\infty} (Pa)$	$\rho_a (kg / m^3)$	$U_{\infty} (m / s)$
Value	101300	998.2	1

9.5 RESULTS AND DISCUSSION

9.5.1 Flow characteristics for fluid flow across a marine riser without dimples

Three dimensional numerical simulations were carried out to study the effect of flow parameters for ocean currents past a bare marine riser. The effect of these flow loads on riser was analysed in terms of different fluid flow parameters. The VIV increased marginally with an increase in flow speed. The results are in reasonable agreement with the experimental data for similar cylindrical structures available in the literature.

Simulation details:

- Velocity = 1 m/s
- Characteristic length = 0.4 m
- Numerical simulation : 3D, Transient, RANS
- Turbulence model = *SST k- ω*
- Condition: Free stream
- Outlet pressure: Atmospheric pressure

It is observed in Figure 9.16(a) that the flow oscillations have a definite pattern in the wake of the cylinder inducing a structural vibration perpendicular to the flow

direction at a velocity of 1 m/s. The corresponding drag on the cylinder as indicated in Figure 9.16 (b) has considerable variation in the initial stages and later attains a steady level.

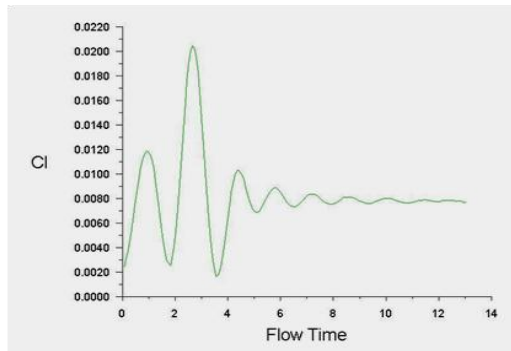


Fig. 9.16(a) Coefficient of lift with flow time

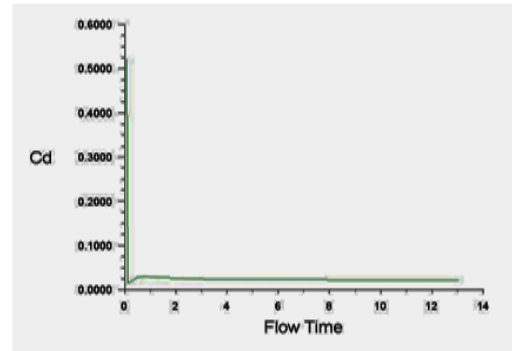


Fig. 9.16(b) Coefficient of drag with flow time

The variation in pressure distribution throughout the domain is shown in Figure 9.17. As similar to the previous case, a low pressure zone formed in the wake of the cylinder has resulted in the flow separation from the structure and thereby initiating vortex shedding. The fluid layer near the riser tends to get separated from top and bottom surfaces alternatively due to the immense pressure drop in the wake of the cylinder inducing VIV on the structure due to the strong adverse pressure gradient. The abrupt change in the pressure resulting in a highly turbulent wake immediately after the structure is depicted in Figure 9.17.

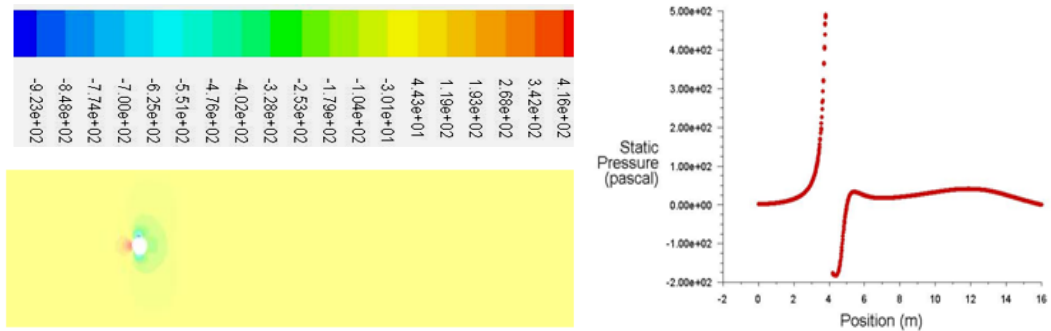


Fig. 9.17 Pressure distribution in the central plane

Velocity fluctuations similar to pressure distributions are detected in the wake of the cylinder as illustrated in Figure 9.18. The fluid on striking the marine riser attains a stagnation state before restoring its velocity towards the end of the domain. The formation of vortices due to the difference in momentum between layers initiates the instability.

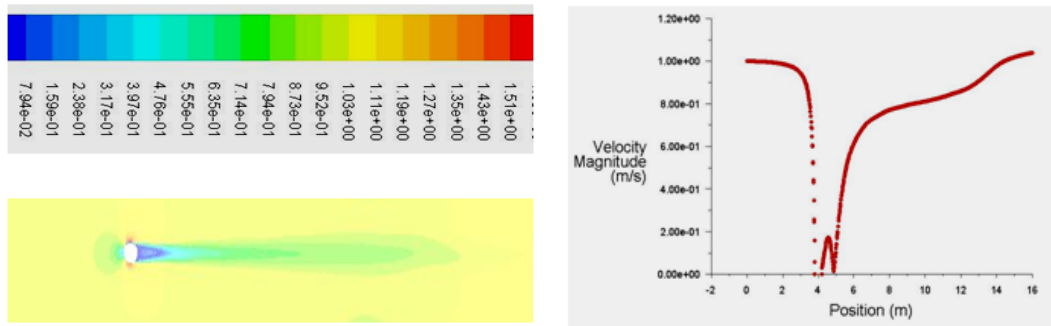


Fig. 9.18 Velocity distribution in the central plane

The vortex shedding phenomenon as displayed in Figures 9.19(a) and (b) indicates the detachment of vortices from both sides of the cylinder aligned as a continuous stream along the cylinder. Initially, large vortices are formed and as it moves away from the structure, gets aligned into single separate streams and finally diffuses into the fluid medium.

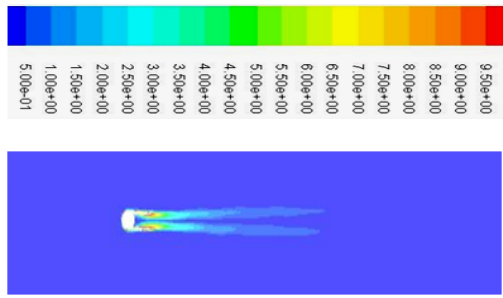


Fig. 9.19(a) Contours of vorticity magnitude

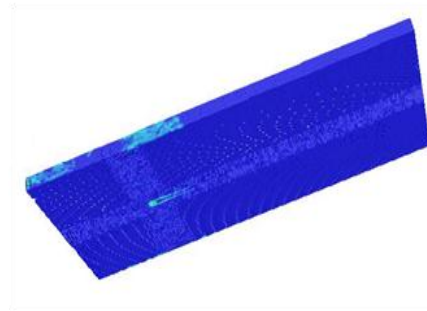


Fig. 9.19(b) 3D view

The Strouhal frequency was computed by converting time domain to frequency domain using Fast Fourier Transform (FFT) available in the software, and Strouhal number was estimated. The Strouhal number estimated as 0.22 for a flow velocity of 1 m/s. This value is in reasonable agreement with the experimental data for cylindrical structures of smaller diameters reported in the literature. The Strouhal frequency and Strouhal number with flow time are shown in Figures 9.20(a) and (b) respectively.

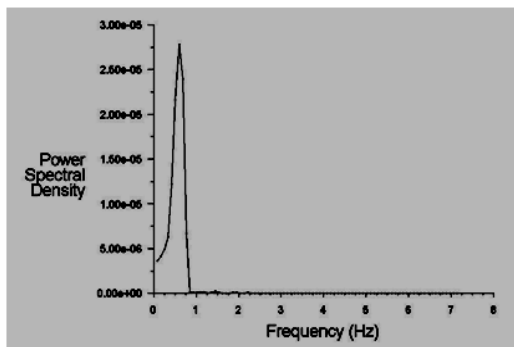


Fig. 9.20(a) Strouhal frequency

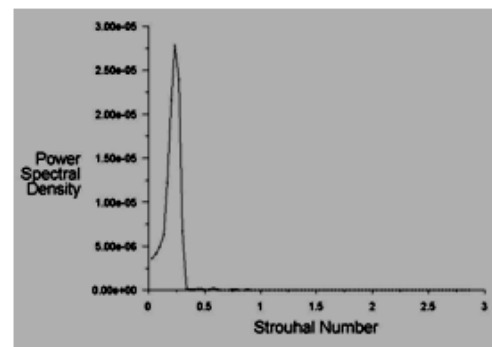


Fig. 9.20(b) Strouhal number

The flow parameters pertaining to lift, drag and their coefficients for a flow past a bare marine riser is tabulated in Table 9.5. The increased rate of detachment of vortices from the structure and large size of the structure may be the reason for

enhancement in Stouhal number. If this value is close to the natural frequency of the structure, structure may fail prematurely. Many researchers have suggested that surface protrusion or depression devices can suppress these vortex shedding phenomenon and reduce the magnitude of VIVs. Engraving dimples on a surface create a thin turbulent boundary layer of fluid that clings to the outer surface of the structure. Hence this novel concept of depressions on the surface with dimples have been tried and analysed in the subsequent sections.

Table 9.5 Flow characteristics across a bare marine riser (without dimples)

Drag (N)	Coefficient of drag	Lift (N)	Coefficient of lift	Strouhal frequency (Hz)	Strouhal number
38.189	0.022	12.985	0.0076	0.55	0.22

9.5.2 Flow over marine riser with dimples on the surface at a velocity of 1 m/s

Numerical simulations were performed in 3D for a long marine riser arranged with dimples all along the surface. A section of marine riser of 0.5 m length with distinct dimples of $0.1d$ diameter and $0.05d$ depth was taken for investigation.

Simulation details:

- Velocity = 1 m/s
- Outer diameter = 0.4 m
- Dimples: Hemispherical, Diameter = $0.1d$, Depth = $0.05d$
- Numerical simulation: 3D, Transient, RANS

- Turbulence model: SST $k\omega$
- Condition: Free stream
- Outlet Pressure: Atmospheric pressure

The domain shown in Figure 9.21 is the same as the domain for a bare marine riser except for the inclusion of the dimples on the surface in a definite pattern. The numerical simulation was carried out with the same boundary conditions.

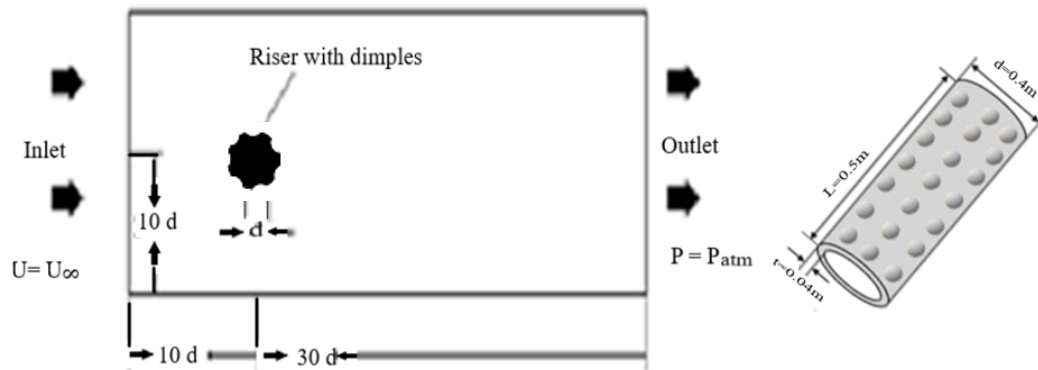


Fig. 9.21 Computational domain for marine riser with dimples on the surface

When the fluid flows past the cylinder with dimples, fluid layer close to the surface was disturbed mainly by the presence of hemispherical dimples on the riser surface. This allows the flowing fluid to get separated a little farther around the back side of the structure, thereby decreasing the size of the wake. Moreover, the tiny vortices that formed near the surface are not significant and the lift force developed for modified dimpled riser is much smaller than that of a bare cylinder.

It is observed that the flow over the surface of structure from the forward stagnation point results in a laminar boundary layer. The hemispherical depressions on the surface induce a complex motion for the fluid while it flows around the circular

surface. As the flow travels over the surface of structure without dimples it encounters an adverse pressure gradient created by the rear stagnation point causing the flow to separate readily from the structure, which in turn creates a large wake resulting in significant drag. When structure containing dimples on its surface is considered, the fluid enters the dimple, initiating pressure differential between the trailing edge region and leading edge region causing the fluid to circulate within the dimple and a cavity flow exists. However, the main flow passes over the cavity, while some enters the cavity and circulates creating turbulence with an amount of energy determined by the main flow. The circulation within the cavity takes place with a strength determined by the velocity gradients present in the cavity. A tremendous interaction between the rotating masses of fluid around the structure surface, leading to significant reduction of the flow separation and VIV is observed in Figure 9.22.

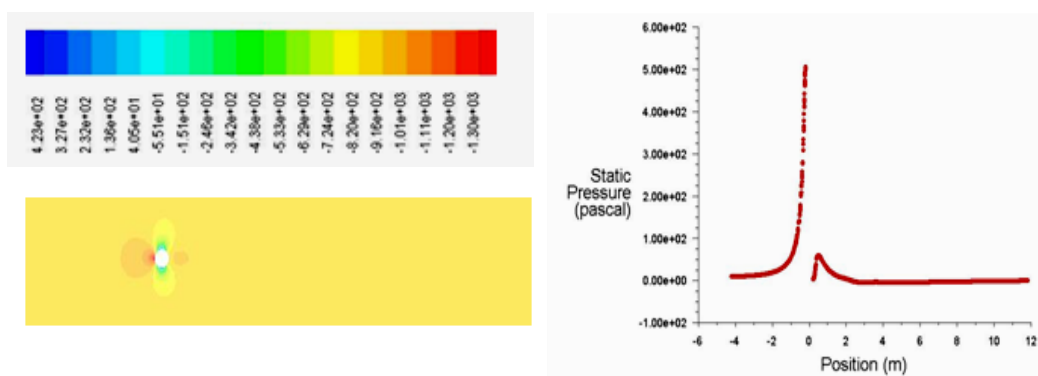


Fig. 9.22 Pressure distribution in the central plane

The velocity distribution in the central plane for fluid flow past a cylinder with a dimpled surface is depicted in Figure 9.23. The velocity plot depicts that restoration of velocity is perfectly smooth in the wake due to the presence of dimples. This may be due to the lesser dispersion of vortices upon leaving the cavity.

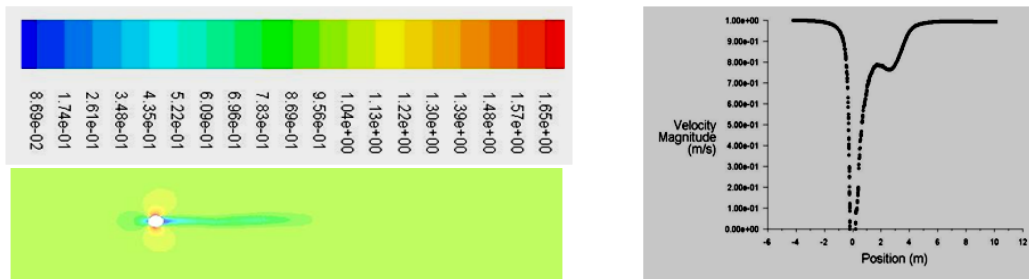


Fig. 9.23 Velocity distribution in the central plane

The contours of vorticity magnitude shown in Figures 9.24(a) and (b) highlight the non-appearance of vortex shedding during the fluid flow past a dimpled structure. Small localised vortices found around the hemispherical depressions with a negligible contribution to the formation of VIV are observed. It may be noted that the energy from the main flow is drained by the less dispersion vortices in the dimples as they leave the dimple cavities and mixing of these two flows occurs.

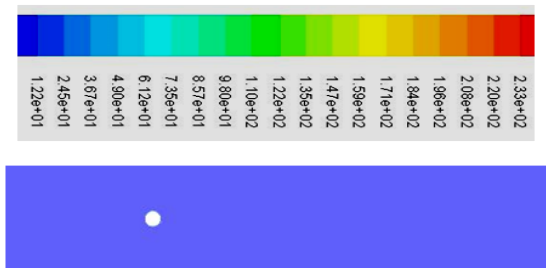


Fig. 9.24(a) Contours of vorticity magnitude in central plane

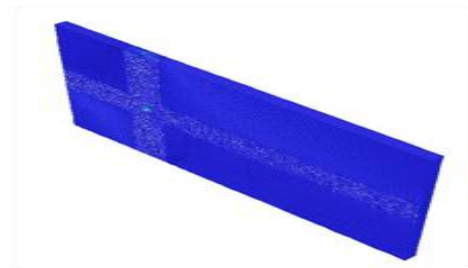


Fig. 9.24(b) 3D view

The resultant Strouhal number and Strouhal frequency are shown in Figures 9.25(a) and (b) respectively. The Strouhal frequency was estimated with the help of Fast Fourier Transform and a significant reduction in the frequency of VIV was observed for the dimpled structure. The reduction in these parameters brings to light the tremendous effect by the presence of the dimples on the surface. The energy drawn out of the main flow by the cavity vortices is imparted to the boundary layer

along the surface of the structure through the flow mixing process. As the fluid travels along the surface of the structure encountering increasing pressure, this energized boundary layer is better able to resist the adverse pressure gradient. The longer, the flow remains attached, the occurrence of smaller wake and drag is observed. Moreover, the smaller vortices formed all along the length of dimpled surface contribute less momentum for the formation of vortex shedding. The phenomenon of longer attachment of the flow with the surface together with smaller vortices results in the enormous reduction of Strouhal frequency and VIV.

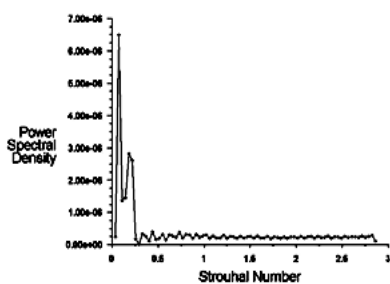


Fig. 9.25(a) Strouhal number

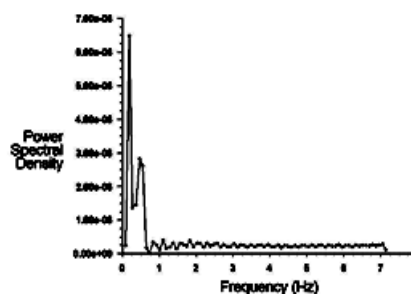


Fig. 9.25(b) Strouhal frequency

The flow parameters of fluid flow past a marine riser engraved with dimples on the surface are shown in Table 9.6. There is a significant reduction in lift and drag forces along the flow field when compared with that of a bare riser. The coefficient of lift, Strouhal frequency and Strouhal number registered a sharp decline in magnitude. The decrease in magnitude of Strouhal frequency ensures reduction in VIV to a much lesser value due to the presence of dimples. Even though the kinetic energy gradients determine the strength of the vortex shedding, the vorticity distribution depends significantly on the velocity gradients present in the flow field. As a result, the frequency of VIV was diminished to a much lesser value of 0.052. A reduction in

Strouhal number up to 67% was attained with the presence of modified cylinder with depressions on the surface.

Table 9.6 Flow characteristics across a cylinder with dimples on the surface

Drag (N)	Coefficient of drag	Lift (N)	Coefficient of lift	Strouhal frequency (Hz)	Strouhal number
33.75	0.0198	-1.3876	0.0007	0.182	0.052

9.5.3 Effect of sizing and sequencing of dimples on the riser surface

The numerical investigations were carried out by changing the sequence of dimples. The number of dimples arranged in a single circular ring was selected as 6, 7, 8 and 10. The same boundary conditions were applied, and the flow velocity kept at 1 m/s. Table 9.7 provides the results of this analysis. The size of the dimple was 40 mm for all the dimples in the ring. However, due to the highly complicated fluid flow field generated by the dimpled surface, no definite pattern was evolved. It seems that flow field and vortex shedding phenomenon varies abruptly with changes in the sequence of dimples on the surface. However, Strouhal number was found to be a minimum for a dimple count of 7 per ring on the riser surface.

Table 9.7 Flow characteristics by varying sequence of dimples on the surface

Number of dimples in one ring	Drag (N)	Coefficient of drag	Lift (N)	Coefficient of lift	Strouhal frequency (Hz)	Strouhal number
6	30.656	0.0097	0.241	0.00007	0.6081	0.2295
7	26.570	0.0848	-4.695	0.0149	0.0225	0.0093
8	44.860	0.0143	-18.314	0.0058	0.1340	0.0437
10	33.750	0.0198	-1.318	0.0007	0.182	0.072

Similar results were observed by changing the size of the dimples arranged in a ring on the surface of marine risers as shown in Table 9.8. The number of dimples in the ring on the outer surface of the riser was kept at 10. The sizes of the dimple selected were 20 mm, 40 mm, 60 mm and 100 mm. No definite trend was obtained by experimenting with the size of dimples. The results showed abrupt changes in flow characteristics in the field with the change in size. It may be due to the highly complicated vortex dynamics induced by the presence of these depressions on the surface. However, Strouhal number was found to be a minimum for a dimple size of 60 mm on the riser surface.

Table 9.8 Flow characteristics by varying size of dimples on the surface

Size of dimples in one ring	Drag (N)	Coefficient of drag (C_D)	Lift (N)	Coefficient of lift (C_L)	Strouhal frequency (Hz)	Strouhal number
20 mm	94.590	0.301	-21.795	0.069	0.0601	0.0239
40 mm	33.75	0.0198	-1.318	0.0007	0.182	0.072
60 mm	57.827	0.0184	4.644	0.0014	0.0556	0.0208
100 mm	64.189	0.0204	3.367	0.0010	0.4320	0.1712

9.6 SUMMARY

Computational analysis of a subsonic incompressible flow of air past a tall chimney fitted with and without helical strakes has been performed using RANS calculations with SST $k-\omega$ turbulence model. The numerical calculations predicted the flow parameters such as coefficient of lift, coefficient of drag and Strouhal number accurately. Strouhal frequency was found to reduce considerably with the addition of helical strakes along the surface of the chimney. The introduction of helical strakes in the fluid flow has decreased the lift along with a reduction in the coefficient of lift and drag. This decrease in the lift force resulted in the suppression of vortex shedding phenomenon. The small vortices formed around the structure close to the strakes are found to be out of phase with one another and led to partial cancellation of the forces at different span-wise positions. Strouhal frequency and VIV registered a decline of approximately 78%. This investigation predicts that the helical strakes can suppress Aeolian vibration and protect a tall chimney from the impending structural failure.

The detailed evaluation of tall chimney fitted with helical strakes gave the following advantages for this method: (i) Vortex induced forces can be reduced by as high as 85 percent, (ii) Strakes can be permanently attached to the surface of structure and (iii) Optimum values for pitch and height can be accurately determined.

Computational analysis of subsonic fluid flow across a marine riser arranged with and without dimples on the surface has been performed using RANS calculations. Strouhal frequency was reduced remarkably with the arrangement of dimples all along the surface in a definite pattern. The introduction of hemispherical depressions on the surface has changed the vortex dynamics and decreased the lift significantly. When depressions are engraved on the surface of the riser, the fluid enters the dimple, initiating pressure differential between the trailing edge region and leading edge region causing the fluid to circulate within the dimple and a cavity flow exists. The energy drawn out of the main flow by the cavity vortices is imparted to the boundary layer along the surface of the structure through the flow mixing process causing the energized boundary layer to resist the adverse pressure gradient. The longer, the flow remains attached on the surface, the smaller is the overall wake and drag. Strouhal frequency and VIV recorded a sharp decline of approximately 67%. However, due to the presence of highly complicated flow field induced, the exact sequence and size of dimples vary with flow conditions. The complicated vortex dynamics induced by the presence of dimples contributes to these predictions. The suitable size and sequence of dimples seem to depend on the size of riser and velocity of fluid flow. This investigation highlighted that dimpled surfaces can protect marine riser from an imminent structural failure due to undesirable shear layer instabilities. The calculations based on Strouhal number revealed that a dimple size of 60 mm and a

dimple count of 7 per ring provided better benefits in reducing vortex induced forces. The detailed evaluation of marine riser engraved with dimples on the surface gave the following advantages for this method: (i) Vortex induced forces reduces by 67 percent, (ii) Dimples can be created on the surface of the structure even at the time of design and construction and (iii) Issue of 'drag crisis' can be solved to some extent by preventing the increase in drag.

CHAPTER - 10

CONCLUSIONS

A comprehensive computational investigation of turbulent subsonic fluid flow characteristics in the wake of the square and circular structures with and without suppression methods have been carried out. The effect of passive devices and active methods in the reduction of vortex induced vibrations was studied in detail. The probes were conducted to study nature of instabilities and its effect on the fluid flow parameters such as Strouhal number, lift and drag forces. A study on the effect of wind load on tall industrial chimneys and water currents over dimpled surface of long marine risers on the possible suppression of vortex induced vibrations was also performed and the effect on the flow-induced forces were examined. A comparison of the predictions obtained from fluid flow past bluff bodies with the experimental data reported in literature reveals some relevant inferences. It may be noted that the structural response due to these forcing functions are not analyzed in the present study as it requires finite element modeling leading to tremendous computational resources.

10.1 ANALYSIS OF FLUID FLOW PARAMETERS ON CIRCULAR AND SQUARE STRUCTURES

The flow characteristics at various Reynolds numbers around the square and circular cylindrical structures showed remarkable variation in properties. At $Re=40$, only recirculation eddies are formed immediately downstream of the square cylinder, and no periodic vortex shedding noticed. The flow separates at the top right corner of the square cylinder, *i.e.* flow wraps the cylinder at the top and bottom face at $Re=40$. However, at $Re>40$, flow around square cylinder becomes unstable and results in an

oscillating flow with the amplitude of oscillation increasing in the downstream direction. Moreover, at $Re=150$, due to its turbulent nature, the flow separates much earlier, *i.e.* at top left corner forming a vortex street. Flow characteristics in the field such as Strouhal number (St), C_L and C_D were computed and the predictions were found to be in reasonable agreement with the available experimental data in the literature.

The characteristics of a flow past a circular cylinder at a low Reynolds number of $Re=5$ reveals that the separation of flow gets much delayed and the stagnation point occurs at the rear of the circular cylinder. However, at $Re=40$, the flow separation occurs at the forwarding stagnation point and only recirculation eddies are observed. When the flow characteristics of the square and circular cylinders at $Re=40$ are compared, similar trends in recirculation eddies are noticed. Nevertheless, the flow separation occurs much delayed in circular cylinders when compared to a square cylinder which is primarily due to the sharp corners of the square cylinder. The coefficient of drag computed for circular and square cylinders remains roughly the same under similar conditions. The Strouhal number calculated for square and circular cylinders for the same Reynolds number without any vortex suppression devices are 0.15 and 0.20 respectively. The non-dimensional recirculation length $Lr/h = 2.688$ reported by De and Dalal (2006) experimentally is in good agreement with the predicted value of $Lr/h = 2.60$ in the present study.

10.2 EFFECT OF SPLITTER PLATE IN THE REDUCTION OF VORTEX INDUCED FORCES ON A SQUARE CYLINDER

An investigation on the suppression of fluid forces around a square cylinder was conducted by employing a splitter plate (passive device) in the wake region. The formation of vortex shedding phenomenon and the associated changes in flow parameters were analysed along the flow field with and without detached splitter plate at various gap ratios (G/d) ranging from 0.5 to 3. The splitter plate thwarted the interaction of fluid masses from the top and bottom layers in the wake of the cylinder. It was observed that the splitter plate is highly effective in interrupting the regular vortex formation, which in turn suppresses the vortex shedding phenomenon and thereby a reduction in flow-induced forces. There is an optimum gap distance ' G ' known as critical gap distance ' G_{cr} ' between the splitter plate and the square cylinder where the drag is seen to be a minimum. It is clearly evident from C_D vs G plot that the coefficient of drag reduces as G approaches $G_{cr} = 2.5D$ and there after it increases. This is in reasonable agreement with the findings of Mittal (2003) that the shortest length required to suppress vortex shedding is at least two cylinder diameters.

10.3 PASSIVE CONTROL OF VORTEX INDUCED FORCES ON A CIRCULAR GEOMETRY FITTED WITH STRAIGHT FINS

Numerical investigations of the flow around a circular cylinder with straight fins were conducted to analyse the flow characteristics around bluff bodies in subsonic flow. As a passive vortex control method, the straight fins are found to be effective in suppressing the vortex induced vibrations of the structures. The modification in the design by varying fin count and orientation provided valuable

information on vortex shedding phenomenon. The investigation was performed for different fin counts (3-8), and orientation (4 fin-0⁰, 4 fin-45⁰). The vortex shedding and Aeolian vibrations were reduced by the use of straight fins fitted on the cylinder surface. A large fin count and an orientation angle of 0⁰ are found to be more effective in reducing the VIV. Although the added benefits of VIV reduction by increasing the fin count is less, selection of proper fin orientation seems to be more critical.

The study on straight fins on structures infers that the lift force gets reduced at the expense of an increase in drag force and the order of its increase has to be evaluated further with the aid of experimental measurements. The study is limited to low and medium Reynolds numbers and confined to incompressible fluid flows alone.

10.4 SUPPRESSION OF VORTEX INDUCED FORCES ON CIRCULAR GEOMETRY FITTED WITH HELICAL STRAKES

Computational study of a subsonic flow of air past a circular cylinder with and without helical strakes has been performed using Reynolds Averaged Navier Stokes calculations coupled with Shear Stress Transport $k-\omega$ turbulence model. The numerical predictions provided valuable information on changes in various flow parameters. The Strouhal frequency was seen to reduce appreciably by fitting helical strakes on the surface of cylindrical bodies. A reduction in VIV of approximately 85% was attained by employing helical strakes. The investigation revealed that the effectiveness of helical strakes improved immensely at an optimum pitch of $5d$ and height $0.15d$. It was detected that the use of helical strakes in the fluid flow has increased the drag marginally due to the obstruction in the flow affecting its smooth movement around the structure, inducing a force in the direction of flow. This

phenomenon known as the drag crisis can be reduced by suitably aligning the surface of the strakes so that the skin friction coefficient can be reduced. Helical strakes seem to have significant role in the reduction of Strouhal frequency and thereby subsequent damages caused on different offshore and onshore structures can be eliminated.

10.5 ACTIVE METHOD OF VIV SUPPRESSION ON A SQUARE STRUCTURE

Numerical study of flow past stationary as well as oscillating square cylinders has been carried out to get an insight into the effect of oscillations provided to the structure to suppress the vortex induced vibrations. This method of supplying energy into the system for VIV suppression is termed as Active method. It is observed that the oscillation of the square cylinder considerably suppresses the vortex shedding phenomenon. Simulations were performed on a square cylinder by providing different amplitudes of oscillation. Strouhal frequency was found to reduce with increase in amplitudes of oscillation. A 20% reduction of Strouhal number was realised in this method at oscillation amplitude of 0.3 m. Beyond certain amplitude, both the coefficients of lift and drag show some unrealistic values. The increase in turbulence and flow instabilities at large amplitudes are very complex and challenging to analyse, resulting in these surreal values. Hence amplitudes less than 0.03 m are considered to be a favourable value of oscillation that could prevent the structure from VIV.

10.6 ANALYSIS OF COMPOUND METHOD IN THE SUPPRESSION OF VORTEX INDUCED FORCES

The flow characteristics due to shear layer instability for a flow past a structure with and without stationary and oscillating splitter plates were also investigated in detail. The compound method, which combines the effect of both passive and active controls for the suppression of vortex induced vibration, was employed. The oscillating splitter plate placed in the wake effectively interrupts the formation of vortex shedding, and the wake becomes more and more turbulent. A reduction in Strouhal frequency along with weakened vortex shedding phenomenon was observed due to forced oscillations of the splitter plate. The fluid layers getting detached from both sides of the cylinder were prevented from interacting with each other in the wake region. At low amplitudes of oscillations, this method reduces the Strouhal frequency to a much lesser value, and this control measure is found to be very effective in the suppression of VIV. However, at higher amplitudes of oscillation, the simulation recorded strong vibrations initiated by the highly turbulent wake. Since the compound method resulted in substantial reduction in the Strouhal frequency, this method is found to be superior to both active and passive methods. A reduction in Aeolian vibration of approximately 72.36% was realised in this method. The compound method as similar to other suppression methods is effective in reducing the VIV, but only on the expense of a marginal increase in the drag forces acting on the structure. This method may be highly effective in preventing the damage to tall structures, and underwater applications that are subjected to hefty fluid flows across them.

10.7 SUPPRESSION OF VORTEX SHEDDING USING HELICAL STRAKES ATTACHED ON A TALL CHIMNEY

Numerical analysis of a subsonic incompressible flow of wind past a tall chimney fitted with and without helical strakes has been carried out. RANS calculations have been used to predict the flow parameters such as coefficient of lift, coefficient of drag, Strouhal number and frequency accurately. The introduction of helical strakes in the fluid flow has reduced the lift considerably together with a reduction in the coefficient of lift and drag. This decrease in the lift force has resulted in significant reduction of vortex shedding phenomenon. Strouhal frequency was found to reduce considerably with the addition of helical strakes along the surface of the chimney. The small vortices formed around the structure close to the strakes are found to be out of phase with one another and led to partial cancellation of the forces at different span-wise positions. Strouhal frequency and lift force registered a sharp decline in VIV. The magnitude of VIV was found to reduce by 78% with the addition of helical strakes along the chimney height for a pitch of $2d$ and strake height of $0.1d$. It may be noted that the Strouhal number calculated with and without attaching helical strakes to the tall chimney are 0.052 and 0.24 respectively. This investigation predicts that the helical strakes can suppress Aeolian vibrations and protect tall chimneys from colossal damage. It also ensures the safety of life and property of people living nearby tall structures and can also address the looming environmental concerns.

10.8 NOVEL CONCEPT OF SUPPRESSION OF VORTEX SHEDDING ON A MARINE RISER ENGRAVED WITH DIMPLES ON THE SURFACE

Computational analysis of a cross-flow of water past a long marine riser engraved with and without dimples on the surface has been performed using RANS calculations coupled with suitable turbulence model. The effect of circular dimples is omni-directional around the cylindrical riser and initiated transcendental changes in the flow domain. The introduction of hemispherical depressions on the surface has changed the vortex dynamics and also decreased the lift considerably. The depressions engraved on the surface of the riser allows the fluid to enter the cavity, initiating pressure differential between the trailing edge region and leading edge region causing the fluid to circulate within the dimple resulting in a cavity flow. It is observed that the energy from the main flow is drained by the less dispersion vortices in the depressions as they leave the dimple cavities. The energy drawn out of the main flow by the cavity vortices is imparted to the boundary layer along the surface of the structure through the flow mixing process causing the energized boundary layer to resist the adverse pressure gradient. The longer, the flow remains attached on the surface, the smaller is the overall wake and drag. The estimated Strouhal number has recorded a sharp decline of approximately 67%. It may be noted that the Strouhal number calculated with and without engraving dimples on the surface of marine riser are 0.072 and 0.22 respectively. However, due to the presence of highly complicated flow field caused by these depressions, the exact sequence and size of dimples vary with flow conditions. The complicated vortex dynamics induced by the presence of dimples contributes to these predictions. The optimum size and sequence of dimples seem to depend considerably on the size of riser and velocity of fluid flow. On

calculating the Strouhal number, it was observed that a dimple size of 60 mm and a dimple count of 7 per ring provided better benefits in reducing vortex induced forces. This investigation highlight that dimple all-around a cylindrical structure in a definite pattern rather than a staggered configuration can suppress the Aeolian vibration and protect marine riser from an imminent structural failure due to undesirable shear layer instabilities.

10.9 FUTURE WORK

Experimental measurements on novel concepts of passive and active methods may be carried out to get more insight into these complex phenomena. Combination of passive and active methods into a compound method with improved control techniques and advanced concepts on forcing function may provide better benefits in VIV reduction. Structural analysis may be carried out by appropriate finite element modelling techniques with proper structural damping and the natural frequencies (eigen values) and mode shapes (eigen vectors) of the structure determined. Finer computational grids keeping wall y^+ less than 1 and numerical methods such as large eddy simulation and direct numerical simulation may be carried out to predict accurate values of flow-induced parameters. Although computational cost and time may increase tremendously, the above simulations may provide better perception into the complex vortex dynamics and flow-induced instabilities.

REFERENCES

Ali M.S.M., Doolan C.J. and Wheatley V. (2009) Grid convergence study for a two-dimensional simulation of flow around a square cylinder at a low Reynolds number. *In: Seventh International Conference on CFD in the Minerals and Process Industries CSIRO, Melbourne, Australia.*

Alok David John, Ajay Gajrola, Eshan Ganju and Anant Gupta (2011) Design wind loads on reinforced Concrete Chimney- An Experimental case study. *Procedia Engineering*, 14, 1252-1257.

Arnab Kumar De and Amaresh Dalal S. (2006) Numerical simulation of unconfined flow past a triangular cylinder. *International Journal for Numerical Methods in Fluids*, 52, 801-821.

Assi G. R. S., Bearman P. W, and Kitney N. (2009) Low drag solutions for suppressing vortex-induced vibration of circular cylinders. *Journal of Fluids and Structures*, 25, 666-675.

Baek H. and Karniadakis G. E. (2009) Suppressing vortex-induced vibrations via passive means. *Journal of Fluids and Structures*, 25, 848-866.

Bearman P.W. and Obasaju E.D. (1982) An experimental study of pressure fluctuations on fixed and oscillating square-section cylinders. *Journal of Fluid Mechanics*, 119, 297–321.

Behr M., Hastreiter D., Mittal S. and Tezduyar T.E. (1995) Flow past a circular cylinder: Dependence of the computed flow field on the location of the lateral boundaries. *Computer Methods in Applied Mechanics and Engineering*, 123, 309–316.

Brika D. and Laneville A. (1997) Vortex-induced oscillations of two flexible circular cylinders coupled mechanically. *Journal of Wind Engineering and Industrial Aerodynamics*, 69–71, 293-302.

Cheng M., Chew Y.T. and Luo S.C. (2001) Numerical investigation of a rotationally oscillating cylinder in mean flow. *Journal of Fluids and Structures*, 15, 981-1007.

Dalton C. (2000) Fundamentals of Vortex Induced Vibration. *College course notes, University of Houston.*

Dong S. and Karniadakis G.E. (2005) DNS of flow past a stationary and oscillating cylinder at $Re=10000$. *Journal of Fluids and Structures*, 20, 519– 531.

- Doolan C.J., Choley V. And Crespel J.** (2012) Vortex shedding during the interaction of a turbulent wake with a cylinder. *Journal of Fluids and Structures*, 31, 141-146.
- Guilmineau E. and Queutey P.** (2002) A numerical simulation of vortex shedding from an oscillating circular cylinder. *Journal of Fluids and Structure*, 16, 773-794.
- Hover F. S., Tvedt H. and Triantafyllou M. S.** (2001) Vortex-induced vibrations of a cylinder with tripping wires. *Journal of Fluid Mechanics*, 448, 175-195.
- Inoue, Iwakam and Hatakeyama** (2006) Aeolian tones radiated from flow past two square cylinders in a side-by-side arrangement. *Physics of Fluids*, 18, 046104.
- Kawcki J. and Zuranski J.A.** (2007) Crosswind vibrations of steel chimneys-A new case history. *Journal of wind Engineering and Industrial Aerodynamics*, 95, 1166-1175.
- Khalak A. and Williamson C.H.K.** (1999) Motions, forces and mode transitions in vortex-induced vibrations at low mass-damping. *Journal of Fluids and Structures*, 13, 813–851.
- Korkischko I. and Meneghini J. R.** (2010) Experimental investigation of flow induced vibration on isolated and tandem circular cylinders fitted with strakes. *Journal of fluids and structures*, 26, 611 – 625.
- Krishnamoorthy S., Price S. J. and Paydoussis M. P.** (2001) Cross-flow past an oscillating circular cylinder: synchronisation phenomena in the near wake. *Journal of Fluids and Structures*, 15, 955–980.
- Kwon K. and Choi H.** (1996) Control of laminar vortex shedding behind a circular cylinder using splitter plates. *Physics of Fluids*, 8, 479-486.
- Lee KeeQuen** (2014) Investigation on the effectiveness of helical strakes in suppressing VIV of flexible riser. *Applied Ocean Research*, 44, 82–91.
- Li J.S., Zhang L., Ding L. and Yang Z.Q.** (2014) Effect of length of splitter plate on flow over a square cylinder in flow channel. *Journal of Zhejiang University Engineering Science Edition*, 48(12), 2172-2180.
- Ming Jyh Chern, Rajesh Kanna P., Yi Jen Lu, Chung Cheng I. and Shang Chung Chang** (2010) A CFD study of the interaction of oscillatory flows with a pair of side-by-side cylinders. *Journal of Fluids and Structures*, 26, 626–643.
- Mittal S.** (2003) Effect of a ‘‘slip’’ splitter plate on vortex shedding from a cylinder *Physics of Fluids*, 15(3), 817-820
- Mohamed Sukri Mat Ali, Doolan J. and Vincent Wheatley** (2012) Low Reynolds number flow over a square cylinder with a detached flat plate. *International Journal of Heat and Fluid Flow*, 36, 133–141.

- Muammer Ozgoren, Engin Pinar, Besir Sahin and Huseyin Akilli** (2011) Comparison of flow structures in the downstream region of a cylinder and sphere. *International Journal of Heat and Fluid Flow*, 32, 1138-1146.
- Nakamura Y., Mizota T.** (1975) Unsteady lifts and wakes of oscillating rectangular prisms. *Journal of Engineering Mechanics Division ASCE*, 101, 855–871.
- Okajima A.** (1982) Strouhal numbers of rectangular cylinders. *Journal of Fluid Mechanics*, 123, 379–398.
- Owen J. C, Bearman P. W. and Szewczyk A. A.** (2001) Passive control of viv with drag reduction. *Journal of Fluids and Structures*, 15, 597-605.
- Ozono S.** (1999) Flow control of vortex shedding by a short splitter plate asymmetrically arranged downstream of a cylinder. *Physics of Fluids*, 11, 2928–2934.
- Ozono S.** (2000) Flow Control of Vortex Shedding by Asymmetrically Arranged Plates. *Theoretical and Applied Mechanics*, 49, 191–196.
- Robert D. Blevins** (1990) Flow Induced Vibrations. Krieger Publishing Co., Florida.
- Robert R. Hwang, AmalenduSau, Sheu T.W. and Yang W.C.** (2003) Interaction of trailing vortices in the wake of a wall mounted rectangular cylinder. *Physics Review E*, 68, 056303, 1-15.
- Roshko, Anatol** (1954) On the Development of Turbulent Wakes from Vortex Streets. *National Advisory Committee for Aeronautics, Washington, D. C.*
- Shan Huang** (2011) VIV suppression of a two-degree-of-freedom circular cylinder and drag reduction of a fixed circular cylinder by the use of helical grooves. *Journal of Fluids and Structures*, 27, 124–113.
- Shan Huang and Andy Sworn** (2013) Hydrodynamic coefficients of two fixed circular cylinders fitted with helical strakes at various staggered and tandem arrangements. *Applied Ocean Research*, 43, 21–26.
- Sohankar A.** (2006) Flow over a bluff body from moderate to high Reynolds number using large eddy simulation. *Computer and Fluids*, 35 (10), 1154 – 1168.
- Strykowski P. J and SreenivasanK. R.** (1990) On the formation and suppression of vortex shedding at low Reynolds numbers. *Journal of Fluid Mechanics*, 218, 71-107.
- Subhankar Sen and Sanjay Mittal** (2011) Free vibration of a square cylinder at low Reynolds numbers. *Journal of Fluids and Structures*, 27, 875–884.
- Sumner D., Heseltine J. L. and Dansereau O. J. P.** (2004) Wake structure of a finite circular cylinder of small aspect ratio. *Experiments in Fluids*, 37(5), 720-730.
- Yunus A. Cengel and John M Cimbala** (2005) Fluid Mechanics: Fundamentals and Applications. *McGraw-Hill Publications*.

Zakir Faruquee, David S. K, Ting, Amir Fartaj, Ronald M. Barron and Rupp Carriveau (2007) The effects of axis ratio on laminar fluid flow around an elliptical cylinder. *International Journal of Heat and Fluid Flow*, 28, 1178-1189.

Zdravkovich M. M. (1981) Review and classification of various aerodynamic and hydrodynamic means for suppressing vortex shedding. *Journal of Wind Engineering and Industrial Aerodynamics*, 7, 145 -189.

Zhao Ming (2015) Numerical simulation of vortex induced vibration of a circular cylinder in a span wise shear flow. *Physics of Fluids*, 27(8), 063101.

Zheng Z.C. and Zhang N. (2008) Frequency effects on lift and drag for flow past an oscillating cylinder. *Journal of Fluids and Structures*, 24, 382–399.

Zhou T., Mohd. Razali S.F., Hao Z. and Cheng L. (2011) On the study of vortex induced vibration of a cylinder with helical strakes. *Journal of Fluids and Structures*, 27, 903–917.

LIST OF PUBLICATIONS

International Journals:

1. Sunil A. S. and Tide P. S. (2017) “An Investigation on Suppression of Vortex Instabilities for Flow Past a Bluff Body Using a Passive Device”. *International Review of Mechanical Engineering*, Vol.11 (2), pp. 132 – 137.
2. Sunil A. S. and Tide P. S. (2019) “An Investigation on the Suppression of Vortex Induced Vibration of a Cylinder Using Compound Method with Oscillating Splitter Plate”, *International Journal of Advanced Research in Dynamical and Control Systems*, Vol.11 (07), pp. 562-569.
3. Sunil A. S. and Tide P. S. (2019) “Numerical Investigations on Suppression of Aeolian Vibrations on a Tall Chimney using Helical Strakes”, *International Journal on Engineering Applications*. Vol.7 (5), pp.152-159.
4. Sunil A. S. and Tide P. S. (2019) “An Investigation on Reduction of Vortex Induced Loads on Marine Risers”. *International Journal of Emerging Technologies and Innovative Research*, Vol.10, pp. 25-33.

International Conferences:

1. Sunil A. S. and Tide P. S. (2014) “An Investigation on Fluid Flow Oscillations for Flow past a Square Cylinder at various Reynolds Numbers”, International Conference on Energy, Environment, Materials and Safety, ICEEMS, pp. 443-450.

CURRICULUM VITAE

1. Name : **SUNIL A. S.**

2. Date of Birth : 22.04.1970

3. Educational Qualifications

1991 Bachelor of Technology (B.Tech)

Institution : Government Engineering College, Thrissur,
University of Calicut, Kerala,

Specialisation : Mechanical Engineering

2006 Master of Technology (M.Tech)

Institution : National Institute of Technology, Calicut, Kerala

Specialisation : Energy Management

Doctor of Philosophy (Ph.D)

Institution : Cochin University of Science and Technology,
Kochi, Kerala

Registration Date : 24.11.2011